Title
Properties of Mesoscale Flows in the Nightside Auroral and Subauroral Ionosphere

Author
Gallardo Lacourt, Beatriz Isabel

Publication Date
2016

UNIVERSITY OF CALIFORNIA

Los Angeles

Properties of Mesoscale Flows in the Nightside Auroral and Subauroral Ionosphere

A dissertation submitted in partial satisfaction of

the requirements for the degree Doctor of Philosophy

in Atmospheric and Oceanic Sciences

by

Beatriz Isabel Gallardo Lacourt

2016

ABSTRACT OF THE DISSERTATION

Properties of Mesoscale Flows in the Nightside Auroral and Subauroral Ionosphere

by

Beatriz Isabel Gallardo Lacourt

Doctor of Philosophy in Atmospheric and Oceanic Sciences

University of California, Los Angeles, 2016

Professor Lawrence R. Lyons, Chair

In addition to the traditional large-scale convection, nightside plasma sheet transport involves a significant amount of meso-scale fast flows that carry a large amount of magnetic flux. Those flows are coupled to the ionosphere, and auroral manifestations of such fast flows include auroral streamers and substorm onset. Sub-auroral polarization streams (SAPS) are another fast-flow phenomenon occurring just equatorward of the electron auroral oval. While in-situ measurements can only detect these mesoscale transient phenomena at a limited number of points or can characterize them statistically, measuring flows and aurora in the ionosphere allows us to evaluate the instantaneous two-dimensional evolution. In this thesis we first investigate the structure of these flow bursts using two-dimensional line-of-sight flow observations from the SuperDARN radars and auroral images from the THEMIS ground-based all-sky imager (ASI) array. Radar echoes captured at horizontal distances <~500 km from the radars were mainly used

to detect small-scale flow structures that would otherwise be missed or poorly resolved in long-range radar echoes. After identifying 135 auroral streamers in the ASI images near radar echoes, we examined the flow evolution and properties of flow channels. Flow bursts and streamers are invariably correlated in all events. The flow bursts are often directed equatorward and appear simultaneously with the streamers. Equatorward flows are located just to the east of the streamers. Less frequently (~10% of the time), a poleward flow enhancement was detected even when a streamer propagated equatorward, the poleward flow enhancement being located to the west of the auroral streamer, or to the east of the equatorward flow enhancement, consistent with the expected spatial relationship between flow shear and upward field-aligned currents in plasma sheet flow bursts. The azimuthal width of the flow channel is on average ~75 km, and the azimuthal offset of the equatorward flow channel relative to the auroral streamer is ~57 km eastward. This study demonstrates the capability of radar-imager pairs for identifying the 2-D structure of localized flows associated with plasma sheet flow bursts.

In the second part of this thesis, we investigated ionospheric flow patterns associated with auroral onset beads using line-of-sight flow observations from the SuperDARN and auroral images from the THEMIS ground-based ASI array. We selected events that occurred when the SuperDARN radars operated in a high temporal resolution THEMIS mode (6 seconds) along northward looking beams, a time resolution comparable to that of the imagers, providing a unique tool to detect properties of flows associated with auroral onset beads. We have found very fast oscillating flows (~1000 m/s) that are correlated with the onset beads propagating across the THEMIS-mode beam meridian. 2-d radar measurements also show a wavy pattern in the azimuthal direction with a wavelength of ~78 km, which is close to the azimuthal separation of individual beads. We also used an imager and SuperDARN in Iceland and identified weak but

significant azimuthal flow modulations associated with beads. These strong correlations (in time and space) between auroral beading and the fast ionospheric flows suggest that substorm onset occurs via an instability in the inner plasma sheet and is associated with intense flow shears. The flow shear is clockwise around auroral beads, consistent with converging electric fields associated with upward field-aligned currents in the shear center.

Finally, we present simultaneous measurements from the THEMIS ASI array and the 2-d SuperDARN radar measurements that share fields of view with the imagers to investigate the association between SAPS flow enhancements and auroral streamers. We first identified auroral streamers in the ASI images to analyze the ionospheric flow variations at subauroral latitudes. We also performed a reverse study starting with flow variations and then analyzed the auroral condition from the ASI. In this study we analyzed a total of 104 events. For the case of streamers observed near the equatorward boundary of the auroral oval, we find average westward flow enhancements of ~700 m/s slightly equatorward of the streamers. Our statistical results show that for the first part of this study (forward study, starting from streamers) 98% of the streamers that reach close to the equatorward boundary lead to SAPS westward flow enhancements. For the reverse study (starting from flow enhancements), we have found that streamers and enhanced convection nearly equally contribute to SAPS flow enhancements. We also characterize the SAPS flow channel width and timing relative to streamers reaching radar echo meridians. The strong influence of auroral streamers on the rapid evolution of SAPS flows suggests that transient fast earthward plasma sheet flows can lead to westward SAPS flow enhancements in the subauroral region, and that such enhancements are far more commonly occurring than during substorms alone, based on the frequent occurrences of streamers under various geomagnetic conditions.

The dissertation of Beatriz Isabel Gallardo Lacourt is approved.

Vassilis Angelopoulos

Jacob Bortnik

Yukitoshi Nishimura

Lawrence R. Lyons, Committee Chair

University of California, Los Angeles

2016

Esta tesis esta dedicada a mis padres Simon y Maria Eugenia, y a mi hermana Carolina, que son mi mayor apoyo.

Table of Contents

List of Figures

List of Tables

Acknowledgments

I would like to thank my advisors, Prof. Larry Lyons and Dr. Yukitoshi Nishimura, for their guidance during these years at UCLA. They have taught me very patiently and enlightened me during moments in which inspiration or motivation was not very easy to reach.

I want to also thank my co-authors and collaborators who contribute greatly to the development of this research work: Prof. Vassilis Angelopoulos, Prof. Richard Thorne and Prof. Jacob Bortnik at UCLA; Prof. Eric Donovan at University of Calgary, Canada; Prof. Mike Ruohoniemi at Virginia Tech; Dr. Evgeny Mishin; and Prof. Nozumo Nishitani at Nagoya University, Japan

I would also like to thanks my friends in AOS and EPSS department for being there with me in the happy and no so happy moments: Tersi Arias, Victor Pinto, Mojhgan Haghnegahdar, Richard Hart, David Gonzalez-Martinez, Baird Langenbrunner, Marla Schwartz, Rose Tseng, Cheng Zheng and Dr. Chih-Ping Wang.

Beatriz Isabel Gallardo Lacourt

Los Angeles, California

May, 2016

Chapter 2 is a modified version of "**Gallardo-Lacourt, B.**, Y. Nishimura, L. R. Lyons, S. Zou, V. Angelopoulos, E. Donovan, K. A. McWilliams, J. M. Ruohoniemi, and N. Nishitani (2014), Coordinated SuperDARN THEMIS ASI observations of mesoscale flow bursts associated with auroral streamers, J. Geophys. Res. Space Physics, 119, doi:10.1002/2013JA019245."

Chapter 3 is a modified version of "Gallardo-Lacourt, B., Y. Nishimura, L. R. Lyons, J. M. Ruohoniemi, E. F. Donovan, V. Angelopoulos, K. A. McWilliams, and N. Nishitani (2014), Ionospheric flow structures associated with auroral beading at substorm auroral onset, J. Geophys. Res. Space Physics, 119, 9150–9159, doi:10.1002/ 2014JA020298."

Chapter 4 is a modified version of "Gallardo-Lacourt, B., Y. Nishimura, L. R. Lyons, E. V. Mishin, J. M. Ruohoniemi, E. F. Donovan, V. Angelopoulos, and N. Nishitani (2016), Influence of auroral streamers on rapid evolution of ionospheric SAPS flows, In preparation to be submitted to J. Geophys. Res. Space Physics"

This research was funded by a Chilean Fellowship (Becas Chile) and a UCLA Dissertation Year Fellowship, along with two National Foundation Aeronomy program grants and an Air Force Office of Science Research Program. All THEMIS data are from THEMIS official website (http://themis.ssl.berkeley.edu/). We thank S. Mende and H. Frey for use of the ASI data. Solar wind data and energetic particle data were obtained courtesy of the SPDF OMNIWeb database and the LANL Energetic Particle Team, respectively. SuperDARN is a collection of radars funded by national scientific funding agencies of Australia, Canada, China, France, Japan, South Africa, United Kingdom, and United States of America. The operation of the Canadian SuperDARN radars is supported by the Natural Sciences and Engineering Research

Council of Canada, the Canada Foundation for Innovation, and the Canadian Space Agency. Auroral observations at Iceland are carried out and provided by the Space and Upper Atmospheric Sciences group in the National Institute of Polar Research, Japan.

Vita

December, 2008	B.S., Physics. Physics Department, University of Santiago, Chile
March, 2012	Engineering Diploma, Physics Engineering. Physics Department, University of Santiago, Chile
November, 2012	M. S., Space Sciences. Department of Atmospheric and Oceanic Sciences University of California, Los Angeles, USA
2009	International Student Travel Grant, AGU Fall Meeting
2010-2014	Chilean Fellowship for Graduate Studies (Becas Chile)
2010	National Student Travel Grant, AGU Fall Meeting
2014	**AGU Outstanding Student Paper Award**
2014	**NSF-CEDAR Best Student Poster Award**
2015	**AOS Morris Neiburger Award**, for excellence in teaching
2015	**UCLA Dissertation Year Fellowship**
2016	Travel Grant, Chapman Conference AGU
2014-2015	Teaching Assistant, Department of Atmospheric and Oceanic Sciences, University of California, Los Angeles, USA.
2011-2014	Graduate Student Research Assistant Department of Atmospheric and Oceanic Sciences University of California, Los Angeles, USA

PUBLICATIONS

1. **Gallardo-Lacourt, B.**, Y. Nishimura, L. R. Lyons, J. M. Ruohoniemi, E. Donovan, V. Angelopoulos, K. A. McWilliams, and N. Nishitani (2014), Ionospheric flow structures associated with auroral beading at substorm auroral onset, J. Geophys. Res. Space

Physics, 119, 9150-9159, doi:10.1002/2014JA02029

2. **Gallardo-Lacourt, B.**, Y. Nishimura, L. R. Lyons, S. Zou, V. Angelopoulos, E. Donovan, K. A. McWilliams, J. M. Ruohoniemi, and N. Nishitani (2014), Coordinated SuperDARN THEMIS ASI observations of mesoscale flow bursts associated with auroral streamers, J. Geophys. Res. Space Physics, 119, doi:10.1002/2013JA019245 **[Featured article]**

3. **Gallardo-Lacourt, B.**, Y. Nishimura, L. R. Lyons, and E. Donovan (2012), External triggering of substorms identified using modern optical versus geosynchronous particle data, Ann. Geophys., 30, 667-673, doi:10.5194/angeo-30-667-2012

4. Lyons, L. R., Y. Nishimura, **B. Gallardo-Lacourt**, Y. Zou, E. F. Donovan, S. Mende, V. Angelopoulos, J. M. Ruohoniemi, K. A. McWilliams, D. L. Hampton, M. J. Nicolls (2016), Dynamics Related to Plasma Sheet Flow Bursts as Revealed from the Aurora, AGU Geophysical Monograph Series: Auroral Dynamics and Space Weather, ISBN: 978-1-118-97870-2

5. Lyons, L. R., Y. Nishimura, **B. Gallardo-Lacourt**, M. J. Nicolls, S. Chen, D. L. Hampton, W. A. Bristow, J. M. Ruohoniemi, N. Nishitani, E. F. Donovan, and V. Angelopoulos (2015), Azimuthal flow bursts in the Inner plasma Sheet and Possible Connections with SAPS and Plasma Sheet Earthward Flow Bursts, J. Geophys. Res. Space Physics, 120, doi:10.1002/2015JA021023.

6. Lyons, L. R., Y. Nishimura, **B. Gallardo-Lacourt**, Y. Zou, E. Donovan, S. Mende, V. Angelopoulos, J. M. Ruohoniemi, and K. McWilliams (2013), Westward traveling surges: Sliding along boundary arcs and distinction from onset arc brightening, J. Geophys. Res. Space Physics, 118, 7643–7653, doi:10.1002/2013JA019334

CHAPTER 1

Introduction

The following chapter serves as introduction to this thesis. Section 1.1 provides a general introduction explaining the structure of the Earth's magnetosphere and basic aspects of magnetosphere-ionosphere coupling. Sections 1.2, 1.3 and 1.4 serve as introduction of chapters 2, 3 and 4, respectively.

1.1 General Introduction

1.1.1 Structure of the Earth's Magnetosphere

The Earth's magnetosphere is the cavity around the Earth formed by the interaction between the solar wind and the Earth's magnetic field. The solar wind is formed as a result of the difference in gas pressure between the solar corona and the interstellar space. This pressure imbalance drives the solar plasma outward. The solar wind is a supersonic flow of plasma and magnetic field that permeates the interplanetary medium. The solar wind consists mainly of protons and electrons with mean velocities of 400-500 km/s, and typical densities of about $5/cm^3$. The solar wind is strongly affected by solar activity that varies according to the 11 year period of the solar cycle and is directly related to the sunspot number at the sun's surface, Figure 1.1 shows the evolution of the solar cycle.

When the solar wind impinges upon the Earth's magnetic field the magnetosphere is formed, compressing the magnetic field lines in the dayside and stretching them in the night side, forming a magnetotail. Since the solar wind travels with supersonic velocities in the interplanetary medium, a bow shock is formed on the dayside. At the bow shock the plasma is decelerated and thermalized. This thermalized plasma then forms a region called the magnetosheath, where the boundary between the magnetosheath and the magnetosphere is called magnetopause. In the nightside magnetosphere, where the magnetotail is formed, several distinct regions can be observed. The magnetotail is mainly populated by protons and electrons coming from the ionosphere and the solar wind. The outer region of the magnetotail is called plasma mantle, and it is a transition region between the magnetosheath and the magnetosphere. At lower latitudes in the magnetosphere are located the tail lobes, which are regions of open field lines with very low density (~0.01/cm^3), but strong magnetic field. The tail lobes are able to store large amounts of magnetic energy. Most of the magnetotail hot plasma is located in the plasma sheet, which is a very dynamic region composed by hot and dense (0.1-1/cm^3) plasma. The inner magnetosphere contains two different confined plasma populations: a cold and dense plasma making up the plasmasphere, and two distinct regions filled with energetic and tenuous plasma called Van Allen Radiation Belts. Figure 1.2 shows the different regions of the Earth's magnetosphere.

1.1.2 Magnetosphere-Ionosphere coupling

In 1961, Dungey et al. [1961] proposed a conceptual mechanism to explain the interaction between the Interplanetary Magnetic field (IMF) and the Earth's magnetosphere, nowadays that mechanism is referred to as Dungey's cycle. In this cycle, magnetic reconnection is explained as the transport of mass energy and momentum into the magnetosphere. In the presence of southward directed IMF, reconnection removes magnetic flux from the dayside and transports it to the nightside (e.g. magnetotail). In the ionosphere this process forms a two-cell convection pattern. Figure 1.3a shows the magnetospheric Dungey's cycle and 1.3b shows the ionospheric two cell convection pattern. This large-scale convection has been also observed and described using measurements from ground magnetic perturbations [Nishida et al., 1968a, b], from electric field measurements in the ionosphere [Heppner, 1972; Weimer, 1995], and from satellite plasma sheet observations [Hori 2000; Wang et al., 2006].

Plasma transport in the magnetosphere-ionosphere system has been traditionally studied from the point of view of this large-scale convection pattern, that occurs over large scale lengths of thousands of kilometers in the ionosphere. Figure 1.3b shows that in the ionosphere, the flow in the convection pattern is observed as anti-sunward flow in the center and a sunward flow at lower latitudes, westward in the dusk sector (pre-midnight) and eastward in the dawn sector (post-midnight). However, localized equatorward flows were discovered in the ionosphere in addition to the large scale convective flows [Sergeev et al., 1990; Kauriste et al., 1996], and these flows are the ionospheric manifestation of earthward flow bursts in the magnetosphere. However, observations showed that these mesoscale flows (10-100km) are capable of transporting large amount of energy (between 60-100 percent of the total) [Angelopoulos et al., 1993]. These mesoscale flows can be recognized in the ionosphere as auroral streamers, flows occuring at the substorm onset and in subauroral regions, among others. The main focus of this thesis is to analyze the mesoscale flow channels associated with these auroral signatures.

1.2 Ionospheric signature of bursty bulk flows

Bursts of earthward flows in the plasma sheet are fundamental to plasma transport in the magnetotail. Satellites in the plasma sheet frequently detect high-speed flows or bursty bulk flows (BBF) with a predominantly earthward propagation [e.g., Angelopoulos et al., 1992, 1994; Baumjohann et al., 1993]. Plasma sheet flow bursts have small cross-tail scale, ~2-3 R_E [Sergeev et al., 1990; Angelopoulos et al., 1996, 1997, Kauristie et al. 2000; Sergeev et al., 2000; Nakamura et al., 2001, 2004]; however, these narrow plasma streams are capable of carrying magnetic flux at a rate comparable to that of large-scale magnetic flux circulation in the magnetosphere [Angelopoulos et al., 1994]. Using three-dimensional MHD simulations, Birn et al. [2004] investigated the dynamics of the magnetotail flux tubes with reduced entropy to address properties of the earthward motion of BBFs. They showed that earthward transport of depleted flux tubes leads to a BBF channel surrounded by Region-1 sense field-aligned currents (FACs), downward field-aligned current on the dawn side and upward FAC on the dusk side. Similar relations between BBFs and field-aligned currents have been obtained by the Rice Convection Model as well [Yang et al., 2011, 2012].

While in-situ measurements can only detect these mesoscale transient phenomena at a limited number of points or characterize them statistically, measuring flows and aurora in the ionosphere allows us to evaluate their instantaneous two-dimensional evolution. It is known that the poleward boundary intensifications (PBIs) and their equatorward extension, auroral streamers, are the ionospheric signature of longitudinally localized earthward flow bursts in the plasma sheet [Henderson et al., 1998; Sergeev et al., 1999, 2000; Lyons et al., 1999, 2002; Kauristie et al., 2000; Zesta et al., 2000; Zou et al., 2010; Zou et al., 2013]. Those studies also found that the flows related to the streamers mapped to the east of the streamers, consistent with the relationship between the aurora and upward FACs on the duskside of the flow [Amm et al., 1999; Nakamura et al., 2001; Birn et al., 2004].

In contrast to the large number of studies of plasma sheet fast flows and conjugate auroral intensifications, localized, transient ionospheric flows in the auroral zone have not received much attention. The DMSP satellites have been used to identify the spatial relationship between equatorward flow channels and auroral streamers [Sergeev et al., 2004]. Recently, Shi et al. [2012] investigated the 2-D pattern of ionospheric flows and auroral streamers using SuperDARN and the Wideband Imaging Camera (WIC) on board of the IMAGE satellite to measure flows and streamers, respectively. They showed that equatorward flow enhancements formed within and to the east of steamers. Their methodology provided an excellent view of the relationship between ionospheric flows and auroral streamers on large-scales, but the low spatial resolution of space-based imaging was a limiting factor. For a full understanding of the link between auroral streamers and flow structures in the ionosphere, higher resolution measurements are required. Pitkanen et al. [2011] used the Kevo all-sky imager and EISCAT VHF radar to identify auroral streamers and flow patterns in the ionosphere, respectively. The authors also reported a good correlation between auroral streamers and flow enhancements in the ionosphere, and suggested that the equatorward flow enhancements are located to the east of the streamer. However, their radar observations were limited to a single line of sight, and the ionospheric backscatters were obtained outside the imager field of view, requiring spatial extrapolation of both radar and auroral observations.

In chapter 2 we present a detailed study of the association between auroral streamers and flow enhancements in the ionosphere using the THEMIS ASIs and Super Dual Auroral Radar Network (SuperDARN) radars that measure flows within the THEMIS ASI field of view. Radar echoes captured close to the radars (~500 km) were mainly used to detect small-scale flow structures that could be missed or would otherwise be poorly resolved in long-range radar echoes. We examined 135 isolated auroral streamers from December 2007 to December 2010 and identified flow patterns and their association with auroral streamers. We show that the equatorward and westward motion of the auroral streamers is well correlated with the flow enhancements. Finally we provide evidence supporting the results obtained in the MHD simulations of Birn et al. [2004] relative to the flow vortex associated with field-aligned current formation.

1.3 Substorms

Substorms are dramatic disturbances of the global magnetosphere-ionosphere system during which solar wind energy stored in the magnetotail is released (Rostoker et al., 1980). In the ionosphere, substorm onset can be identified as an explosive brightening of a quiet auroral arc near the auroral equatorward boundary that subsequently expands both poleward and azimuthally [Akasofu, 1964]. The following section explains the full observational development of the substorm onset.

1.3.1 Auroral signatures of substorms

The development of the auroral substorm was first described by Akasofu [1964] by using several all-sky-imagers (ASIs). In his description, during a disturbed period it was possible to observed 4 or more substorm over a period of 12 hours. In his paper, Akasofu described two of the three substorm stages that we know, the expansion and the recovery phase. In the expansion phase he described the intensification and poleward expansion of a pre-existing east-west aligned auroral arc. During the recovery phase the luminosity of the aurora decreases. Figure 1.4 shows the auroral substorm described by Akasofu [1964].

In the magnetotail, the classical understanding of a substorm includes three stages: initially the solar wind energy is stored in the tail during the growth phase under southward IMF. This energy is subsequently released during the expansion phase after the onset, and then the magnetosphere returns to its quiet state during the recovery phase [Rostoker et al., 1980]. The different phases of the substorm described above are associated with characteristic changes in the auroral morphology, such as poleward and equatorward expansion of auroral activity following the initial brightening along a preexisting arc during the expansion phase.

1.3.2 Physics of the substorm auroral onset

A long standing question in magnetosphere-ionosphere coupling system is the process responsible for substorm onset. In the aurora, the substorm onset is identified by an explosive brightening of a quiet auroral arc near the auroral equatorward boundary that subsequently expands both poleward and azimuthally [Akasofu, 1964]. While there has been intense debate on the pre-onset event sequence [e.g., Angelopoulos et al. 2008; Lui et al., 2009], the THEMIS spacecraft observations have shown that the onset is preceded by magnetotail reconnection [Angelopoulos et al. 2008; Lin et al., 2009]. The sequence of events leading to substorm onset can generally be visualized in the ionosphere as auroral disturbances along the auroral poleward boundary, referred to as PBIs [Lyons et al., 2002], followed by an auroral streamer moving equatorward towards the onset latitude, roughly following the preexisting flow pattern around the Harang flow shear of the duskside convection cell, though occasionally turning eastward within the dawnside convection cell. Then a substorm auroral onset occurs when the streamer reaches near the onset location [Oguti, 1973; Nishimura et al., 2010]. Figure 1.5 from Nishimura et al. [2010], illustrates the sequence of events described above. Streamer coupling to the inner magnetosphere has also been reported by Henderson et al. [2002], who found coupling of dawn cell streamers to dawnside auroral omega bands.

In the magnetosphere, a possible explanation for this process can be described as transport of low-entropy plasma from the open-closed field line boundary toward the near-Earth plasma sheet along an azimuthally narrow flow channel [Sergeev et al., 2000]. Coordinated observations using radars and ASIs have shown mesoscale flows that move from the polar cap to the auroral oval give rise to PBIs, and have given a suggestion that mesoscale flows coming from deep within the polar cap may contribute to the triggering of earthward propagating flows that subsequently lead to substorm auroral onset [Lyons et al. 2011; Zou et al., 2014]. This indicates that localized enhanced reconnection and low entropy flow channels that lead to onset within the inner plasma sheet may originate from the mesoscale, polar-cap flows impinging on the polar cap boundary

At the substorm auroral onset, the initial brightening along a preexisting or a newly formed arc is often observed in the form of a wavy auroral pattern [Elphinstone et al., 1995; Voronkov et al., 1999, 2000], which is referred to as auroral beads [Donovan et al., 2006; Liang et al., 2008; Sakaguchi et al. 2009]. The beads then grow, first as periodic waves along the arc and then showing more dynamic and nonlinear evolution. Figure 1.6 from Sakaguchi et al. [2009] shows the temporal evolution of the auroral beads for an event occurring on January 15, 2008. In this case, auroral brightening appeared along the poleward boundary of a diffuse auroral arc and then developed westward. The wavy auroral forms have characteristic wavelength of ~10-100 km and azimuthal propagation speed of roughly 5 km/s. Recently, Motoba et al. [2012] showed simultaneous beading observations in the northern and southern hemispheres suggesting the existence of a common driver in the magnetotail equatorial region that controls the major temporal evolution of the beads. Thus, the bead structure has been considered as the auroral manifestation of an instability that occurs in the near-Earth plasma sheet. Figure 1.7 shows Motoba's simultaneous observations in the northern and southern hemisphere.

To understand the instability that leads to auroral beading at substorm onset, it is important to understand the flow pattern and field-aligned current (FAC) structure associated with the beads. Radars can measure the ionospheric flow structure, and thus can be used to infer important information on the plasma sheet flow patterns associated with the beading during the onset process. Voronkov et al. [1999] found vortical auroral structures along the preexisting arc with temporal evolution comparable to that of the observed ionospheric currents at the onset. However, the temporal and spatial resolution provided by the instruments used in their study was not able to resolve the small-scale structures in the plasma flow. More recently, Hosokawa et al. [2013] studied an event in which strong flows measured by the Pykkvibaer (pyk) Super Dual Auroral Radar Network (SuperDARN) were associated with auroral beading; however, the sparse echoes measured by the radar at the time of the beading do not provide enough information to resolve the flow pattern surrounding the beads. In addition, in their study it was not possible to determine the orientation of the flows relative to the arc due to the oblique orientation of the radar beam.

Chapter 4 of this thesis is dedicated to determining the ionospheric flow pattern associated with substorm auroral onset beads using ASIs and SuperDARN radars, which occasionally are operated in high-time resolution. Different orientations of the radar beams relative to the onset arc for different events allow us to distinguish between north-south and east-west flows. We have found a remarkable correlation of the substorm auroral onset beads with oscillating, extremely fast flows that are more intense in the north-south direction. We inferred a clockwise flow shear around the beads, indicating that an upward field aligned current in the center of the shear gives rise to the individual beading structures.

1.4 Subauroral polarization streams

Another important manifestation of plasma transport in the duskside ionosphere is Subauroral Polarization Streams or SAPS, which are strong westward flows lying just equatorward of the electron auroral oval and thus of enhanced ionospheric conductivities of the auroral oval. This phenomenon was first observed with satellite data [Galperin et al., 1973; Spiro et al., 1979] and then through incoherent scatter radar data [Yeh et al., 1991]. Several terms have been used to describe this phenomenon, such as polarization jets [Galperin, 2002] or subauroral ion drift (SAID) [Anderson et al., 1991]. Foster and Burke [2002] used the term subauroral polarization stream (SAPS) to include both phenomena.

Magnetosphere-Ionosphere (MI) coupling processes have been recognized as important drivers of SAPS. A quasi-steady picture of SAPS flows is now well understood; Anderson et al. [1993] proposed a production mechanism for SAPS flows as an establishment of poleward subauroral electric field through closure of region-2 field-aligned currents (R2 FACs) in the low-conductivity subauroral ionosphere. In the pre-midnight region, R2 FACs flow into the ionosphere at lower latitudes (downward FAC) and towards the magnetosphere at higher latitudes (upward FAC). To keep ionospheric current continuity, these FACs close through a poleward directed Pedersen current, which is associated with a poleward directed electric field, which gives westward drifts and reduction of the electron density (also known as the plasma trough).

Traditionally, SAPS intensifications have been associated with substorm onset. Using DE-2 satellite data, Anderson et al. [1993] reported that SAPS intensified soon after substorm onset and were observed extending well equatorward of the auroral oval. The connection between SAPS intensification and substorm onset has been supported by several other studies [e.g., Anderson et al., 1993, 2001; Erickson et al., 2002; Galperin, 2002; Mishin et al., 2002, 2003, 2004; Foster et al., 2004; Mishin and Burke, 2005]. While SAPS are known to intensify due to substorm injections [Makarevich and Dyson, 2007, Nishimura et al., 2008, Zou et al. 2009] and are usually associated with periods of disturbed geomagnetic conditions, Clausen et al [2012] showed that the maximum westward SAPS velocity is considerably variable and that this large variability is generally not correlated with geomagnetic indices.

Recently, Makarevich et al. [2011] used IMAGE FUV and radar data to present a case study in which a large enhancement of SAPS flows was suggested to occur in association with an auroral streamer. Similar results were found by Lyons et al. [2015]. Auroral streamers are roughly north-south aligned arcs that extend from the auroral poleward boundary, and are commonly recognized as the auroral signature of longitudinally localized earthward flow bursts in the plasma sheet [Henderson et al., 1998; Sergeev et al., 1999, 2000; Lyons et al., 1999, 2002; Kauristie et al., 2000; Zesta et al., 2000; Zou et al., 2010]

If the connection between auroral streamers and SAPS intensification is common, it would imply that transient fast earthward plasma sheet flows are an important driver of westward SAPS flow enhancements, and that such enhancements would far more commonly contribute to

SAPS because streamers occur under various geomagnetic conditions much more frequently than substorms. However, the Makarevich et al. [2011] and Lyons et al. [2015] studies were limited to single cases and by the spatial and temporal resolution of global imaging.

In this study we investigated systematically the association between SAPS flow enhancements and auroral streamers by using the THEMIS all-sky imagers (ASIs) and the SuperDARN radars that share fields-of-view (FOVs) with the ASIs. We examined data from December 2007 to April 2013. We also used the Defense Meteorological Satellite program (DMSP) satellite and Meridian Scanning Photometer (MSP) data to assist in the identification of the auroral equatorward boundary. Results of our study reveal that the association between SAPS flow enhancements and auroral streamers is common. We also characterized properties of SAPS flow enhancements and related streamers.

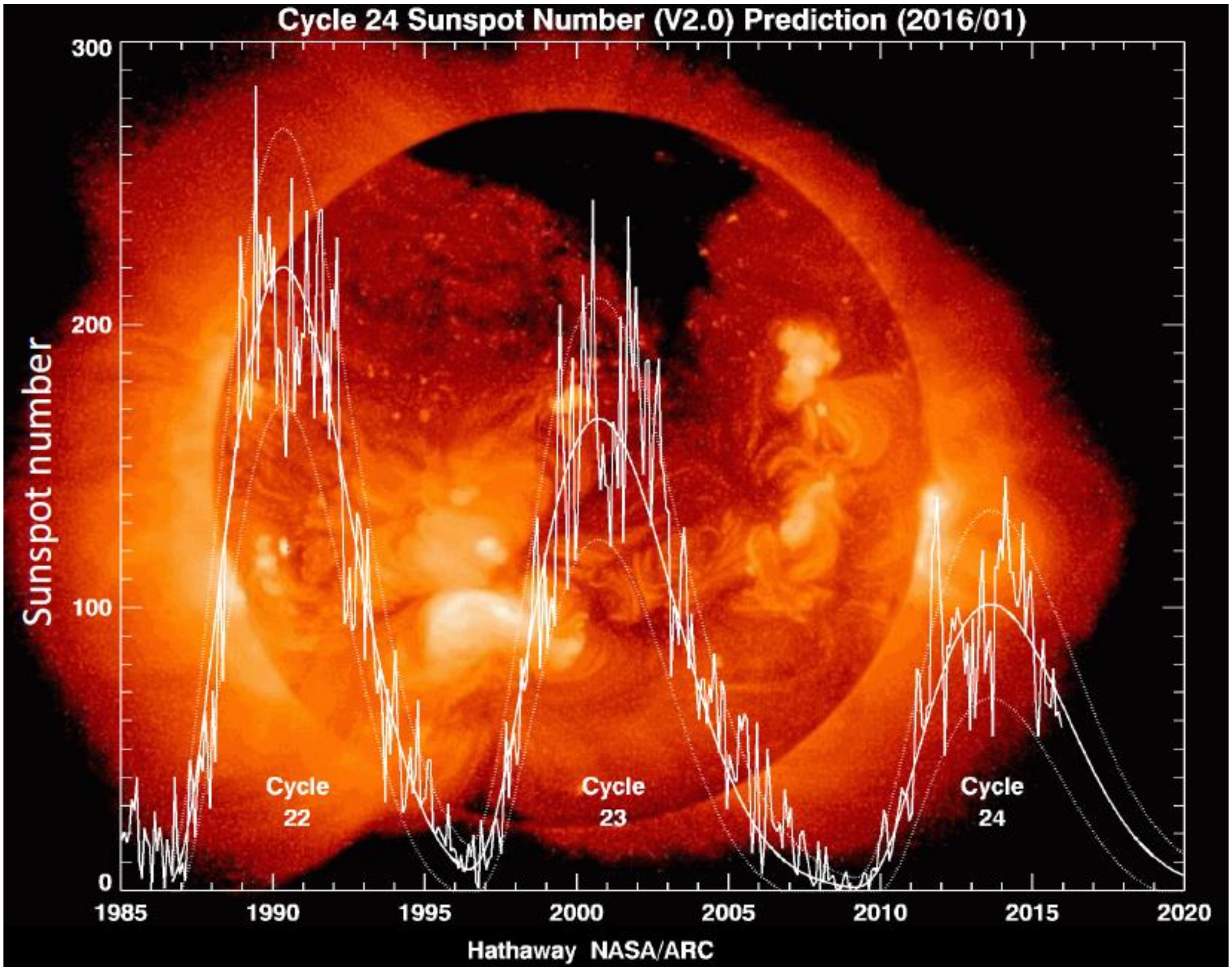

Figure 1.1. Solar cycle evolution.

(source: http://solarscience.msfc.nasa.gov/images/Cycle22Cycle23Cycle24big.gif)

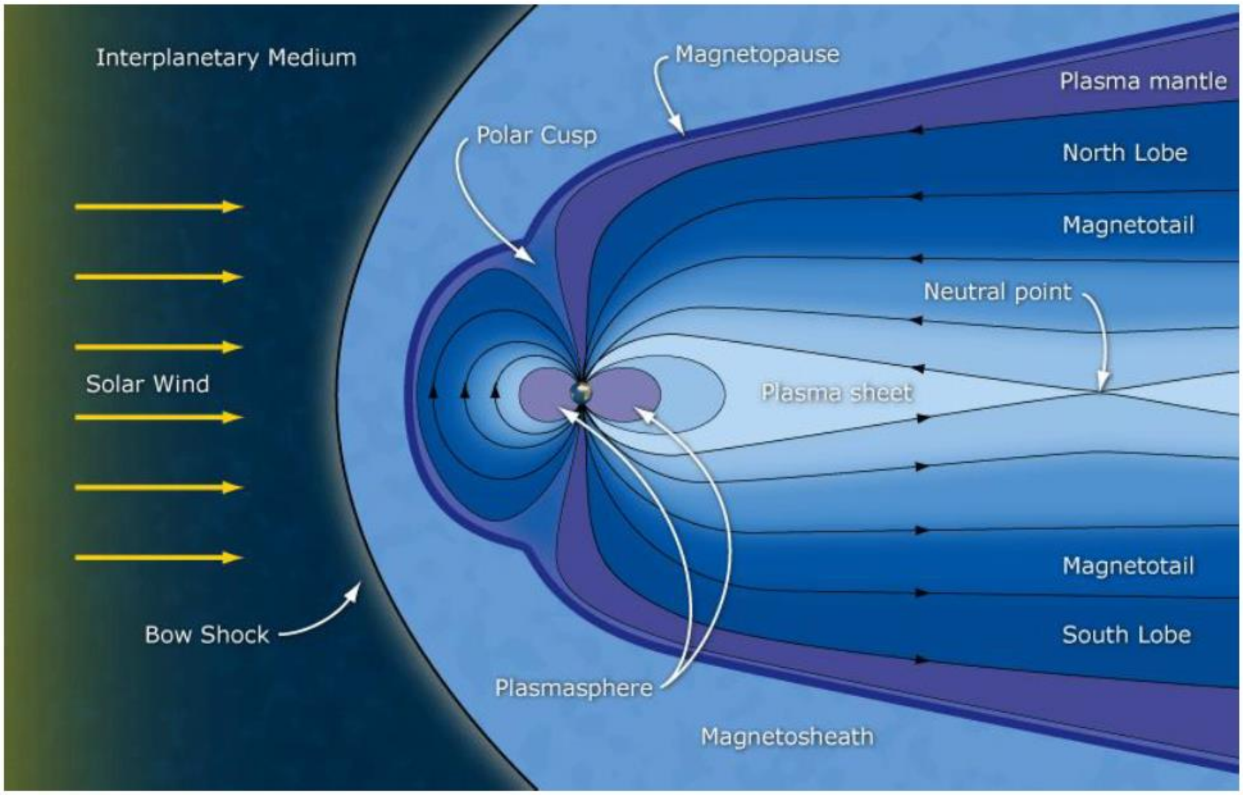

Figure 1.2. Principal regions of the Earth's magnetosphere

(source: http://www.nasa.gov/images/content/517890main_Earth-Magnetosphere.jpg)

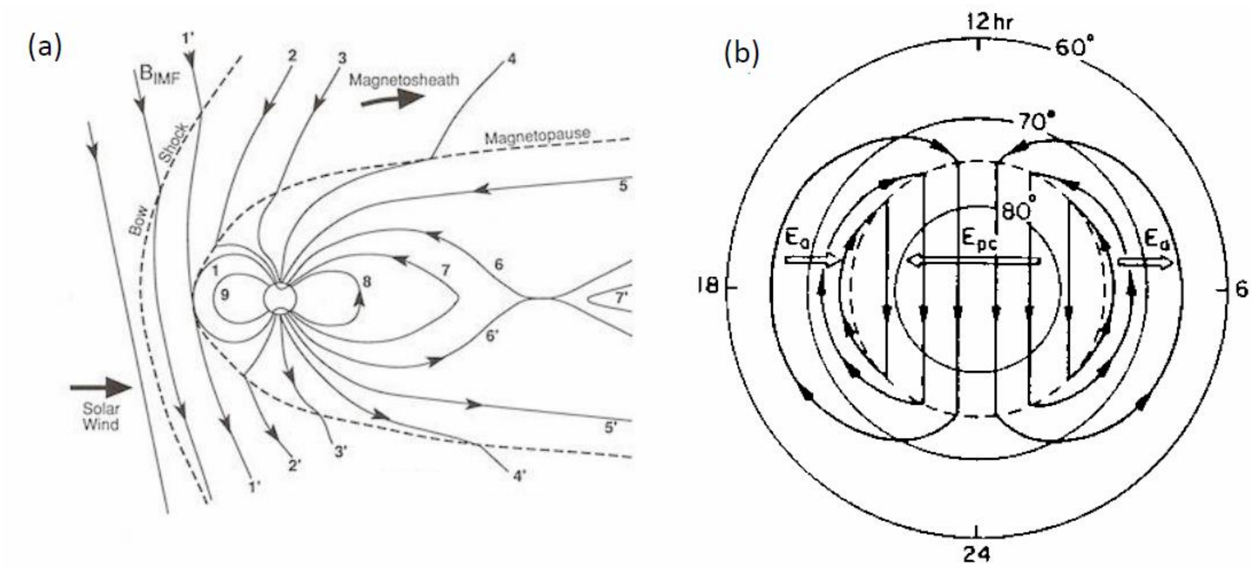

Figure 1.3. Dungey's cycle in the (a) magnetosphere and (b) ionosphere

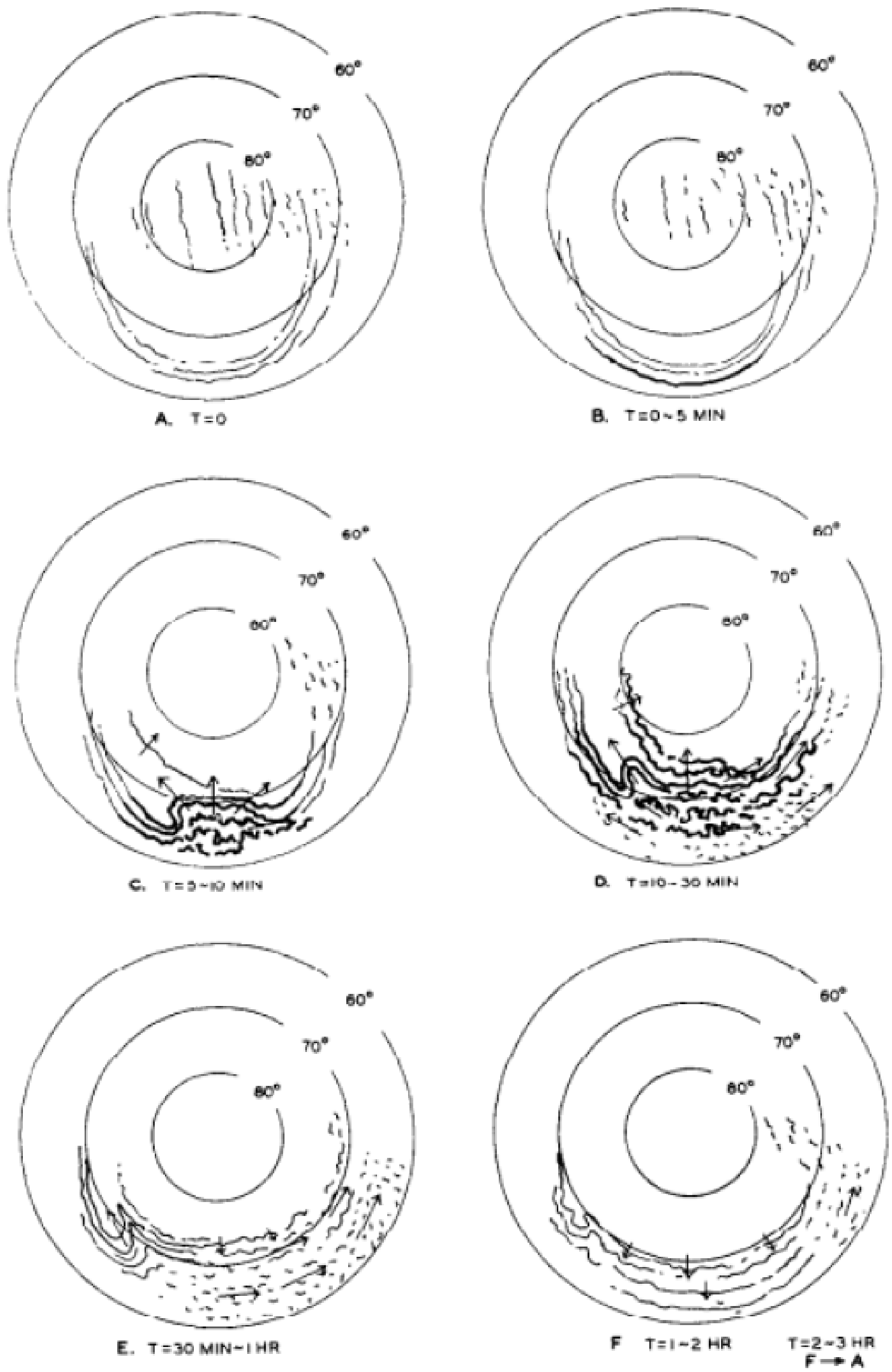

Figure 1.4. Substorm evolution described by Akasofu [1964]

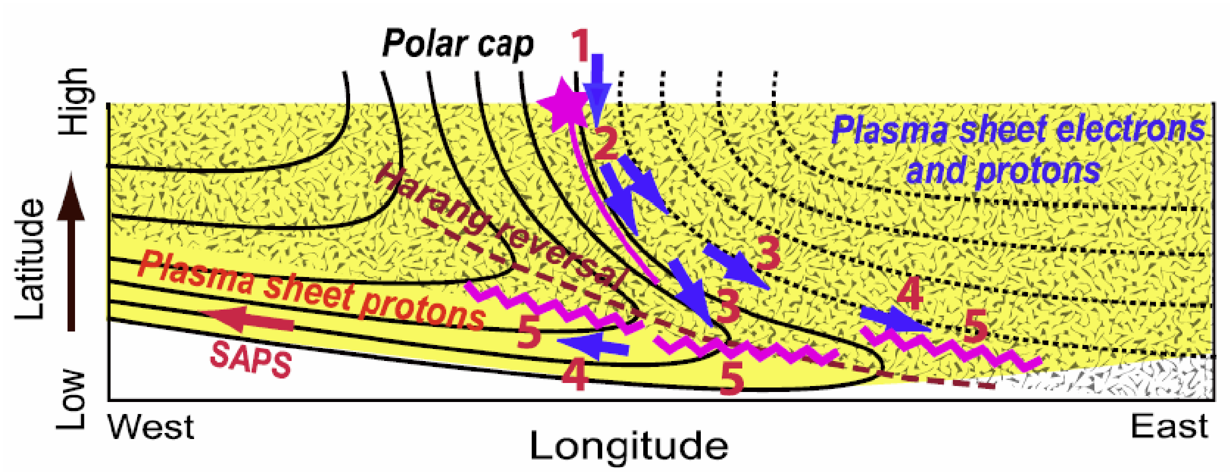

Figure 1.5. Schematic illustration of pre-onset auroral evolution and its relationship with nightside ionospheric convection. From Nishimura et al. [2010].

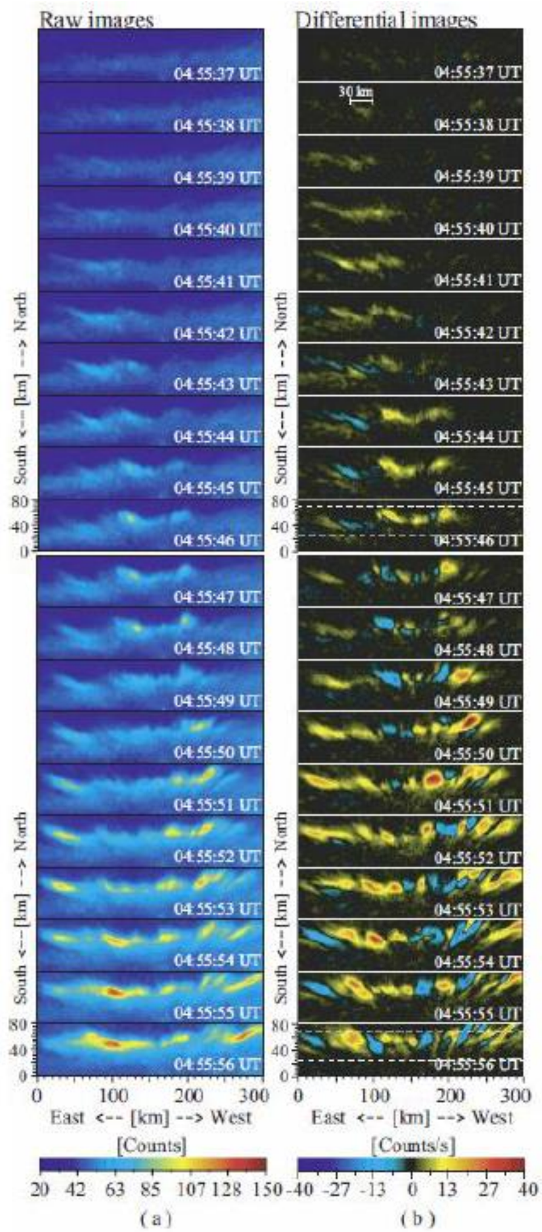

Figure 1.6. Time series evolution of auroral beading at the substorm auroral onset occurring at Gillam on January 15, 2008. (a) Left column consists of averaged images over 0.1 s in false color. (b) Right column consists of differential images, showing increase

(yellow-red) and decrease (blue) of auroral intensity during 1 s. From Sakaguchi et al., [2009]

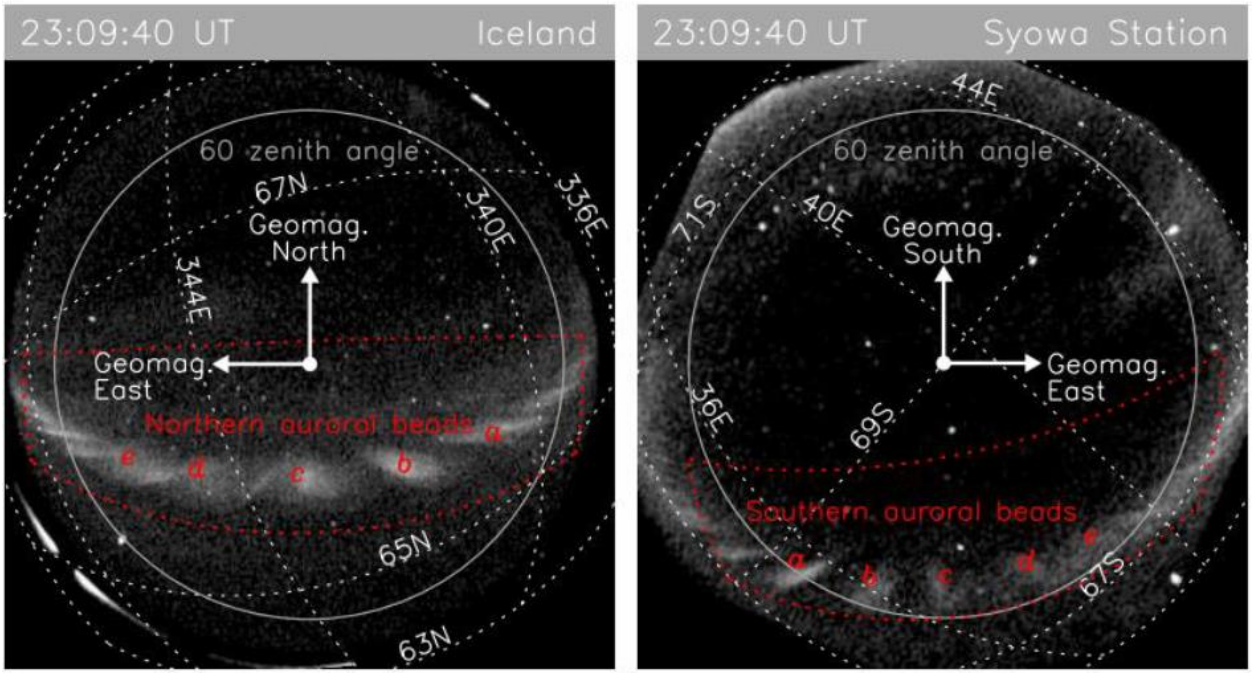

Figure 1.7. Simultaneous observations of auroral beads at the substorm auroral. Left (right) panel represents observations in the northern (southern) hemisphere. From Motoba et al., [2012].

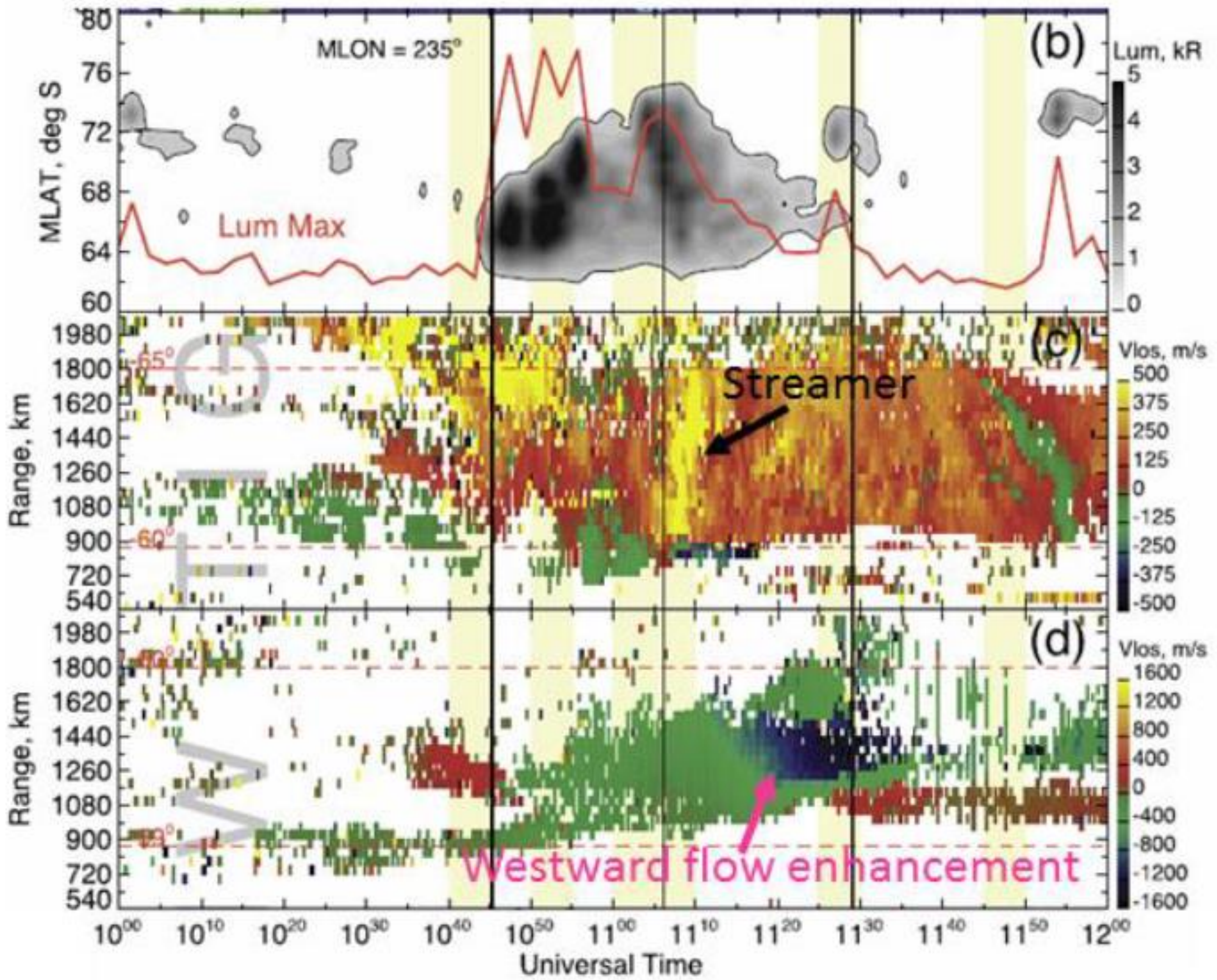

Figure 1.8. Example of an event showing association between an auroral streamer and SAPS intensification. (b) Keogram along the magnetic meridian of 235°. The red thick line indicates the maximum luminosity at 235°. (c) l-o-s velocity measured by the TIGER Bruny Island beam 4 and (d) the TIGER Unwin (UNW) beam 0. From Makarevich et al. [2011].

CHAPTER 2

Coordinated SuperDARN-THEMIS ASI observations of mesoscale flow bursts associated with auroral streamers

Nightside auroral zone localized flow channels, typically associated with auroral poleward boundary intensifications and streamers, are an important component of the high-latitude ionospheric plasma. Here we present a detailed study of the association between auroral streamers and flow enhancements in the ionosphere using the Time History of Events and Macroscale Interactions during Substorms (THEMIS) all-sky imagers (ASIs) and Super Dual Auroral Radar Network (SuperDARN) radars that measure flows within the THEMIS ASI field of view

2.1 Data set and methodology

We use the THEMIS ASIs [Mende et al., 2008] to identify auroral streamers. The ASIs are white light charge- coupled device imagers, where each imager has a latitudinal coverage of ~9° and a longitudinal coverage of slightly more than 1 h in magnetic local time (MLT) with time resolution of 3 s The SuperDARN radars were used to measure ionospheric flows. SuperDARN is a chain of high- frequency coherent scatter radars that measure the ionospheric E and F region flow velocity in the line-of-sight (l-o-s) direction with temporal resolution of 1 or 2min [Greenwald et al., 1995]. The SuperDARN radars scan through 16 beams (from east to west) of azimuthal separation of ~3°, where each beam is divided into ~100 (variable be- tween radars) range gates. The radars used here are in Rankin Inlet (rkn), Inuvik (inv), Saskatoon (sas), Prince George (pgr), and Kapuskasing (kap), where their field of views (FOVs) are directed roughly poleward in the auroral zone and overlap with the FOVs of the Rankin Inlet, Gillam, Fort Smith, Forth Simpson, and Athabasca THEMIS ASIs. Since short-range radar echoes are generally E region echoes, where, because of collisions, the Doppler speed magnitude is not the full electric field drift, we do not compare the flow speed and auroral propagation speed but focus on flow structure, although we calculate average flow speeds. Even though the echoes are mainly due to E region backscatters, and thus, the magnitude of their Doppler speeds may be underestimated and limited below the ion acoustic speed (~400 m/s) [Haldoupis, 1989; Koustov et al., 2005], this does not influence our results because we do not discuss the exact flow magnitude, but rather focus on relative flow changes.

We examined THEMIS ASI data during fall and winter months (October to April) from mid-2007 to 2010. Auroral streamers are defined as roughly north-south-aligned arcs that originate from or near the poleward boundary of the auroral oval and propagate equatorward [Zesta et al., 2002]. While some streamers are highly tilted to the east or west depending of the convection pattern [Zesta et al., 2006; Zou et al., 2009, 2010], we only selected streamers oriented roughly parallel to the radar l-o-s directions so that flows tangential to streamers can be measured by the radars. Tangential flows are generally stronger than normal flows for stable arcs [Aikio et al., 2002], and such a pattern is also expected for auroral streamers since converging Pederson currents are believed to drive both stable arcs and streamers. In order to obtain flows associated with streamers, streamers should be measured within or adjacent to available radar echoes. We require that streamers are roughly parallel to the radar l-o-s direction and this frequently occurs within ±3 h of MLT around magnetic midnight, with maximum intensities higher than 3000 count/s. The longitudinal extension of the streamers should be fully covered within the avail- able ASI FOVs. We further required that streamers are isolated, i.e., that there be no other streamer within the FOV of the observing radar at the same time. Fast flows should be more than 200 m/s to be easily identifiable. We found 135 isolated streamers that satisfied the criteria above. Most of these, 90%(121 events) showed equatorward flow enhancements associated with the streamers, 10% (11 events) showed poleward flows, and 3% (4 events) showed both equatorward and poleward flows. Figure 2.1 shows the MLT distribution of these equatorward (Figure 2.1a) and poleward (Figure 2.1b) flow events. On average, streamers with equatorward flows were more frequently identified before magnetic midnight, and streamers with poleward flows appeared to be more frequently observed around magnetic midnight. It is interesting to notice that there are no streamer events after 2 MLT in this study, and also, there are no streamers associated with poleward flows before 23 MLT. The number of poleward flow events at each MLT is less than one third of that of equatorward flows, and we do not reach a conclusion about the relatively higher occurrence of poleward flows at post-midnight. The lack of streamers before 21 MLT and after 2 MLT is probably because we focus on streamers nearly parallel to the radar l-o-s direction, which is roughly in the north-south direction. When considering the large-scale two-cell-flow pattern, equatorward flows near midnight turn azimuthally and propagate sunward as they propagate away from midnight. Such azimuthally oriented flows and streamers are not included in our study.

2.2 Results

In this study we examined 135 isolated auroral streamers from December 2007 to December 2010 and identified flow patterns and their association with auroral streamers. The first part of the result sections is dedicated to the case study with the most representative cases. In the second part of this section we discuss the statistical study results.

2.2.1 Case study: Representative Cases

In this section, we analyze in detail four events that illustrate the relationship between streamers and flow channels. [10] Figure 2.2 shows a streamer moving equatorward within the Rankin Inlet radar FOV on 14 January 2008. The black- white images were obtained using the THEMIS ASI and the colored rectangles correspond to the l-o-s velocity measured by the SuperDARN radar, which is located near the center of the imager FOV. Warmer colors correspond to l-o-s flows toward the radar (roughly equatorward) and colder colors are flows away from the radar (poleward). Figure 2.2a shows a snapshot before the poleward motion of an arc along the auroral poleward boundary. The l-o-s velocities were small except for a moderate flow near the western edge of the radar FOV. The western portion of the poleward boundary arc moved poleward in Figures 2.2b–2.2d. Figure 2.2b shows that enhanced equatorward and poleward flow developed poleward of the arc, which could be related to the channels of enhanced polar cap flows recently reported by Zou et al. [2013]. Then, a streamer (>5000 c/s in intensity) originated from the eastern side of the poleward moving arc and propagated into the radar FOV (Figures 2.2c and 2.2d). Associated with this auroral streamer, an equatorward flow enhancement of ~300m/s was observed just to the east of the auroral streamer. The streamer propagated further equator- ward roughly aligned with the radar l-o-s direction, and the enhanced equatorward flow also extended equatorward (Figures 2.2e–2.2g). Also, a poleward flow enhancement was detected to the east of the equatorward flow (Figure 2.2e) and further enhanced in Figures 2.2f and 2.2g.

In Figure 2.3, we present another event showing the association between the flow pattern and an auroral streamer. Figure 2.3a shows a flow and auroral structure that lasted for 4min before the streamer of interest. Preceding this, slowly drifting streamers were detected, and flows were weak except for a moderate flow near the western edge of the radar FOV. Figure 2.3b at 0718UT marks the initiation of the streamer in the northwestern portion of the radar FOV and of an equator- ward flow enhancement. While the enhanced flow appears to extend deeper equatorward than the streamer, this is likely due to the limited time resolution of the radar (2 min), and the streamer did extend down to ~73° MLAT in the next minute (Figure 2.3c). The streamer propagated further equatorward almost parallel to the radar l-o-s direction in Figures 2.3d–2.3f and the equatorward flow remained enhanced. Another streamer formed in the northwestern portion of the radar FOV at 0723UT (Figure 2.3e) and propagated equatorward along the same path. During the propagation of this second streamer, the enhanced equatorward flows extended significantly (~0.2– 0.5h in MLT) to the east of the streamer and were aligned with the streamer. In addition, at 0723–0724UT, the radar measured a poleward flow enhancement further to the east of the radar FOV. In both examples shown above, the existence of an equatorward flow just to the east of a streamer is consistent with an upward FAC on the western edge of a plasma sheet BBF [e.g., Birn et al., 2004]. The poleward ionospheric flows on the eastern side of the equatorward ionospheric flows would correspond to tailward plasma sheet flows as part of flow vortices. The resultant counterclockwise ionospheric flow vortex is an indication of a downward FAC sheet, the counterpart of the upward FAC flowing on the streamer field lines. Thus, the combination of auroral imaging and ionospheric flow observations allows us to infer the 2-D structure of the FAC pair and related flows

The streamer in Figure 2.4 shows a westward drift in addition to its equatorward propagation. As tracked by the white arrows, the streamer was initially located to the east of the radar FOV and then reached near the center of the radar FOV. The azimuthal motion of this long-lasting streamer allows us to scan the 2-D distribution of the l-o-s flow as it drifted across the radar FOV. In Figure 2.4a, a very strong poleward flow was measured in the middle of the radar FOV to the west of the streamer. As the streamer moved westward in Figures 2.4b–2.4f, the poleward flow region also moved in the same way and an equatorward flow appeared near the eastern edge of the radar FOV. The streamer marks the boundary between the poleward and equatorward flows, consistent with an upward FAC sheet at the clockwise flow shear. The streamer intensified, and the intensification rapidly propagated equatorward from Figure 2.4e to Figure 2.4i, and the equatorward flow intensified and also moved equatorward with the streamer.

In limited occasions, when the streamers extend through the FOVs of the two consecutive radars with sufficient echoes, it is possible to observe the flow enhancements associated with streamers in both radars at the same time. Figure 2.5 shows one example of a latitudinally long streamer starting in the Rankin Inlet FOV and reaching the poleward region of the Saskatoon radar FOV. In Figure 2.5a, a streamer started to intensify near the center of the ASI image and fast flows toward the radar were observed by the Saskatoon (sas) radar. Another streamer was present to the east of it and was gradually fading. This streamer was oriented perpendicular to the radar l-o-s direction and thus would not affect the measured flows. The streamer near the center of the imager FOV further intensified and extended equatorward and westward (Figures 2.5b and 2.5c), and a fast equatorward flow channel was then observed in both the Rankin Inlet and the Saskatoon radar FOVs just to the east of the streamer. This event demonstrates that enhanced flow channels are not limited to the latitudinal extent of the radar FOV but can extend over wide latitude ranges (~10° in this case) adjacent to the streamers.

2.2.2 Statistical Study

Using all 135 streamer-flow conjunction events, we examine if the flow structure obtained in the above cases is common. To accomplish this, we calculate the azimuthal width and offset of the equatorward and poleward flow enhancements relative to that of the auroral streamers and the average values of the maximum intensity of the auroral streamer and the average flow speed.

Six longitudinal cuts along the radar FOV were made every two or three range gates (depending on the echo avail- ability) to determine the azimuthal width and location of enhanced flows. An example for one of the events is shown in Figure 2.6 (left). The auroral intensity and flow velocity along each slice are shown on the first and second columns. At the time of the flow channel width measurements, echoes were available at ≥70% of the radar measurement locations within the overlapping portion of the radar and ASI FOVs. In addition, the flow channel width was calculated when the edges of the channel were more than one beam width away from the eastern and western edges of the radar FOV. For this time, we fit a Gaussian curve around the maximum flow velocity to calculate the full width at half of the maximum(FWHM) for each cut and then we calculate the width as the average FWHM over the cuts. We also calculate the azimuthal shift of the location of the maximum flow speed with respect to the location of the maximum intensity of the auroral streamer. In this example, the peak flow velocity is shifted to the east of the streamer by ~1° on average and the azimuthal width of the flow enhancement is ~100km (2.3°).

Figure 2.7 shows the azimuthal offset of the flow channels relative to the associated streamer. The x axis gives the flow speed. Negative (positive) flow speeds represent poleward (equatorward) motion. The y axis is the azimuthal offset of the maximum flow speed relative to the position of the associated auroral streamer's maximum intensity. Positive offsets correspond to flow channels to the east of their respective streamers. We see that all equatorward flow enhancements (positive flow speeds) are located to the east of their respective auroral streamer.

In contrast, poleward flow enhancements are mostly to the west of the auroral streamers, although a few do not follow this trend. For a few events (e.g., Figure 2.6), it was possible to observe an equatorward flow enhancement to the east of the streamer and a poleward flow to the west of the streamer within the same radar FOV, and both are included in Figure 2.7. This three-direction structure of flows (poleward-equatorward-poleward) is consistent with the plasma flow shears around a BBF channel [Birn et al., 2004]: The streamers coincide with the upward FAC sheet at the western edge of the equatorward flow channel, that is associated with a flow shear exhibiting a clockwise ionospheric flow vorticity (viewed from space). A downward FAC sheet is expected at the eastern edge of the equatorward flow channel, within a flow shear that exhibits a counter- clockwise flow vorticity. Note in Figure 2.7 that there are fewer points with poleward flows than with equatorward flows. While flows will be sometimes missed due to the limited size of the radar FOV, our criteria for event selection should not favor equatorward flows over poleward flows, or poleward flows to the west of streamers than those to the east. Based on the Birn et al. [2004] simulations, a reasonable explanation of the lower number of observations of poleward flow enhancement is that the poleward flows (tailward in the plasma sheet) do not extend as far in latitude as do the equatorward (earthward) flows (see Figure 18 in the work of Birn et al. [2004]). Such poleward flows are expected to be located at the equatorward portion of the auroral oval, which map to the near-Earth plasma sheet, where earthward flows deflect and form flow vortices. Since the Rankin Inlet radar is typically located at the high latitude portion of the auroral oval, many of the poleward flows would be located equatorward of the radar FOV. Also, it is particularly difficult to detect the poleward flows to the east of the equatorward flows, since those are quite far away from the streamers, and we require the streamers to be located within or adjacent to the radar FOV. However, based on a frequent occurrence of poleward flows to the west of the streamer, we consider that the pole- ward flows are commonly associated with the streamers and are a useful indicator of the FAC pair locations.

The first and second columns in Table 2.1 show the width and average flow speed for equatorward and poleward flow enhancements, and the third column shows the maximum intensity of the auroral streamer. We see that the azimuthal widths of the flow enhancements are essentially the same, 73 ± 24 km and 76 ± 29 km for the equatorward and poleward flow enhancements, respectively. The average flow speeds of poleward and equatorward flows are also about the same, as we can also see in Figure 2.7. We note that, while these flow channel widths are much narrower than the radar FOV width (207km at 75° MLAT), our short-range echoes are not able to capture wide flow channels as were analyzed by Shi et al. [2012]. Our data set focuses on mesoscale flow channels and streamers that are more frequently seen.

We also calculated the azimuthal shift as the difference between the positions of the maximum flow velocity with respect to the maximum intensity of the auroral streamer. The average azimuthal shift for both equatorward and poleward flow enhancements is about 58 km (Table 2.2). The four events for which it was possible to observe both equatorward and poleward flows within the radar FOV on either side of the streamer were also considered in this part of the analysis.

Based on the AL index during these streamer events, 53% of events occurred during the recovery phase of substorms (slow recovery of AL after a sharp intensification), while the rest 47% are observed during quiet times (AL>-100 nT). We do not have expansion phase events, although intense streamers are often seen during the expansion phase. This is because expansion phase streamers are so dynamic and frequent that it is difficult to find isolated streamers.

2.3 Discussion and conclusions

Taking advantage of the high-spatial and temporal resolution of the THEMIS ASIs and the high-spatial resolution of the short-range SuperDARN radar that overlap spatially with the ASI imagers, we investigated statistically the properties of ionospheric flows related to auroral streamers.

By selecting 135 isolated streamers roughly aligned with the radar l-o-s directions, we found that all streamers are correlated with fast flows around the streamers, and most of them were directed equatorward. The equatorward flows invariably lie just to the east of their respective streamer. While observed less frequently, we found evidence for two poleward flows to the east and west of the equatorward flow, giving a three-flow structure as illustrated in Figure 2.8. The western edge of the equatorward flow is collocated with the streamer, which highlights an upward FAC sheet. While the eastern edge of the equatorward flow does not have any auroral emission, it is likely the location of a downward FAC sheet that is a counterpart of the upward FAC. We calculated the azimuthal width of the equatorward and poleward flow enhancements obtaining an average of about 74km for both cases. We also calculated the azimuthal shift of the maximum flow speed relative to the maximum intensity of the streamer obtaining an average of 58km for both equatorward and poleward flow enhancements.

The flow structure we found is consistent with MHD simulations [Birn et al., 2004] and multi-satellite observations [Keiling et al., 2009] during BBFs in the plasma sheet. Our results suggest that ground-based observations are very useful for identifying the 2-D structure of localized flows and FACs that cannot be easily obtained by in situ observations in the plasma sheet.

We have mapped the flow channel widths for the case studies from the ionosphere to the magnetosphere using Tsyganenko 2001 as an external model and the International Geomagnetic Reference Field (IGRF) model for the Earth's magnetic field, and we obtained an average flow channel width of 1.5RE. Here the flow channel width is defined as the FWHM of the radar observations. However, there is a considerable amount of flow enhancement outside this range, and if we lower the flow magnitude threshold to 100m/s, the corresponding magnetospheric width increases to 2.6RE. Both numbers are roughly consistent with the result obtained by Nakamura et al. [2004] within the plasma sheet.

	Average Width (km)	Flow Speed (m/s)	Intensity (c/s)
Equatorward flow	73 ± 24	427 ± 171	5375 ± 1991
Poleward flow	76 ± 29	-453 ± 70	4075 ± 807

Table 2.1. First and Second Column Represent Average Width and Flow Speed Relative to the Flow Enhancement, and Third Column Shows the Auroral Streamer Maximum Intensity for Events Shown Equatorward and Poleward Flow Enhancements, Respectively.

	Azimuthal Shift (km)	% Total Events
Eastward shift	58 ± 13	90
Westward shift	56 ± 13	10

[a]Eastward (westward) shift correspond to maximum flows speed located to the east (west) of the streamer maximum intensity.

Table 2.2. Average Azimuthal Shift[a]

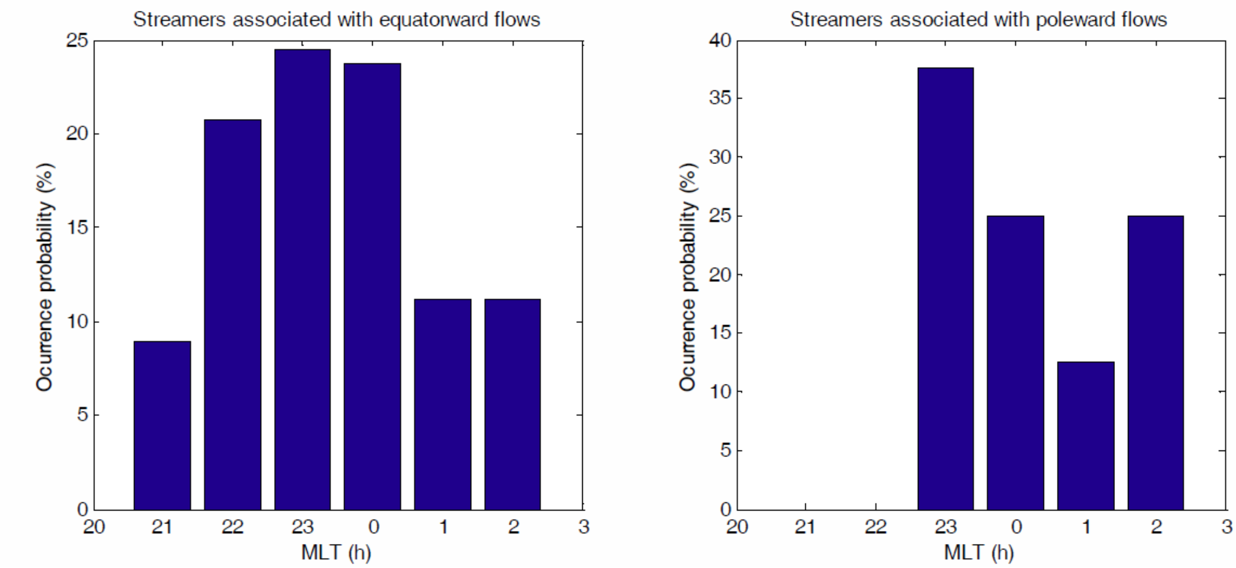

Figure 2.1. MLT distribution of the selected streamer events.

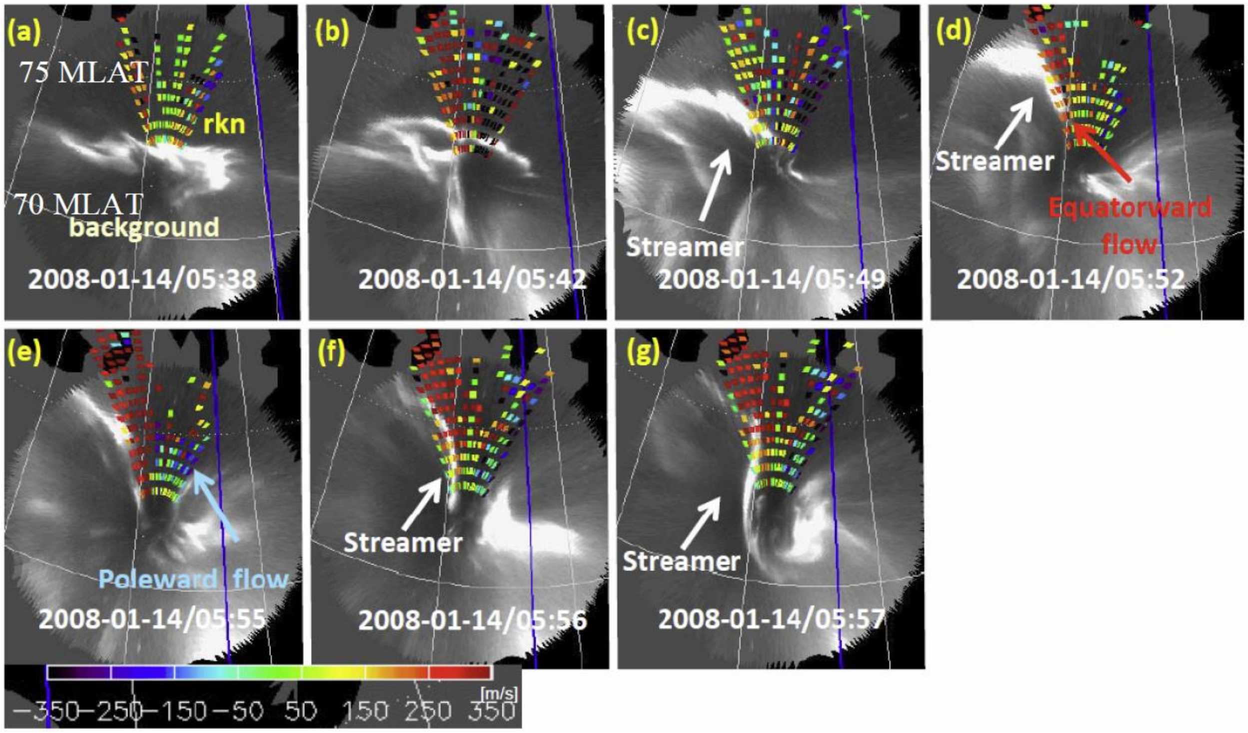

Figure 2.2. Equatorward motion of the auroral streamer and the ionospheric flow channel obtained using the THEMIS ASI and Rankin Inlet SuperDARN radar on 14 January 2008. (a) The background flows before the auroral streamer propagated into the radar FOV. (b–g) The sequence of flow and auroral streamers. The solid blue line indicates magnetic midnight. The white lines correspond to 75 and 70 MLAT contours, respectively.

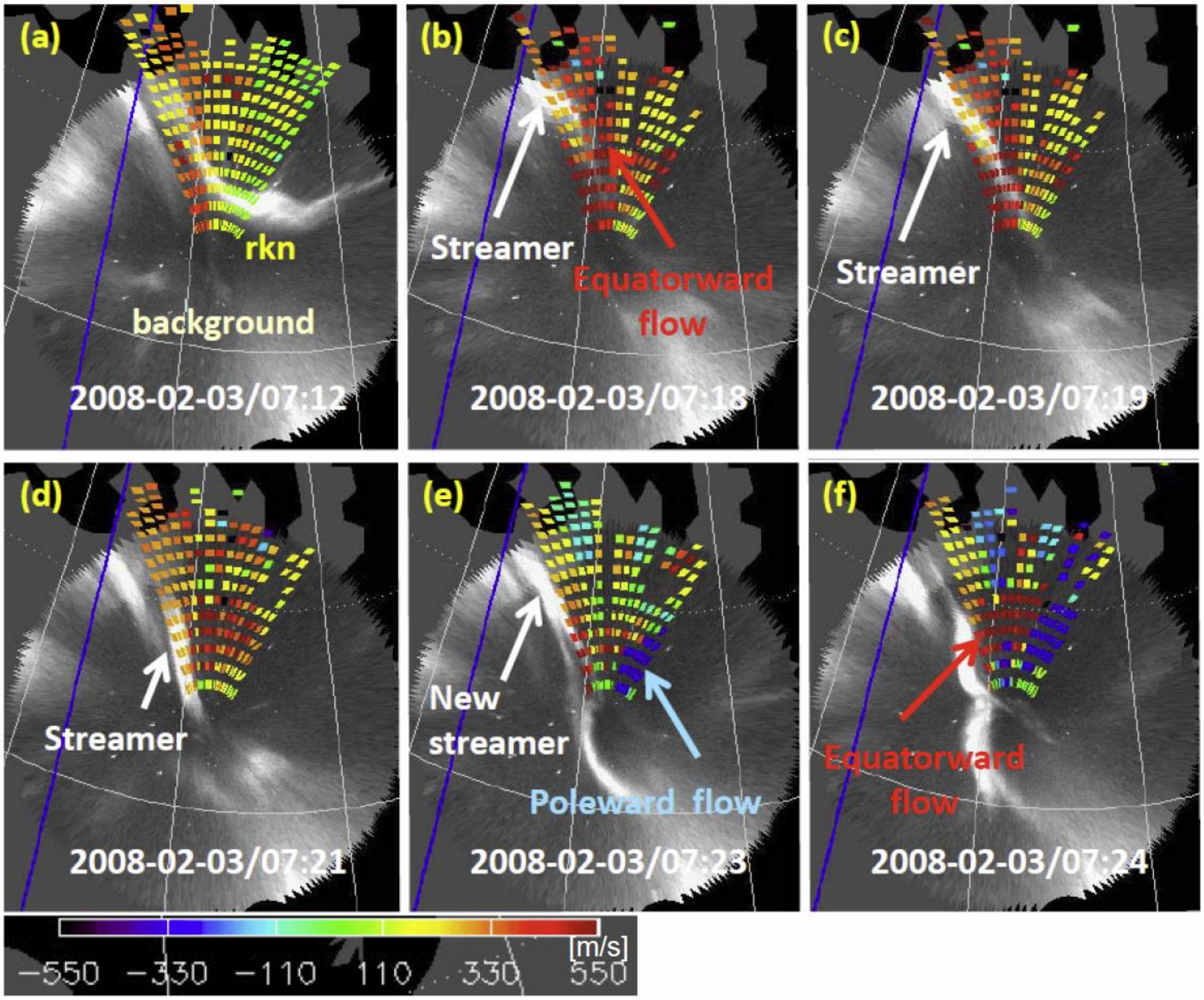

Figure 2.3. Panels represent the equatorward motion of the streamer and the related flow channel on 3 February 2008. The format is the same as in Figure 2.2.

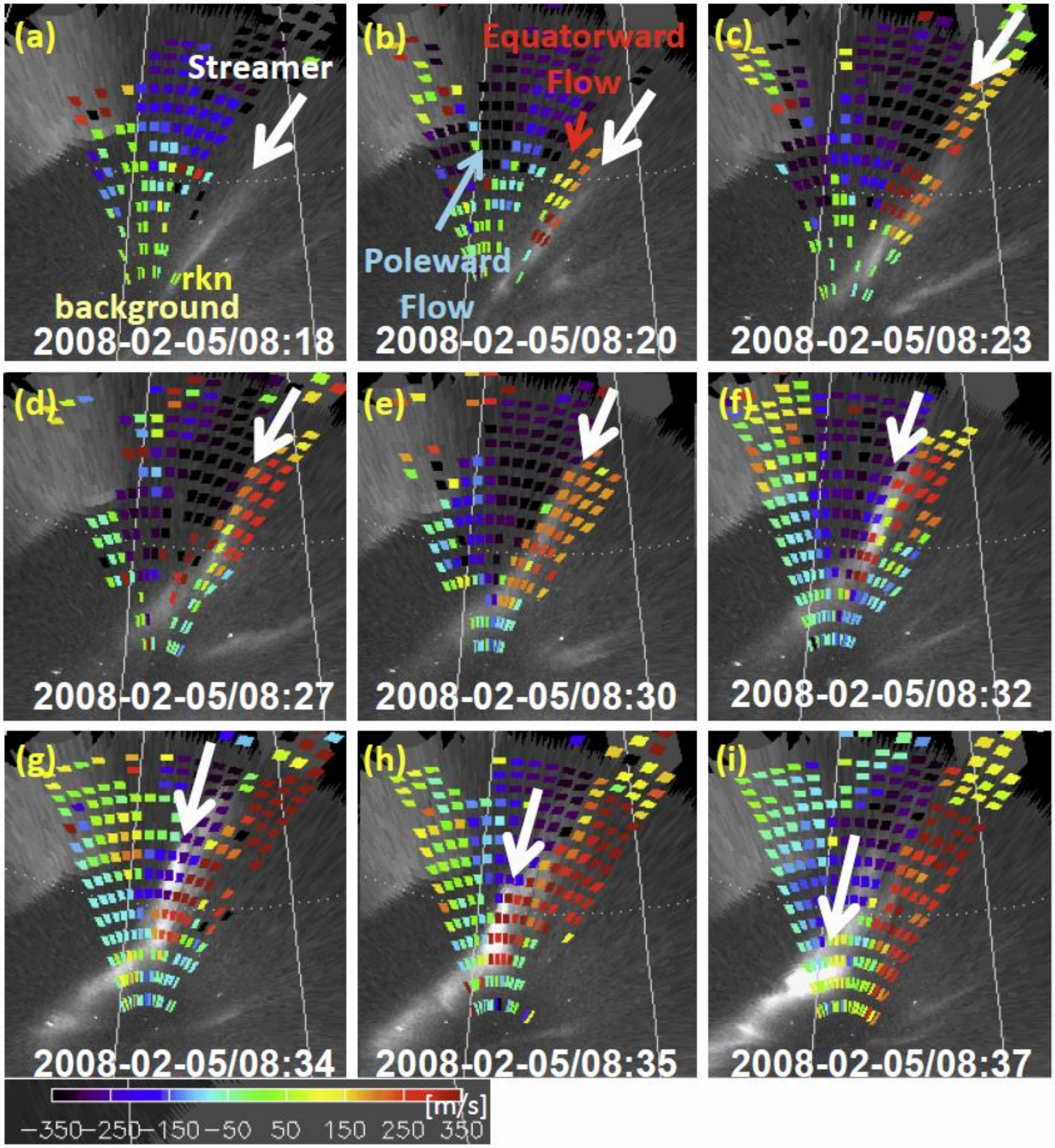

Figure 2.4. 5 February 2008 event illustrating the azimuthal and equatorward motion of the streamer and the correlation with the flow channel.

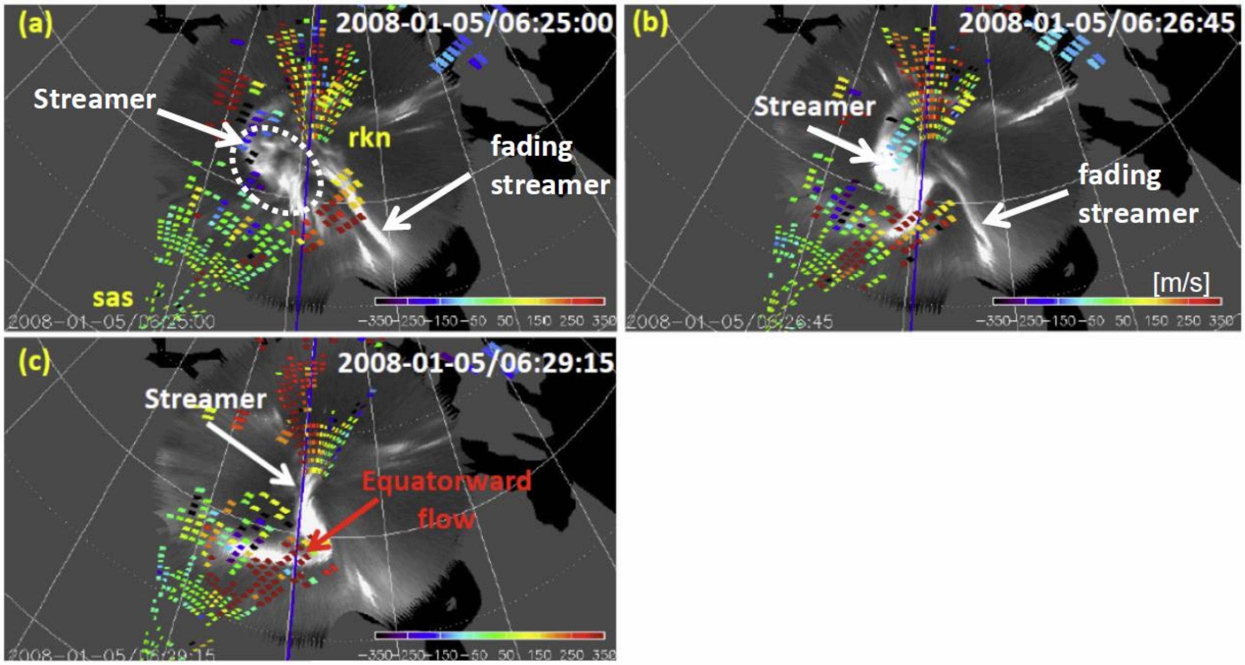

Figure 2.5. Flow channel associated to the auroral streamer detected in two radars.

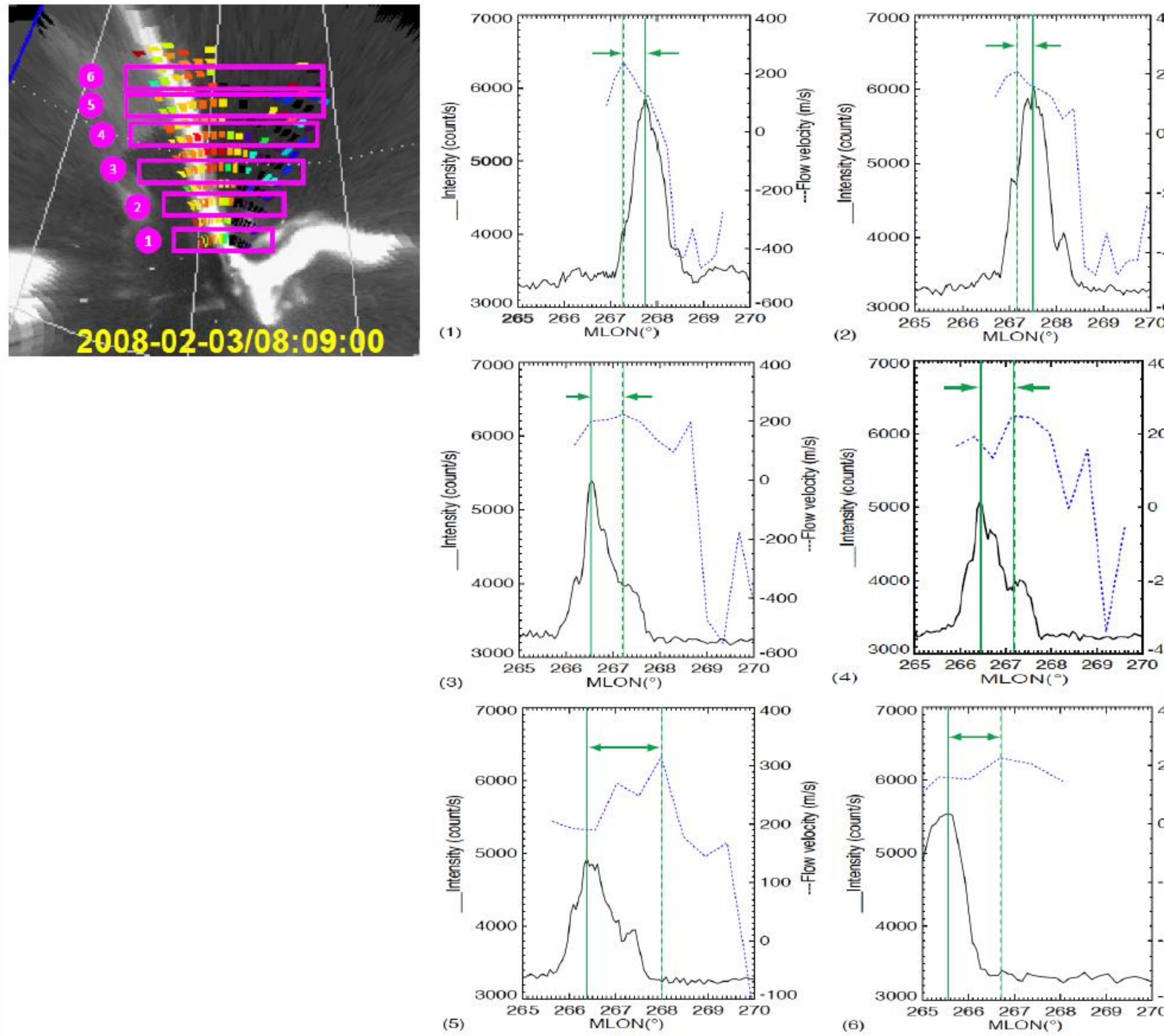

Figure 2.6. Latitudinal cuts along the radar FOV to determine the azimuthal width and shift of each auroral streamer. The left figure shows an example of six latitudinal cuts made for the 3 February 2008 event. The right panels represent auroral intensity (solid back line) and flow speed (blue dashed line), both as a function of magnetic longitude for each of the cuts shown in the figure on the left. The vertical solid (dashed) green lines correspond to the streamer's maximum intensity (maximum flow velocity). The green arrows indicate the azimuthal shift for each cut.

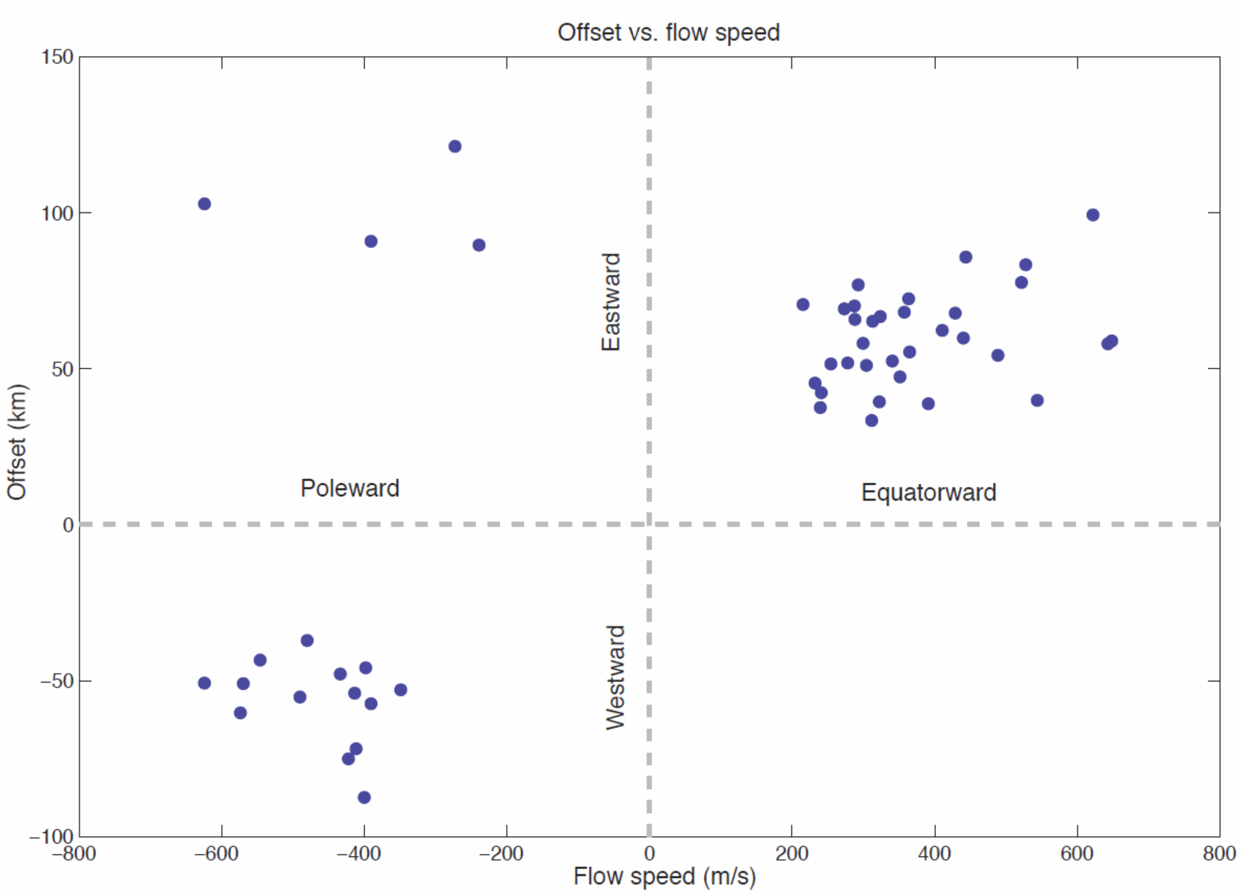

Figure 2.7. Azimuthal offset of ionospheric flow channels as a function of flow speed. Positive values of flow speed indicate equatorward flow enhancement and negative values represent poleward flow enhancement.

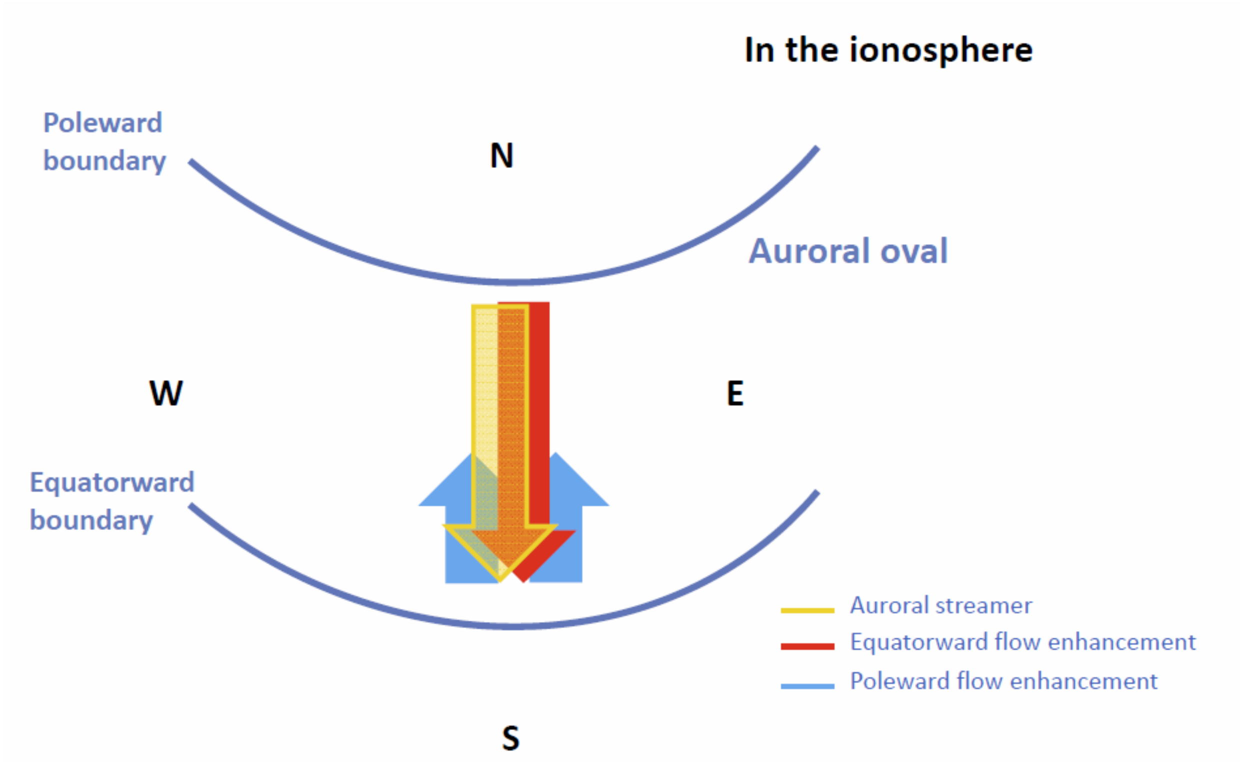

Figure 2.8. Schematic illustration of the association between auroral streamers and flow enhancements in the ionosphere.

CHAPTER 3

Ionospheric flow structures associated with auroral beading at substorm auroral onset

Auroral observations have shown that brightening at substorm auroral onset often consists of azimuthally propagating beads forming along a pre-existing arc. However, the ionospheric flow structure related to this wavy auroral structure has been poorly understood. Here we investigated ionospheric flow patterns associated with auroral onset beads using line-of-sight flow observations from the Super Dual Auroral Radar Network (SuperDARN) and auroral images from the Time History of Events and Macroscale Interactions during Substorms (THEMIS) ground-based all-sky-imager (ASI) array.

3.1 Data set and methodology

We use the THEMIS ASIs and an ASI located in Iceland for auroral observations, and the SuperDARN radars to measure ionospheric flows. The white light all-sky CCD camera installed in Tjörnes Iceland since 2009 acquires images with a temporal resolution of 1 sec. SuperDARN is a chain of high frequency coherent scatter radars that measure the ionospheric E and F region flow velocity in the line-of-sight (l-o-s) directions. SuperDARN utilizes an array of electronically phased antennae that can be steered to look in 16 or more beam directions stepping in azimuth every 3.3 degrees with temporal resolution of 1-2 min [Greenwald et al., 1995]. For each direction, the radar detects backscatter beginning at 180 km and extend to a maximum range of about 3500 km. In addition, during THEMIS tail conjunctions, SuperDARN radars have a capability to operate in the THEMIS mode, which provides measurements along a single beam with 6 s resolution.

The radars used in the first part of this analysis are in Saskatoon (sas) and Prince George (pgr) where their field of views (FOVs) are directed roughly poleward in the auroral zone and overlap with the FOVs of Athabasca (ATHA), Gillam (GILL), and Forth Simpson (FSIM). For sas and pgr radars, the THEMIS mode operates on beams 6 and 12, respectively. The north-south orientation of these beams provides a unique tool to detect flows perpendicular to a typical east-west orientation of onset auroral arcs with high temporal resolution. Note that east-west flows relative to the beading are not obtainable from the high-time resolution beam.

THEMIS ASIs and SuperDARN radars have been continuously operating since 2007 to present, providing a large data set. The SuperDARN THEMIS mode operates sporadically (about one third of the time) allowing us to perform a multi-event study of the north-south flow pattern at the substorm auroral onset.

Substorm auroral onset events seen by the THEMIS ASIs are identified from an extended version of the catalog created by Nishimura et al. [2010], and we searched for auroral onsets happening within or adjacent to a SuperDARN radar FOV. If the onset location is adjacent to the FOV, propagation of the beads across the radar FOV can occur making possible the measurement of flow pattern associated with the beading. We have found four events satisfying this criteria, and in this work we show three events with good echo coverage to establish the north-south flow structure associated with the beading. Strong oscillating flows are also observed for the event that is not shown.

The fourth event allows us to detect east-west flows relative to the auroral beading. This is the event reported by Motoba et al. [2012] for which simultaneous beading was observed in both hemispheres. For this event, the Pykkvibaer (pyk) radar beams overlap with beading as seen by the all-sky camera in Iceland. pyk radar operates in the myopic mode that enables higher (20 seconds) time resolution in all 16 radar beams, and the roughly east-west aligned easternmost looking of these beams *provides measurements of tangential flows relative to* the structure and propagation of the beads. This complements the normal component of the flow pattern associated with the substorm auroral beading seen in the previous three events.

3.2 Results

In this study we examined 135 isolated auroral streamers from December 2007 to December 2010 and identified flow patterns and their association with auroral streamers. The first part of the result sections is dedicated to the case study with the most representative cases. In the second part of this section we discuss the statistical study results.

3.2.1 North-south flows during onset using radars and imagers in North America

Figure 3.1a shows a merger of ASI images and SuperDARN Radars for an event on 28 February 2008. The ASIs are Inuvik (INUV), Rankin Inlet (RANK), GILL, and ATHA. We also present the l-o-s ionospheric flows measured by the Rankin Inlet (rkn), sas, and pgr SuperDARN radars. The left panel of figure 3.1a shows mostly uniform westward flow structures in the pgr and sas radars, the systematic variation in the line l-o-s velocity with azimuth is consistent with a fairly uniform westward flow, and equatorward flows in the rkn radar before the auroral beading started. The aurora near the equatorward boundary of the auroral oval (~62 deg) was quiet, while the poleward portion of the oval was active. At 0537:45 UT (right panel on 1a), a new auroral brightening can be seen within and adjacent to the sas radar FOV. This is the substorm auroral onset and is associated with auroral beads that extended eastward. At this time, the flow pattern at the sas radar drastically changed from the westward flow pattern to a highly structured pattern of strong flows. The 2-d radar measurements for this and later events show a wavy pattern associated with the substorm auroral onset with an azimuthal wavelength of ~80 km, estimated roughly from the occasions where the 2-d radar measurement show equatorward flow enhancement along a radar beam, surrounded by single radar beams showing poleward flow enhancements. This azimuthal wavelength is comparable with the separation of the individual beads. In contrast, radars away from the onset region (rkn and pgr) did not see such structured flows, indicating that the structured flows at sas are related to the auroral onset.

Although the slow (2-min) radar scan does not allow investigating the evolution of the wavy flow structure, the high temporal resolution (6 s) data from the THEMIS mode beam (6) can resolve flows associated with each bead that moves azimuthally across the beam. Figure 3.1b shows the temporal evolution of the auroral beading observed by the ATHA ASI and the flow measured by the sas radar along beam 6. Before the auroral beading started (panel A), sas radar beam 6 detected weak and fairly uniform flows with equatorward l-o-s velocity of roughly 150 m/s. At the time when the first auroral bead propagated eastward towards the radar beam longitude, the equatorward flow intensified to about 300 m/s (panels B-D). Once the first bead crossed the radar beam FOV, the direction of the flow drastically changed exhibiting very strong poleward flow enhancements of about ~800 m/s (panels E-F). Nine seconds later, when the second bead approached the radar beam longitude from the west, the radar measurements showed a strong equatorward flow enhancement of more than 700 m/s (panel G). This flow enhancement changed direction once the second bead crossed the radar beam, reaching more than 500 m/s directed poleward. The same flow direction changes associated with bead crossing were observed for the following 2 beads; strong equatorward flow enhancements before each bead reached the radar beam FOV (panels I and K) and strong poleward flow enhancements after each bead crossed the radar beam (panels J and L). A very interesting characteristic of these flow enhancements is their large speed. Typical auroral signatures such as auroral streamers are associated with average flow speeds of about 400 m/s [Gallardo-Lacourt et al. 2014]. Compared to those, the flow oscillations associated with the auroral onset are twice as fast and evolve in much shorter time scales.

The association between the flow oscillations and beads can also be seen in a time-series format in Figure 3.2. The two panels in Figure 3.2a show an auroral ewogram (east-west slice across the ASI FOV) along the magnetic latitude of the beading and the latitudinal profile of the flow velocity measured by beam 6 of sas radar. Note that the auroral beads have a ray structure that extends to high altitudes and appear as features that converge to the center of the auroral images, since the images map all aurora to a fixed altitude. Thus, for the keograms and ewograms in all the events, we have tracked the edge of the auroral beading that appears at the furthest location from the FOV center to most accurately represent the precise time when each bead crosses the radar beam. This figure clearly illustrates that strong oscillating flows are related to the onset and are only observed for the few minutes after the auroral onset time, which is marked by the red line. To further analyze the association between the fast oscillating flows and auroral beads, we zoomed in around the time where the beads are observed in Figure 3.2b. From top to bottom, the panels show an auroral keogram (north-south slice in the images) along the sas radar beam 6, an ewogram along the magnetic latitude of the auroral beading (east-west slice), the average flow velocity along the sas radar beam 6, and the latitudinal profile of the flow velocity from beam 6. The vertical gray dashed lines represent the times when each bead crosses the radar beam longitude (white horizontal line in the ewogram) according to the 2-D images presented in Figure 3.1b. Each auroral bead is marked by a white dashed line in the ewogram, and the numbers are consistent with those presented in Figure 3.1b. The orange and blue arrows in the third panel represent equatorward and poleward flow enhancements, respectively. For each auroral bead crossing of the radar beam longitude, we can see an equatorward flow enhancement followed by a poleward flow enhancement. Since the onset arc is oriented essentially perpendicular to the north-south radar beam orientation, the measured flows can be interpreted as flows across the arc rather than a projection of flows tangential to the arc.

The second event, on 25 March 2009, is presented in Figure 3.3. The left panel of figure 3.3a shows mostly uniform flows in sas radar, when the aurora in GILL ASI was quiet. At 0506:21 UT (right panel on 3a), large, structured equatorward and poleward flows (encircled by the orange dashed line) associated with the beading are observed. Figure 3.3b shows the auroral onset beading observed in the GILL ASI FOV and the associated ionospheric flows measured by the Saskatoon radar beam 6 operating in the THEMIS mode. At 0504:18 UT, three auroral beads were observed close to the western edge of the ASI FOV. Before the first auroral bead crossed the radar beam, an equatorward flow enhancement was observed. The flow direction reversed once the bead crossed the radar beam and strong poleward flow enhancement was detected at 05:04:24 UT. For this event, we were able to identify 4 beads before the evolution of the beading became nonlinear, and they are clearly seen in the time-series plot in Figure 3.3c. From top to bottom, the time-series plots present an auroral keogram along the radar beam, an ewogram along the beading, the average flow velocity, and the latitudinal profile of the flow velocity in Saskatoon beam 6 containing the THEMIS mode. Equatorward flow enhancements were detected ahead of the beads (orange arrows), and poleward flow enhancements after the bead crossed the radar beam (blue arrows). This flow and aurora relation is consistent with the previous event, and the peak flow magnitude reached ~1000 m/s.

Figure 3.4 presents the third event, on 04 April, 2010, which show the oscillation of strong equatorward and poleward flow enhancements surrounding the auroral beads. In this case, the beading occurred in the FSIM ASI FOV and the strong flows were detected by the pgr SuperDARN radar. The left panel of figure 3.4a shows mostly uniform flows in pgr radar prior to the onset. At 0755:54 UT (right panel of 3.4a), large, structured flows directed equatorward and poleward (encircled by the orange dashed line) are observed in association with beading within the radar FOV. During this event, the beads propagated eastward and the auroral rays are seen in by the imager align nearly parallel to the radar beam 12, which operated in the THEMIS mode, and can be identified even though they became occasionally obscured by trees within the ASI FOV. Figure 3.4b shows a strong equatorward flow enhancement of more than 300 m/s ahead of the first bead (left panel). This flow direction changed once the bead crosses the radar beam (right panel). The time series presented in figure 3.4c follows the same format as figure 3.3c. The imager data we have used to construct the keogram and ewogram (first and second panels in figure 3.4c) are relatively noisy due to the trees which can be identified as the dark areas across the beads highlighted with white dashed lines. Despite this, the auroral beads can be seen in the keogram and ewogram. In this event, the first bead crosses the radar beam longitude (horizontal dashed white line) at about ~0755:50 UT (first vertical gray dashed line), and an equatorward flow enhancement was detected ahead of this bead, and then a reduction of the flow speed is observed once the bead crosses the radar beam. A new bead started propagating eastward at the time when the first bead had crossed the radar FOV; however, this bead fades away before reaching the radar beam longitude. Several seconds later, the second bead propagates eastward, exhibiting the same flow feature before and after the bead. At about 07:56:40 UT, a strong equatorward flow enhancement of ~1000 m/s was observed by the radar beam as the third bead reaches the radar beam longitude, and then this flow dramatically changes to poleward reaching ~1000 m/s. By the time the fourth bead reached the radar beam, the amount of echoes became limited, but the average flow velocity shows the presence of equatorward flow enhancement prior to the bead followed by a flow speed decrease. For the fifth and sixth beads, we observed strong equatorward flow enhancement around the crossing time and a clear flow decrease several seconds later. This event thus shows the same flow and auroral correlation as the previous two events.

3.2.2 East-west flows during onset using radar and imager in Iceland

The fourth event was obtained using the ASI in Tjörnes and the pyk radar on 30 September, 2011. Figure 3.5 shows the temporal evolution of the beading during this event and the related ionospheric flows. At 2305:00 UT in Figure 3.5a we observed a preexisting arc located poleward of 65 deg MLAT and moderate eastward directed flows, consistent with being within the dawnside convection cell, of about 200 m/s. In figure 3.5b, it is possible to observe the initiation of the beading along the preexisting arc and simultaneously a reduction of the eastward flows measured by beams 13, 14 and 15 (eastward most beams encircled by the orange dashed ellipse in figure 3.5a). Figure 3.5c shows a further eastward propagation and intensification of the beading and flow structure. At 23:15:00 UT, in Figure 3.5d, a small auroral poleward expansion is observed within the TJO FOV.

Figure 3.6 shows the time series for the event described above. From top to bottom, panels are a keogram across the radar beams 13, 14 and 15, an ewogram along the magnetic latitude where beading is observed, and the median flow velocity detected in the eastward looking beams 13, 14 and 15. The pink dashed lines in the ewogram correspond to the bottom edge of each auroral bead designated by numbers. We drew the same lines in the third panel. Although the flow speeds are small, it is possible to identify for each bead a reduction in the eastward flow. This flow reduction indicates the presence of westward flow perturbations associated with the auroral beading; and moreover, it demonstrates that the tangential component of the flow pattern also corresponds to a clockwise flow shear associated with each bead.

3.3 Discussion and conclusions

Taking advantage of the high temporal resolution data provided by the ASIs and SuperDARN radars, we identified the flow structure associated with the auroral beading observed at substorm onset. In all three of our events over North America, we found extremely fast (~1000 m/s), longitudinally narrow, flows with a strong flow shear simultaneously with the initiation of the auroral beading. We have found excellent temporal and spatial correlations between the beading and the alternation of fast equatorward and poleward flows. For the event in Iceland (eastward-looking radar beams), westward flow perturbations were associated with eastward propagating beads, although the flow magnitude (~100 m/s) was much smaller than the north-south flows found in the north-south looking beam events.

The measured flow oscillations observed in all the events can be interpreted as a spatial structure passing across the radar beam that maintain its wavy pattern as it grows in time for several wave periods. The flow pattern of one wavelength as inferred from our observations is illustrated schematically in Figure 3.7. Clockwise flow shears are associated with upward

FACs in the center of the flow shear and can be seen as the auroral beads, and counter-clockwise flow shears between the beads are associated with downward FAC. An important feature is the clear difference between the flow magnitudes measured in the north-south (N-S, events 1-3) direction compared with the east-west (E-W, event 4) direction, with the azimuthal component of the flows being significantly slower than that in the north-south orientation. A possible explanation for the difference observed in the N-S and E-W flows is that the N-S flows are confined to a longitudinal width that is much shorter than the latitudinal extend of the flows. The broad latitudinal extent of the N-S flows is an indication that the E-W flows connecting to these N-S flows extend substantially poleward and equatorward of the onset arc.

We roughly estimated the magnetotail size of the observed structure by mapping the beads observed by the all-sky cameras to the equatorial plane using the Tsyganenko 2001 magnetic field model. We obtained an azimuthal wavelength of ~1800 km (0.28 Re), similar to what was obtained by Motoba et al. [2012]. Also, the latitudinal extent of the flow oscillation in the ionosphere is ~3.5° or larger (limited by the echo coverage), which corresponds to >~4R_E extension in the x-direction in the magnetotail, although this number likely has a large uncertainty that depends on the magnetic field configuration.

The present study suggests that the substorm onset process involves formation of fast earthward/tailward flow structures. Several theoretical approaches have been proposed to explain formation of wavy structures in the plasma sheet [e.g., Pu et al., 1999; Lui, 2004; Cheng, 2004]. Roux et al. [1991] proposed a simplified model in which the ballooning mode will act as the instability trigger in the plasma sheet. Several other studies have proposed ballooning instability as one of the main candidates to explain the substorm onset [e.g., Henderson et al., 2002, 2009]. More recently, Pritchett and Coroniti [2010, 2011, 2013] performed particle-in-cell (PIC) simulations to study the structures and consequences of the kinetic ballooning/interchange instability (BICI) modes that can be exited in the plasma sheet. Formation of fast (~600-900 km/s) and very narrow (~2000 km) earthward and tailward flows are observed in the simulation, and those flows map to roughly ~1000 m/s and ~70 km in the ionosphere. This result is consistent with the observations reported in the present thesis work, indicating that BICI modes may be a viable candidate for the instability that is responsible for the auroral beading and initiates the auroral onset. We, however, do not rule out other potential mechanisms for substorm onset, and more quantitative comparisons are needed for determining the onset mechanism.

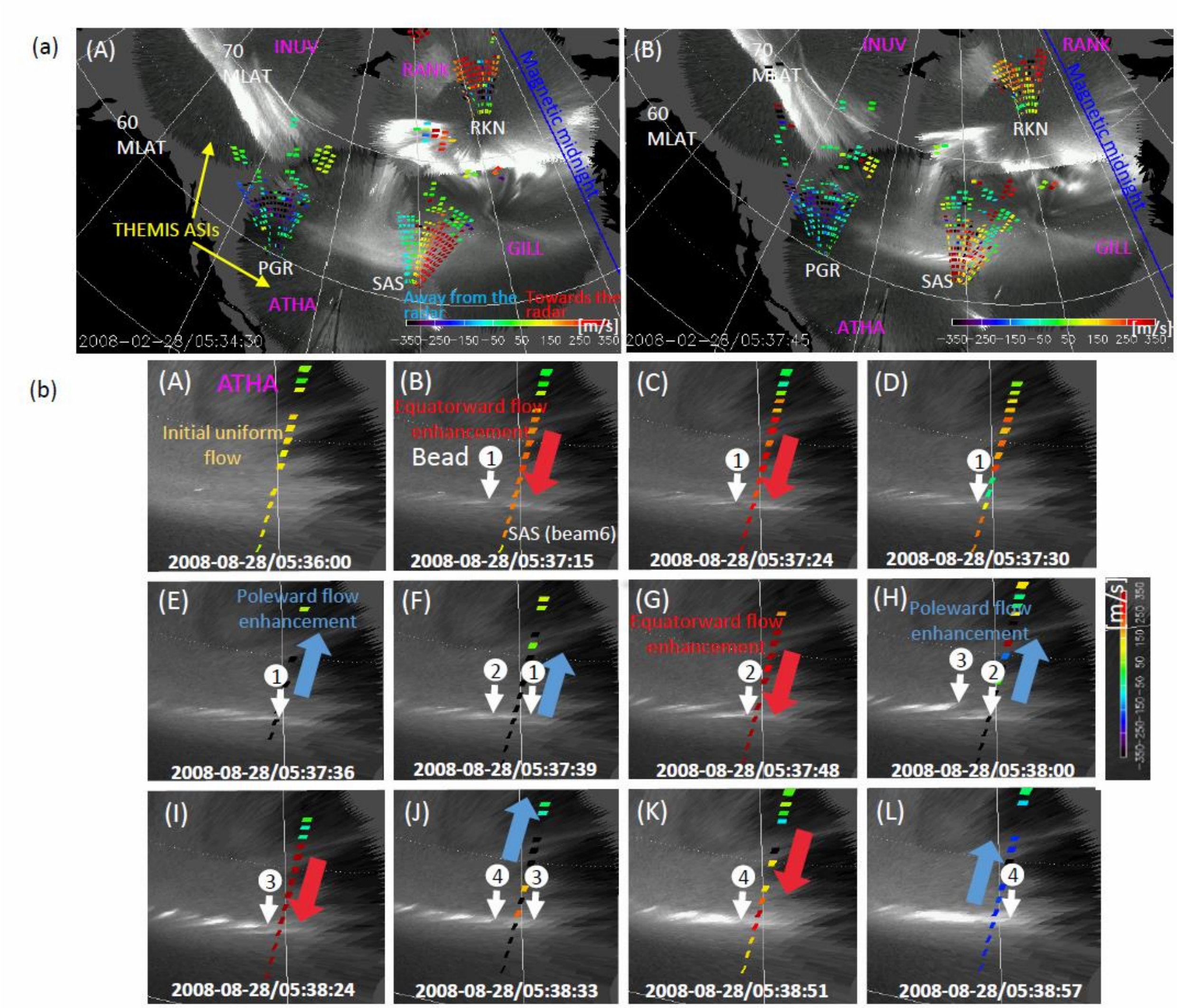

Figure 3.1. Coordinated observations from THEMIS ASIs and SuperDARN radars showing l-o-s flows associated with the auroral beading at the onset time on February 28, 2008. For this event the SuperDARN radars complete a full scan every 2 minutes. (a) Large-scale view of the auroral oval. (b) Temporal evolution of the auroral beading measured in the eastern portion of the ATHA ASI, and the ionospheric flows measured by sas beam 6 in the THEMIS mode. Radar velocities are positive toward the radars. The magnetic north is to the top and the blue line marks the magnetic midnight meridian. The latitude and longitude contours are given every 5 and 15 deg.

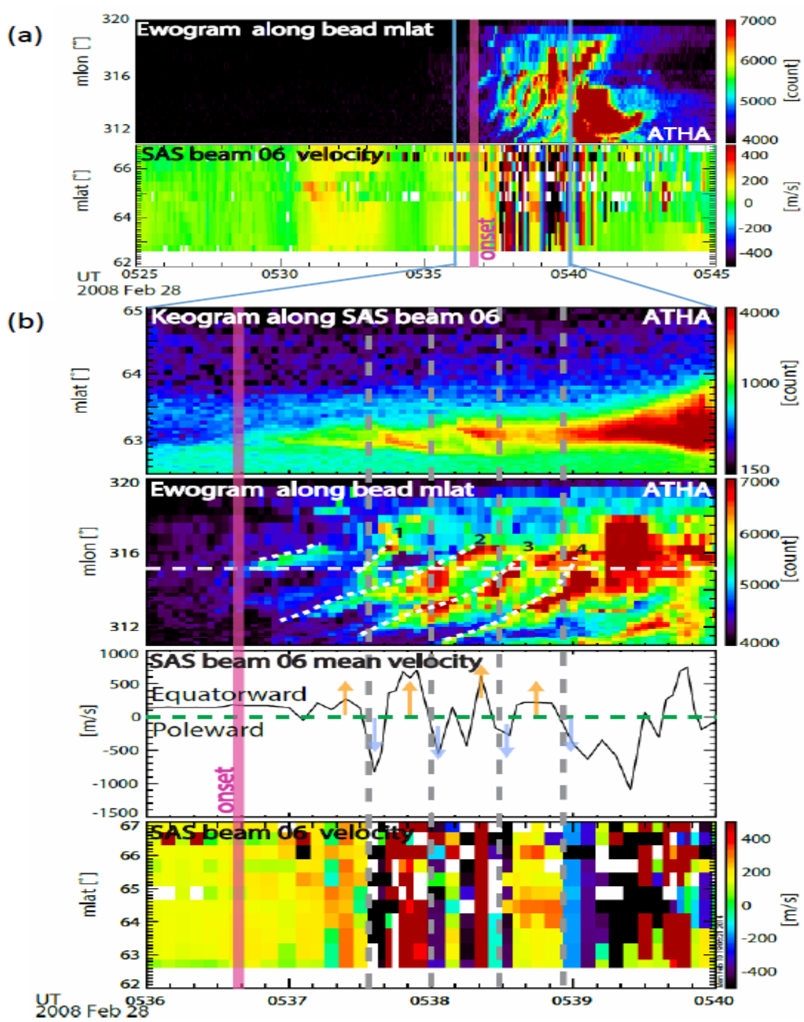

Figure 3.2. (a) From top to bottom panels show an ewogram (east-west slice) of ATHA ASI along the bead magnetic latitude (~63 deg) and the ionospheric flow velocity measured by sas beam 6 operating in the high resolution THEMIS mode. (b) Shorter temporal interval of the previous figure. From top to bottom the panels show a keogram along the sas radar beam 6, an ewogram along the beading magnetic latitude, the average flow velocity measured by sas beam 6, and l-o-s velocity for sas beam 6. Pink vertical line indicates the onset time. The gray vertical dashed lines show the time when each bead crosses the radar beam longitude (horizontal white dashed line in the ewogram). Orange and blue arrows in the third panel show equatorward and poleward flow enhancements respectively.

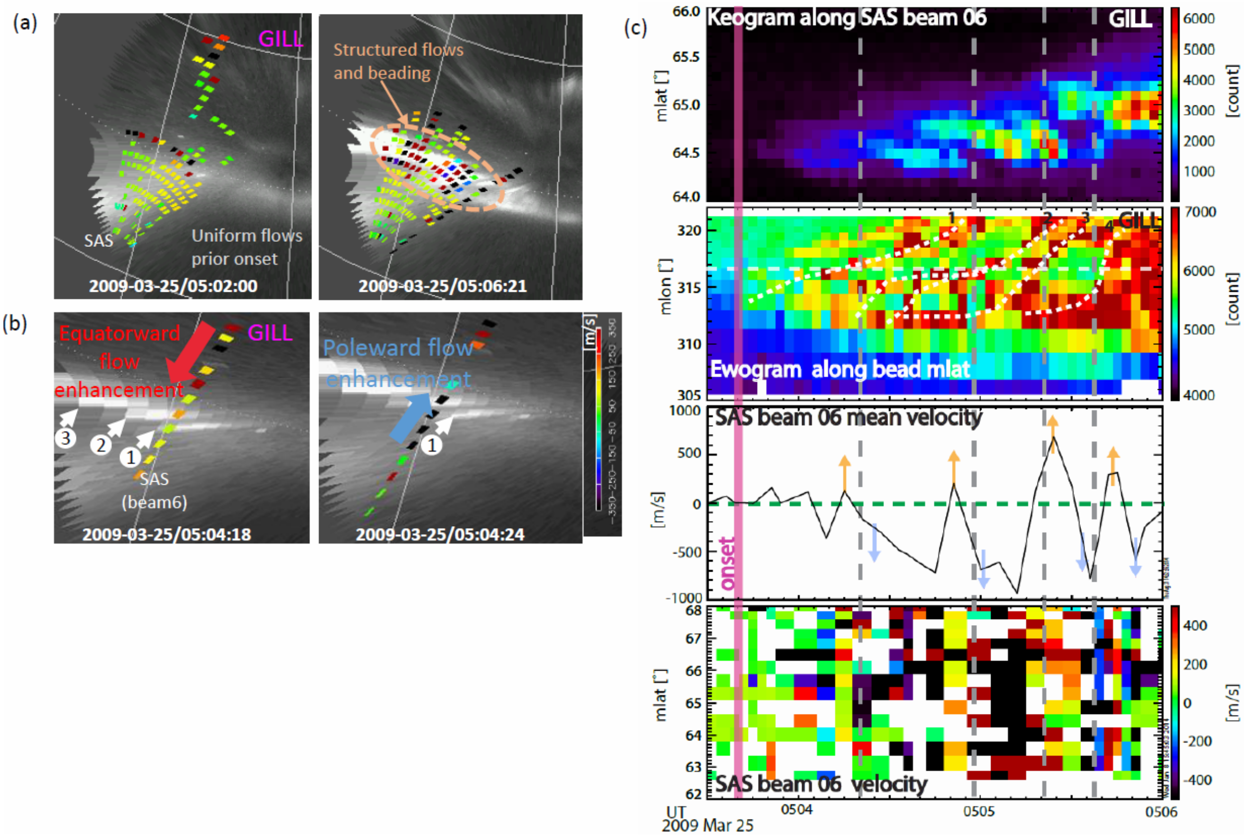

Figure 3.3. (a) Coordinated observations from THEMIS ASIs and SuperDARN radars showing l-o-s flows associated with the auroral beading at the onset time on March 25, 2009. Left panel shows uniform flows within sas FOV prior to the onset. Right panel shows oscillating equatorward and poleward flow enhancements associated with the auroral beading. (b) Temporal evolution of the auroral beading and ionospheric flows observed in sas beam 6. (c) Time series of imager and radar data. The format is the same as in figure 2.

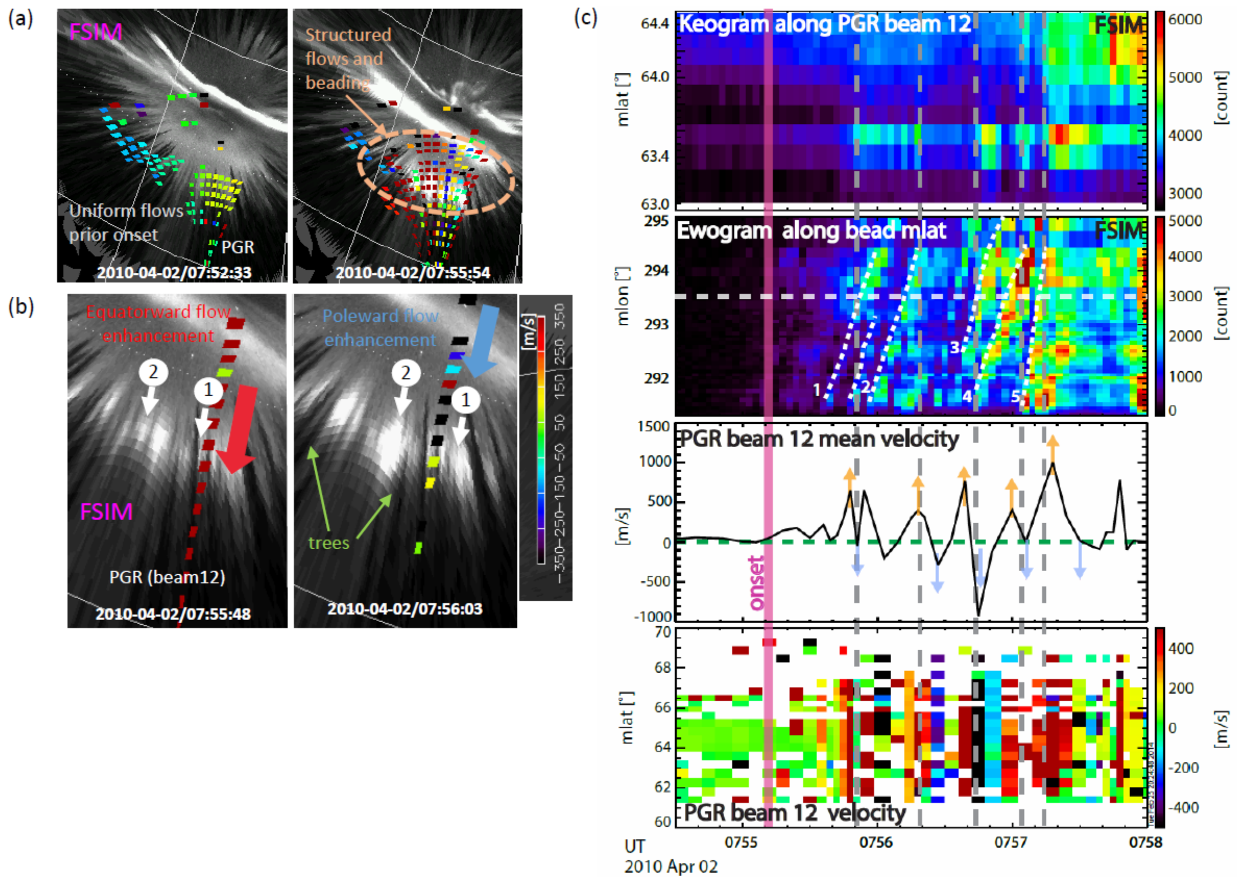

Figure 3.4. (a) Coordinated observations from THEMIS ASIs and SuperDARN radars during a onset time on April 2, 2010. Left figure shows uniform flows within pgr FOV prior to the onset. Right panel shows oscillating equatorward and poleward flow enhancements associated with the auroral beading. (b) Temporal evolution of the auroral beading and ionospheric flows observed in pgr beam 12 during a substorm onset occurring on April 02, 2010. (c) Time series of imager and radar data. The format is the same as in figure 2.

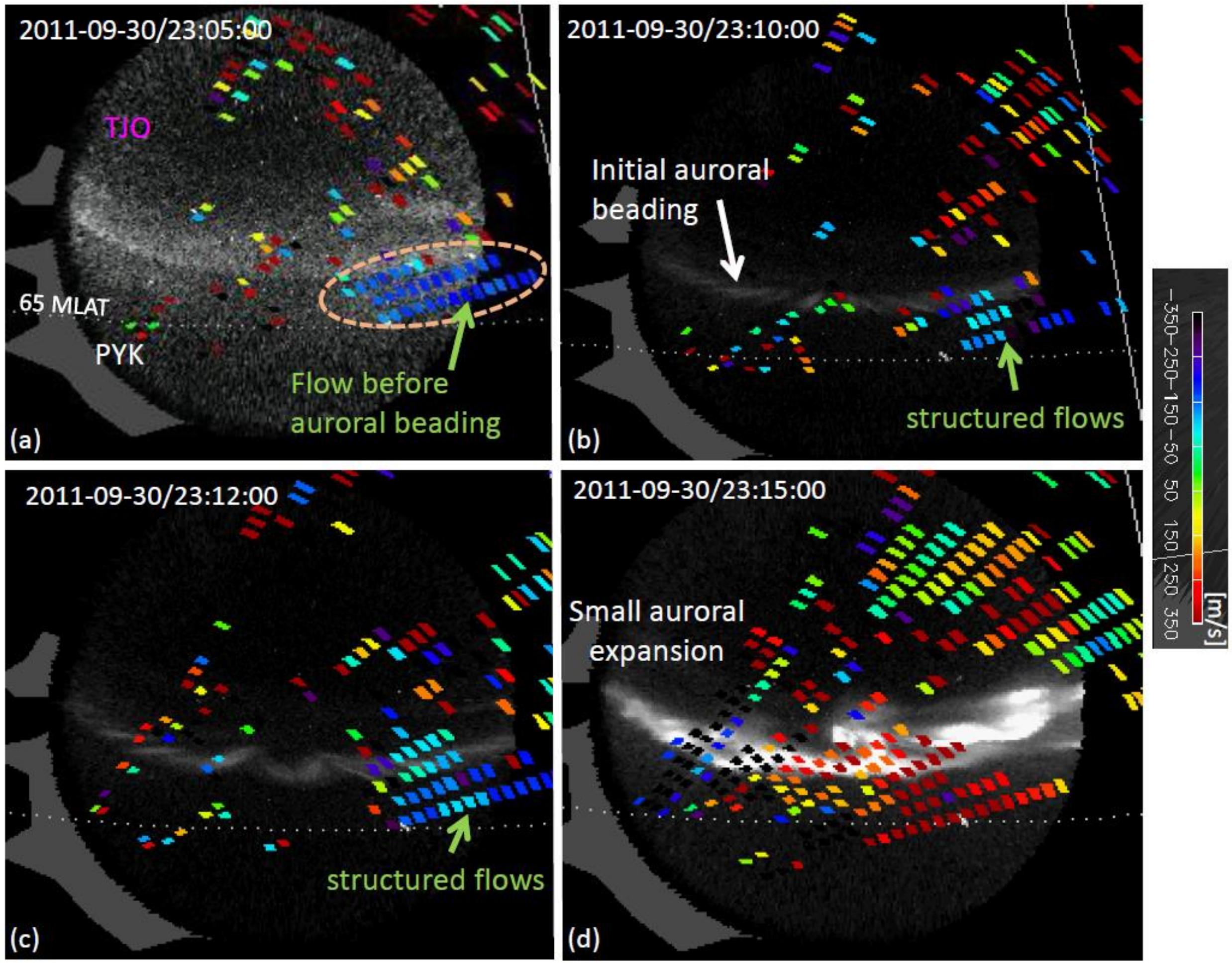

Figure 3.5. Temporal evolution of the auroral beading observed in TJO ASI and ionospheric flows measured by pyk radar for a substorm auroral onset occurring on September 30, 2011.

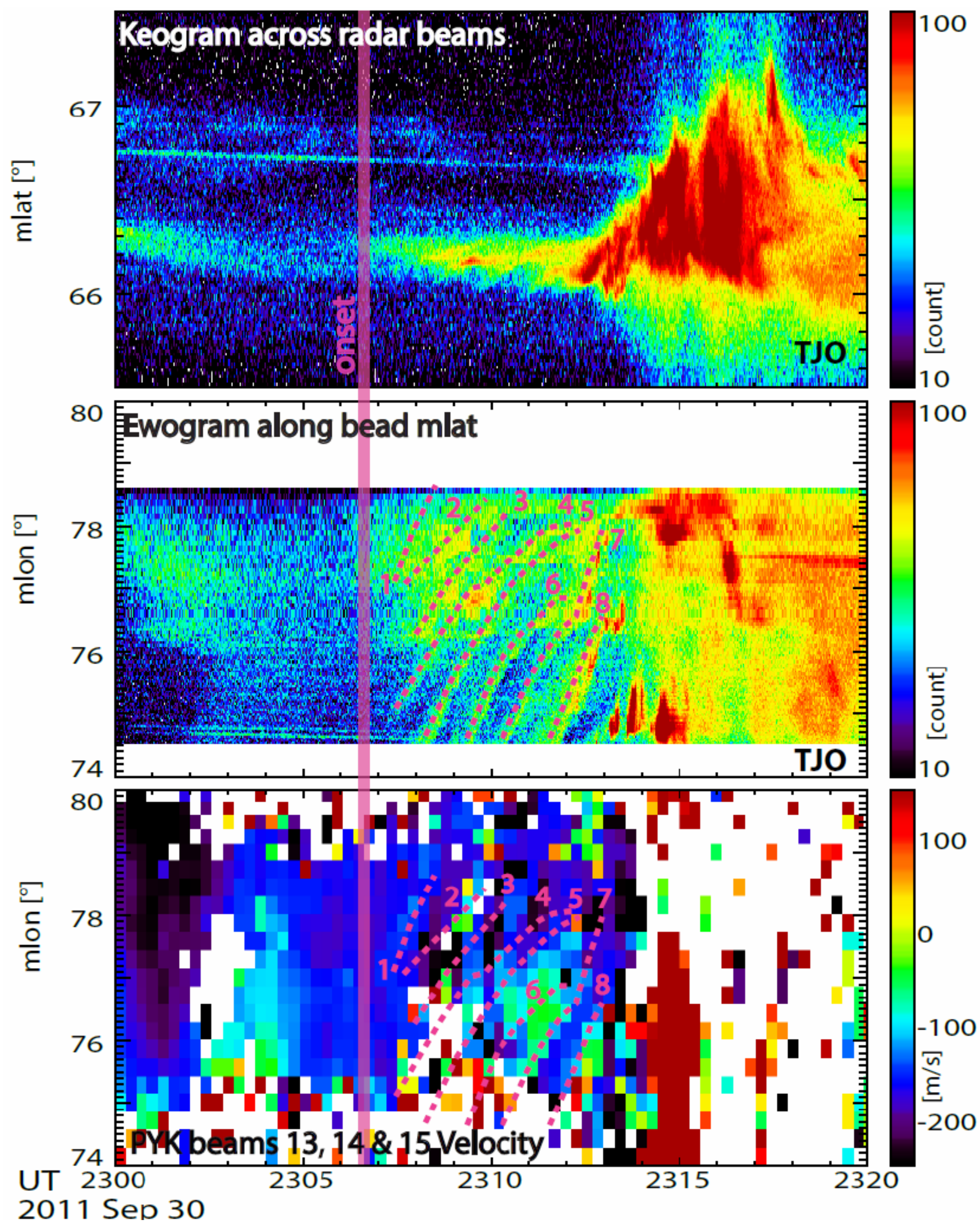

Figure 3.6. Time series of the substorm auroral onset occurring on September 30, 2011. From top to bottom the panels represent a keogram across the radar beams, an ewogram across the magnetic latitude of the beading, and the median of the flow velocity observed by pyk radar in beams 13, 14 and 15. The vertical pink line indicates the onset time. Pink dashed lines in the ewogram correspond to each bead highlighted by the numbers. The same lines are copied on top of the radar data to illustrate the relationship between auroral beading and flow enhancement.

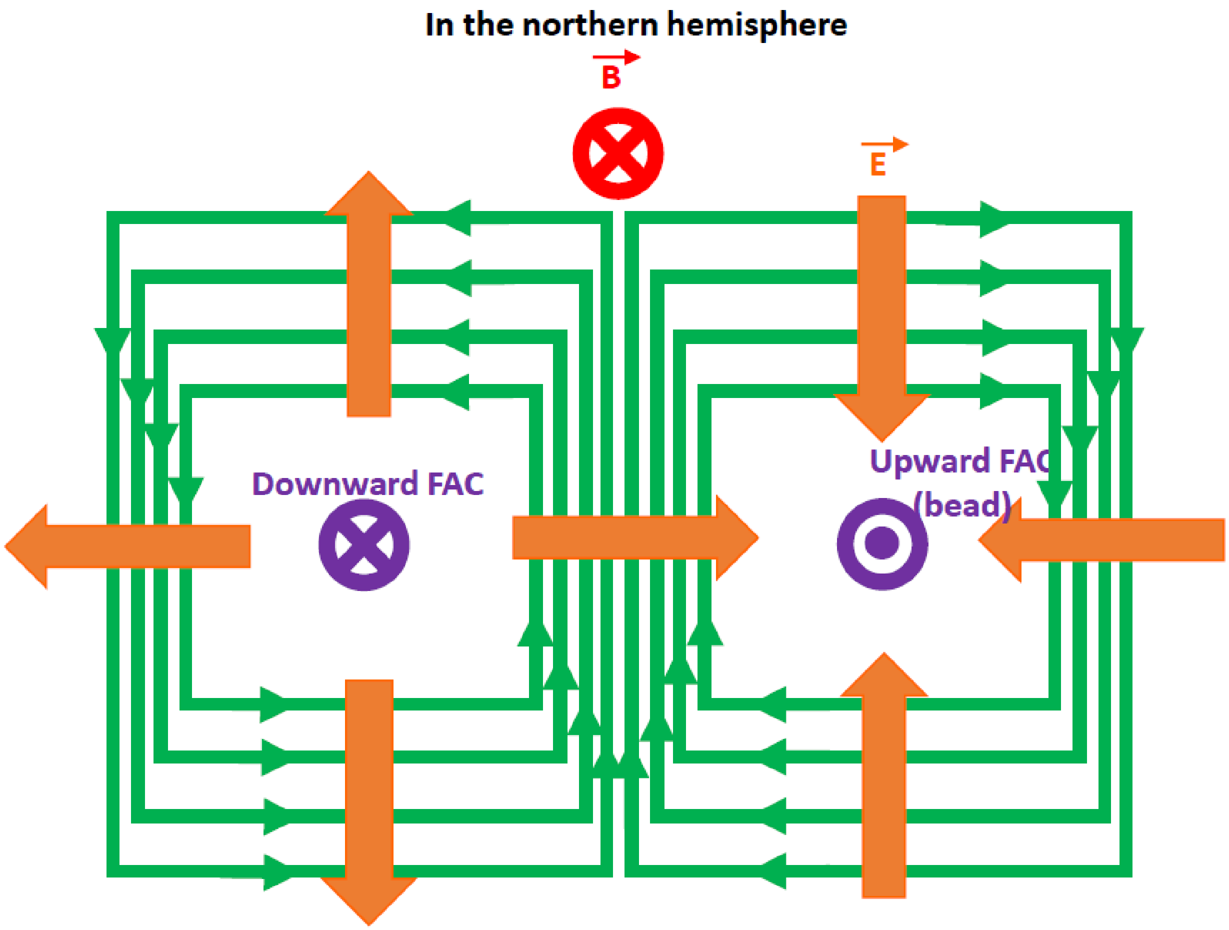

Figure 3.7. Schematic illustration showing the relationship between clockwise flow shear surrounding the auroral beads and FACs.

CHAPTER 4

Influence of auroral streamers on rapid evolution of SAPS flows

While SAPS are known to intensify due to substorm injections, recent studies showed that large variability of SAPS flow can occur well after substorm onset and even during non-substorm times. These SAPS enhancements have been suggested to occur in association with auroral streamers that propagate equatorward, a suggestion that would indicate that plasma sheet fast flows propagate into the inner magnetosphere and increase subauroral flows. In this chapter we investigate systematically the association between SAPS flow enhancements and auroral streamers by using the Time History of Events and Macroscale Interactions During Substorm (THEMIS) and the Super Dual Auroral Radar Network (SuperDARN) radars to measure ionospheric flows within the THEMIS ASIs field-of-view (FOV). We examined data from December 2007 to April 2013. In this study we use the Defense Meteorological Satellite program (DMSP) satellite data and Meridian Scanning Photometers (MSP) to clearly identify the auroral equatorward boundary. The results of our study reveals that the association between SAPS flow enhancements and auroral streamers is relatively common. We also characterize the SAPS flow enhancements and their driver streamers.

4.1 Data set and methodology

The THEMIS ASIs are white light CCD imagers. Each imager has a latitudinal coverage of ~9^0 and longitudinal coverage of ~2.5 h MLT with time resolution of 3 s and spatial resolution of ~100 m near zenith [Mende et al., 2008]. The THEMIS ASIs consist of 21 cameras that cover a large section of the auroral oval and provide 2D auroral observations with high temporal and spatial resolution.

SuperDARN is a chain of high frequency coherent scatter radars that measure ionospheric E and F region flow velocities in the line-of-sight (l-o-s) directions. SuperDARN utilizes an array of electronically phased antennae that can be steered to look in 16 or more beam directions stepping in azimuth every 3.3 degrees with temporal resolution of one to two minutes [Greenwald et al., 1995]. For each direction, the radar detects backscatter echoes beginning at 180 km and extends to a maximum range of about 3500 km. The radars used in this study are located in Saskatoon (sas), Prince George (pgr), King Salmon (ksr), Fort Hays East (fhe), Fort Hays West (fhw), Christmas Valley East (cve) and Christmas Valley West (cvw). The fhe and fhw radars were available from November 2009, and the cve and cvw radars were available since January 2011.

We analyzed data from December 2007 to April 2013. Auroral streamers were identified as roughly north-south aligned arcs that form near the poleward boundary and propagate equatorward, reaching close to the electron equatorward boundary (an example is shown in Figure 4.1). We required that streamers are within ±2 MLT from the radar echo locations, with maximum intensities higher than 3000 count/s. Our analysis focused on isolated streamers, i.e., that there are no other streamers within the FOV of the observing radar at the same time, and long-lasting events with multiple streamers. Observed westward flow velocity should increase by more than 50 m/s l-o-s (which usually correspond to about 100 m/s in the westward direction), and last for more than 3 minutes to be considered as a correlated event. Also, more than 70% of the echoes were available at the time of the measurement. As in the Figure 4.1 snapshot, radar l-o-s velocity magnitudes generally have a minimum in the northward-looking beam, and increase with the angle from north. This indicates that the true flow is close to the azimuthal direction. When positive velocities are seen in eastward looking beams (cve in Figure 4.1) and negative velocities are seen in westward looking beams (cvw in Figure 4.1), the true flow can be deduced as westward. To calculate the maximum westward flow speed, we decomposed the l-o-s flow velocity for 5 different radar beams and calculated the maximum average westward flow velocity.

Our forward study starts with streamers and examines if SAPS flow enhancements occur. We also performed a reverse study, starting from ionospheric flow variations and then analyzing auroral signatures. The same flow enhancement threshold required for the forward analysis was used for the reverse study (flow velocity ≥50 m/s l-o-s). Also the flow enhancement lasted for at least 3 minutes.

In total, 104 events were analyzed that satisfy the aforementioned forward and reverse selection criteria. We have obtained 63 events from the forward analysis and 103 events from the reverse study. The forward analysis is comprised of streamers associated with westward flow enhancements and one uncorrelated event for which we observe an auroral streamer without flow enhancement. The reverse study consists of the same 62 previous events in which streamers were associated with westward flow enhancements, 38 enhanced convection events, 2 interplanetary shock events, and one uncorrelated event for which SAPS flow enhancement is not associated with auroral streamers. We have divided all the events into two main categories: correlated and uncorrelated. Correlated events are those that showed an association between auroral streamers and westward flow enhancements. The uncorrelated events were divided into four sub-categories. Uncorrelated sub-category 1 consists of events with streamers but without flow enhancements; Uncorrelated sub-category 2 corresponds to events with westward flow enhancements in absence of auroral streamers (from the reverse study); The uncorrelated sub-category 3 corresponds to interplanetary shock events. The last uncorrelated sub-category (4) corresponded to events found in the enhanced convection sub-category, which corresponds to events with Interplanetary Magnetic Field (IMF) southward turnings and equatorward motion of the auroral oval. The IMF conditions for these events were obtained by using OMNI database 1-min time resolution.

In addition, we have used MSP and DMSP satellite data closer to the event location to identify the equatorward boundary for all of the events in which the boundary was not clearly identifiable from optical data.

4.2 Results

4.2.1 Case study: Representative Cases

Figure 4.2a-f shows mergers of the THEMIS ASI and SuperDARN radars on February 22, 2008. The figure illustrates a relatively isolated streamer event associated with SAPS westward flow enhancements. Initially at 06:45:00UT (Panel a) the l-o-s flow velocity observed by the pgr SuperDARN radar has a small magnitude of ~100 m/s. At the same time, an auroral streamer began to propagate from the poleward portion (~72° MLAT) of the auroral oval and started moving equatorward. The auroral equatorward boundary seen in the white light imagers was at ~67 MLAT, and this auroral brightening does not seem to be a substorm but a poleward boundary intensification. The same streamer was observed in panel b after it bifurcated and continued propagating equatorward (i.e. closer to the radar's FOV). At that time, the l-o-s flow velocity increased to ~200 m/s. In panel c, the streamers reached about 67 mlat and drifted westward to reach the pgr radar FOV. The l-o-s flow velocity at this stage reached ~250 m/s. Panels d and e show a decay of the streamer and flow. In panel f, the streamer was no longer observed within the ASI FOV and the flows were significantly reduced.

The same sequence of events described above can be observed in the time series plot in figure 4.2g-j. The two first panels (g and h) show keograms (north-south slice across the ASI FOV) from Fort Simpson (FSIM) and Fort Smith (FSMI), respectively, in which the color scale represents auroral luminosity The two last panels (i and j) show the latitudinal profile of the flow velocity measured by the combination of beams 4 and 5, as well as 6 and 7. Note that the initial flow velocity measured by pgr is about -100 m/s, and, at around 06:46:00UT (as shown by the first vertical pink line), the first auroral signature starts to propagate slowly equatorward. At the same time, westward flow enhancements of ~50m/s occur at beams 6 and 7. Another auroral streamer started to develop from a PBI and then propagated equatorward, reaching closer to the optical equatorward boundary at ~68 deg MLAT at ~06:52:00UT. At this time the westward flow reached ~250m/s and the enhancement lasted for around ten minutes. After the auroral streamers are no longer visible within the ASI FOV, the corresponding flows decreased to the original uniform background level.

Figure 4.3 shows another isolated event. The figure on the left (Figure 4.3a-d) illustrates the sequence of the event that occurred on March 15, 2009. The available ASIs used for this event were Snap Lake (SNAP) and Rankin Inlet (RANK). On top of the imagers we have overlaid ionospheric flows from the Saskatoon (sas) SuperDARN radar. Panel 3a shows a clockwise loop of auroral form (Harang aurora), and the flow within the sas FOV was weak and uniform. Four minutes later (Panel 3b) a long auroral streamer developed from the previously observed Harang aurora and reached closer to the radar location. Additionally, to the east of this streamer another streamer was seen at higher latitude propagating equatorward. This is clearly different from a substorm because there is no growth phase arc or poleward expansion. At that time, the sas radar started measuring enhanced flows towards the radar. Panel 3c shows the equatorward streamer drifting westward at the same time that the sas radar measured a SAPS flow enhancement of ~ 200 m/s. Finally, panel 3d illustrates the reduction of the westward flow once the streamers were no longer observed within the ASIs/radar FOV.

Figure 4.3e-g shows the time series plot illustrating the main characteristics of the event described in figure 4.3a. The first panel shows a keogram from RANK. The second panel (f) is from SuperDARN radar sas beam 06 l-o-s flow velocity (High 6s time resolution, THEMIS mode). Panel g is from the MSP red line (6300Å) emission that is used to identify the auroral equatorward boundary. In the first panel, the equatorward moving auroral form or auroral streamer is clearly propagating towards lower latitudes. At this time the westward flows measured in sas beam 06 were uniform and around 0 m/s. After the auroral streamer moved closer to the equatorward boundary, the radar detected a flow increase of about 100 m/s. In this event, the equatorward half of the measured flows were in the subauroral region since the equatorward boundary is at ~67° mlat as detected in the MSP red light emission (panel g).

Figure 4.4 shows an example of the association between westward flow enhancements and auroral streamers during a more active event that occurred on March 2, 2013. Figure 4.4a-f shows the sequence of this event. Initially, it is possible to identify moderate westward flows that were measured by the mid-latitude radars cve and cvw. Panel b shows an auroral streamer moving equatorward poleward of the cvw FOV. This radar measured an increase in the SAPS region flows in the poleward portion of the available echoes. In panel c, three auroral streamers propagate equatorward at the same time as an enhancement in the westward flows is observed by the mid-latitude radar cvw. Panel d shows an auroral streamer reaching closer to the optical equatorward boundary (~63 MLAT), and cvw measured a westward flow enhancement together with an equatorward penetration of these flows. Panel e shows the last auroral streamer observed within the ASI FOV while the mid-latitude radars detected a westward flow enhancement and equatorward penetration. When auroral streamers are not present in the camera's FOV, the mid-latitude radars measured a decay in the westward flow enhancement (Panel f).

Figure 4.4g-i shows the time series plot describing this event. The first two panels (g and h) correspond to keograms from different locations of the FSMI ASI, and the third panel shows the mean values for cvw beams 12 and 14 l-o-s flow velocity. The two first panels clearly show four auroral streamers propagating equatorward after an auroral substorm onset at ~035415 UT. The flow velocity did not change at the substorm onset but showed multiple enhancements during the expansion phase. The pink magenta vertical lines highlight major SAPS flow enhancements in this time period. At the time the first streamer is observed, the radar measured a l-o-s flow increase of ~100 m/s. The second streamer is observed at ~4 UT together with a further flow enhancement. Interestingly, the third streamer is associated with a new westward flow enhancement and an equatorward penetration of the flow, extending from ~62° mlat to ~56° mlat. The fourth and last streamer is associated with a similar flow enhancement of ~ 100 m/s, and we also observed an equatorward penetration of these flows.

Figure 4.4j-k shows data from the DMSP 17 satellite in which the equatorward boundary for this event was identified to be at ~63° mlat based on a sharp drop of ~1 keV electron fluxes. The trajectory of DMSP 17 can be seen in Figure 4.4a. The location of the equatorward boundary indicates that the observed flows are indeed in the subauroral region and comprise the SAPS flows.

The three events described above show two different types of events: isolated streamer events (events one and two, figures 4.2 and 4.3) and a more active case in which a series of streamers are observed within the ASI FOV (event three, figure 4.4). The third event is similar to the Makarevich et al. [2011] event in a sense that multiple flow enhancements were detected during the substorm expansion phase. In all cases, these events are associated with SAPS westward flow enhancements.

Figure 4.5 shows another type of event that occurred on March 30, 2013. In this case, proton aurora intensifications were observed in association with auroral streamers. This type of association was reported by Nishimura et al. [2014]. In this case, the available ASIs were Chibougamou (CHBG) and Kapuskasing (KAPU). On top of the ASIs, we have plotted the flows from the mid-latitude radar fhe. In panel a, weak uniform flows can be seen at the time when the aurora was quiet within the ASI FOV. At 01:22:15UT (Panel b), a faint auroral streamer can be seen propagating equatorward while a westward flow enhancement is observed within the radar FOV. Nearly two minutes later (Panel c), a diffuse east-west auroral structure is observed equatorward of the auroral oval. This can be identified as subauroral proton aurora because the electron oval was located above 62 MLAT based on DMSP data (see below), and the isolated and transient nature of the aurora as shown by Sakaguchi et al. [2007]. Panel d shows more auroral streamers propagating equatorward together with a further westward flow enhancement. A new proton aurora intensification is observed in panel e at 01:33:15UT. In panel f, it is possible to identify the equatorward edge of the auroral streamers at the same time as the radar measured westward flow enhancement. Several minutes later a last proton aurora intensification is observed in panel g. Panel h shows the decrease of the flows in absence of auroral streamers or proton aurora intensifications.

Figure 4.6a-e shows the time series plot that summarizes the event described in Figure 4.5. The first three panels (a, b and c) show keograms from the CHBG and KAPU stations. Panels d and e correspond to fhe beam 09 and 10, respectively. Initially, an auroral streamer was observed propagating equatorward and in connection with a proton aurora intensification (highlighted with the magenta dashed line in the panels a and b). At the same time, an eastward flow enhancement is observed within fhe radar beam 09 and 10 (indicated by the pink vertical line). Sometime later, a new aurora structure is observed in the keograms associated with a new proton aurora intensification as shown in the keogram from KAPU station (panel b). At the same time, a westward flow enhancement is observed by the radar beams. The last proton aurora intensification is observed first at the eastward station, CHBG, and then in KAPU ASI. At this time the radar measured a further increase in the l-o-s flow velocity. Figure 4.6f-g provides the DMSP 17 satellite data in the southern hemisphere that was used to identify the equatorward boundary. From the data, we determined that the southern hemisphere equatorward boundary is located at ~-60° mlat; this boundary was traced from the southern hemisphere to the northern hemisphere using Tsyganenko 2001 as an external model and the International Geomagnetic Reference Field (IGRF) model for the Earth's magnetic field. From this analysis, it was determined that the equatorward boundary is located at ~62° mlat in the northern hemisphere. Thus most of the enhanced flows can be identified as SAPS flows.

The last event in this case study corresponds to an uncorrelated event that occurred on March 10, 2011. Figure 4.7 shows a temporal sequence in which an auroral streamer is observed in absence of westward flow enhancement. The available ASIs in this event were Rankin Inlet

(RANK), Gillam (GILL), Fort Smith (FSMI), Forth Simpson (FSIM) and The Pas (TPAS). This event is notable for its good echo coverage from the mid-latitude SuperDARN radars (specifically cvw, cve, fhw, and fhe). Panel a shows an initial and relatively quiet auroral oval, with a clear poleward (~68° mlat) and equatorward (~63° mlat) boundaries. The mid-latitude radars measured uniform flows of ~0 m/s in the l-o-s direction. In panel b, an auroral streamer propagated towards the equatorward boundary roughly 45 seconds later. At this time the mid-latitude radars did not measure any change in the ionospheric flows. Next, the auroral streamer propagates further equatorward and reached the optical equatorward boundary at ~63° mlat without changes in the radar measurements (Panel c). The same streamer bifurcates and propagates east and west in panels d, e and f. It should be noted here that the mid-latitude radars did not detect any significant (>50 m/s) flow change during the whole duration of this event in spite of the clear streamer activity.

4.2.2 Statistical Study

Using 104 streamer-flow conjunction events in which the electron equatorward boundary was clearly identified, analyses were conducted to determine if the association between westward SAPS flow enhancement and auroral streamers is common. To accomplish this, we started first by looking for auroral streamers in the data set and then we analyzed the ionospheric flows from the radar data. A reverse study was also performed in which all flow enhancements higher than the threshold were identified, and then the corresponding auroral conditions at the time of the flow enhancement were examined.

The pie charts in figures 4.8a and 4.8b show the distribution of events for the forward and reverse studies. From figure 4.8a, (1) Forward Study: 63 events total, 98% (62 events) correlated, and 2% (1 event) uncorrelated. Thus streamers almost always lead to SAPS enhancements. From figure 4.8b, (2) Reverse Study: 103 events total, 60% (62 events) occurrence for flow enhancements associated with streamers, 37% (38 events) were not correlated with streamers but were associated with IMF southward turnings and an equatorward motion of the auroral equatorward boundary, implying an enhancement in the large-scale convection, which was seen when sufficient radar echoes were available; 2% (2 events) correspond to shock events, having structured large-scale convection flows; and 1% (1 event) in which flow enhancement was observed in absence of auroral structures, IMF southward turning or interplanetary shock events. Thus streamers and enhanced convection nearly equally contributes to SAPS flow enhancements. For events without direct solar wind triggering, streamers are important. No events at substorm onset.

The uncorrelated events subsequently were grouped into four sub-categories: 1. Streamers without flow enhancement (from the forward study, for an example refer to Figure 4.6). We have found only one event that fell into this category, comprising only 2% of the uncorrelated cases. We obtained the other three uncorrelated subcategories from the reverse study. 2. Enhanced large-scale convection corresponded to 91% of the uncorrelated subcategory (38 events) 3. Interplanetary shock events, in which two events were observed, comprising 5% of the uncorrelated cases. 4. Flow enhancement without streamers, for which only one event was observed (2% of the uncorrelated cases). Table 4.1 summarized the results for the subcategories of uncorrelated events.

In addition, for the correlated events we have characterized ionospheric flow enhancements and streamers. Median properties are summarized in Table 4.2. The average westward SAPS flow enhancements are 713 m/s, with a typical flow duration (for isolated and non-isolated streamer events) of 55 min. Here, the duration was calculated as the time period between the flow velocity exceeding 50 m/s and falling below 50 m/s with respect to a preceding background flow velocity. For isolated events, this correspond to the duration of a SAPS flow enhancement, while a group of SAPS enhancements is counted for non-isolated streamer events. This approach was chosen because it is difficult to determine the duration of individual SAPS flow enhancements when multiple flow enhancements occur as in the Figures 4.4 and 4.6 cases. This flow duration is comparable to the streamer duration (isolated and non-isolated), which is 57 minutes. Additionally, the median flow duration for the isolated cases (8 min) is comparable to the isolated streamer event duration (7 min) and a typical streamer intensity reaches almost 8000 count/s. To measure the streamer orientation, the north-south direction was defined as 0° and east-west direction as 90°. Before reaching the equatorward boundary, the measured streamer orientation is roughly north-south with a slight tilt to northeast (8.8°). For the streamers that are able to be measured after reaching the equatorward boundary, the average orientation is 87° (almost an east-west alignment). Finally, the azimuthal extent of streamer activity is ~1.7 hours in MLT.

The correlation between westward SAPS flow speed and streamer intensity is shown in Figure 4.8c. We have found a weak correlation between these two parameters (r2=0.3). This indicates that intense flow bursts in the plasma sheet (intense streamers) tend to drive intense SAPS flows probably by enhancing the ring current pressure more than by weak flow bursts. Figure 4.8d shows a correlation between flow duration and streamer duration for all the events. The correlation is remarkably high (r2=0.8), meaning that the duration of plasma sheet flow bursts determines the duration of enhanced SAPS flow enhancements (or a group of flow enhancements).

4.3 Discussion and conclusions

While a quasi-steady picture of SAPS has been well documented, subauroral ionospheric flows often show large variabilities, and it has not been fully understood what drives transient SAPS flow enhancements. In this section we evaluated the connection of these characteristic phenomena in the auroral and subauroral regions by taking advantage of the high-resolution simultaneous observations from the THEMIS ASIs and SuperDARN radars. Additionally, we determined the influence of plasma sheet flow bursts, as seen via auroral streamers, on SAPS flow evolution to understand the role of transient flows in the plasma sheet in driving the subauroral ionosphere and its conjugate region within the magnetosphere.

By selecting 104 events from December 2007 to April 2013, we found that 60% for our events SAPS flow are associated with auroral streamers. Our analysis revealed that typically before the streamers are present within the ASI, the radars measure a uniform flow of ~0-100 m/s. Once the streamers are observed closer to the radars FOV, the flow increases to ~700 m/s on average. Streamers then propagate equatorward and drift westward in the pre-midnight region following the large-scale convection pattern. When the streamers no longer appear closer to the radars FOV we observed a decrease in westward flow velocity.

The remaining 40% of the events corresponds to uncorrelated cases in which westward flow enhancements are not associated with streamers; most of these events (90%) are composed of enhanced convection events. These events typically present changes in the IMF conditions (southward turnings) and a southward propagation of the auroral oval equatorward.

We have also characterized typical parameters of auroral streamer and SAPS flow enhancements for the aforementioned correlated events. In doing so, we determined that a good correlation exists between streamer duration and flow duration for isolated and non-isolated events (r2=0.8). In addition, we established a rough correlation (r2=0.3) between westward flow enhancement and streamer intensity. The high occurrence probability and high correlation between streamers and SAPS flows indicate that plasma sheet-inner magnetosphere-subauroral ionosphere coupling by transient fast flows is important for driving transient SAPS flow enhancements.

Our previous studies suggest a three-flow structures associated with streamers at auroral latitudes [Gallardo-Lacourt et al., 2014], in which an equatorward flow enhancement is located to the east of the streamer and surrounded by two poleward flow enhancements. Figure 4.9 shows a schematic illustration of our proposed flow system associated with the auroral streamer and its relationship with the SAPS flows. At higher latitudes, the flows within the auroral oval are consistent with the description above (i.e. an equatorward flow enhancement surrounded by two poleward flow enhancements). The auroral streamer then propagates to lower latitudes with part of the equatorward flow enhancement located to the east. Once the streamer reaches the equatorward boundary and turns westward following the large-scale convection pattern in the pre-mid-night sector, the corresponding equatorward flow enhancement also turns westward to follow the streamer and consequently produces a transient increase in the SAPS region flows.

Our analysis is supported by MSP and DMSP satellite data to clearly identify the equatorward boundary. The observed flow enhancements are located equatorward of the auroral emissions; therefore, these flows are detected in the suburoral ionosphere. These results suggest that ring current modulations are due to particle injections into the inner magnetosphere, and that the ring current is highly variable. This variability is associated with auroral streamers and westward SAPS flow enhancements.

Subcategory of uncorrelated events	Percentage (%)	# of events
Streamer without flow enhancement	2	1
Flow enhancement without streamer	2	1
Enhanced convection events	91	38
Interplanetary shock events	5	2

Table 4.1. Subcategories of uncorrelated events. First column represents the percentage of uncorrelated cases and second column corresponds the number of events.

	Average value
Westward SAPS flow speed	713 m/s
Flow duration (all events)	55 min
Flow duration (isolated events)	8 min
Streamer activity duration (all events)	57 min
Isolated Streamer duration	7 min
Streamer intensity	7829 count/s
Streamer orientation before turning	8.8°
Streamer orientation after turning	87.1°
Azimuthal extent of streamer activity	1.67 h mlt

Table 4.2. Average values of characteristic parameters for SAPS flow enhancements and auroral streamers for correlated events.

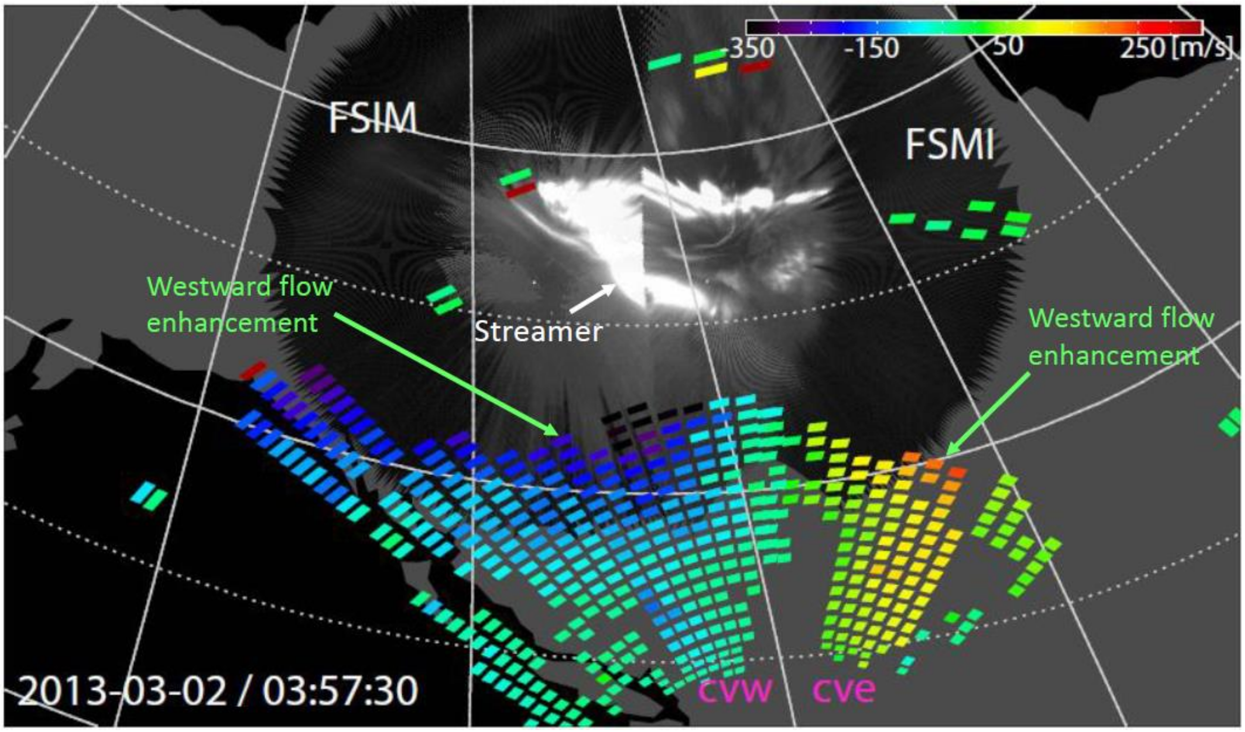

Figure 4.1. Coordinated observations from THEMIS ASIs and SuperDARN radars showing l-o-s flows at subauroral latitudes on March 2, 2013. The ASIs used here are FSIM and FSMI and we have overlaid two midlatitude SuperDARN radars, *cvw* and *cve*. The color scale represents the l-o-s flow velocity measured by the radars. In this time frame, an auroral streamer is observed propagating equatorward. At the same time westward flow enhancements are observed within the radar FOV. Notice that a westward flow enhancement appears as a positive flow (towards the radar) in the eastward looking radar (*cve*) and as a negative flow (away from the radar) in the westward looking radar (*cvw*).

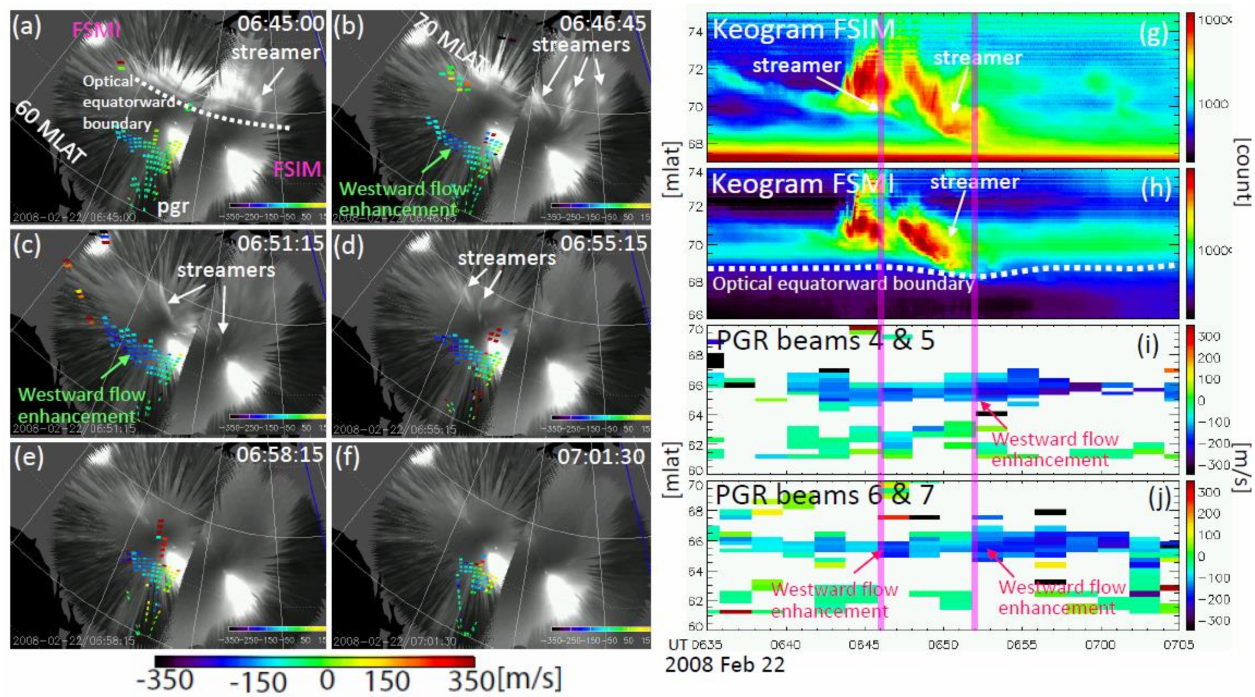

Figure 4.2. (a-f) Temporal evolution of SAPS flow enhancements associated with auroral streamers on February 22, 2008. The white arrows indicate the location of the streamers. The color scale corresponds the l-o-s flow velocity measured by *pgr* SuperDARN radar. (g-j) From top to bottom, the panels show two keograms (north-south slice in the imager) from FSIM and FSIM, respectively. Third and fourth panel show the combined averaged value of *pgr* radar l-o-s flow velocity for beams beams 4 and 5, and 6 and 7, respectively. The pink vertical line indicates the time when we observed westward flow enhancements.

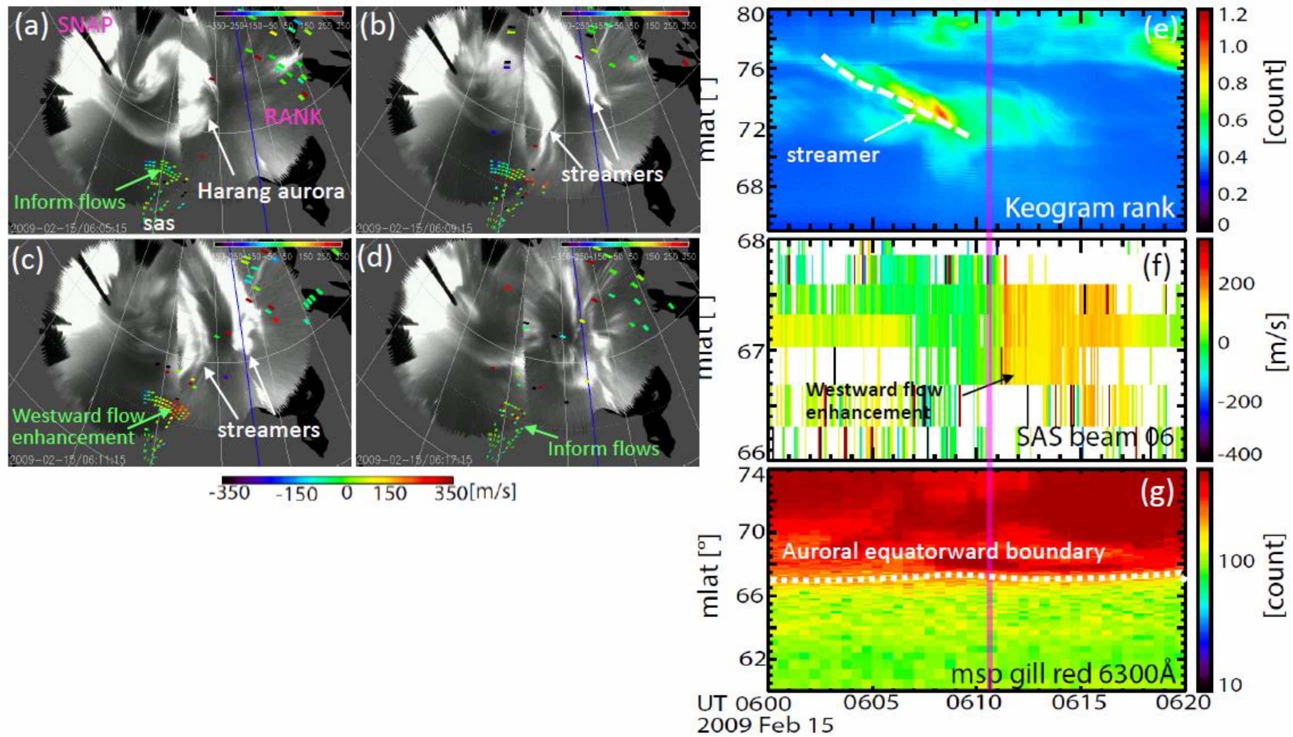

Figure 4.3. (a-d) Temporal evolution of SAPS flow enhancements associated with an isolated streamer event on February 15, 2009. White arrows indicate the location of the streamer and the Harang aurora. The color scale corresponds the l-o-s flow velocity measured by *sas* SuperDARN radar. (e-g) From top to bottom, the panels show a keogram from rank ASI. Second panel correspond to the sas beam 06 l-o-s flow velocity, operating in high temporal resolution 6s THEMIS mode. Third panel show Gillam (gill) MSP red light 6300 Å, here the horizontal white dashed line indicated the location of the equatorward boundary. The pink vertical line indicates the time when we observed westward flow enhancements.

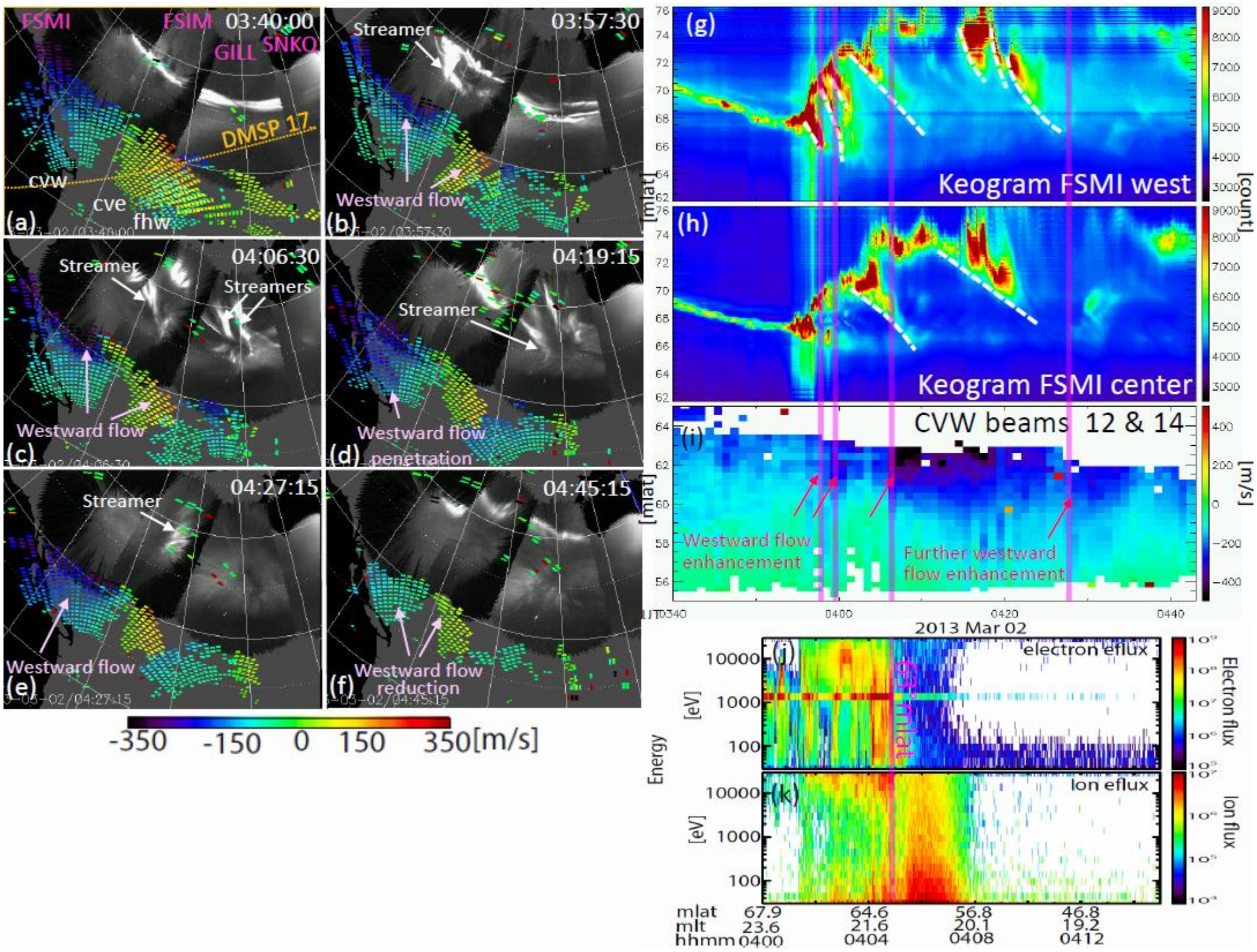

Figure 4.4. (a-f) Temporal evolution of SAPS flow enhancements associated with several auroral streamers (non-isolated event) on March 02, 2013. White arrows indicate the location of the streamers. Orange dash line correspond to the DMSP 17 satellite track. The format is the same as in figure 3. (g-i) From top to bottom, the first and second panels show two keograms from FSMI ASI west and central, respectively. Third panel shows the combined averaged value of *cvw* radar l-o-s flow velocity for beams beams 12 and 14. The pink vertical line indicates the time when we observed westward flow enhancements. (j-k) From top to bottom the panels represents the energy flux for electrons and ions measured by DMSP 17. Pink vertical line indicates the location of the electron equatorward boundary at 63° mlat.

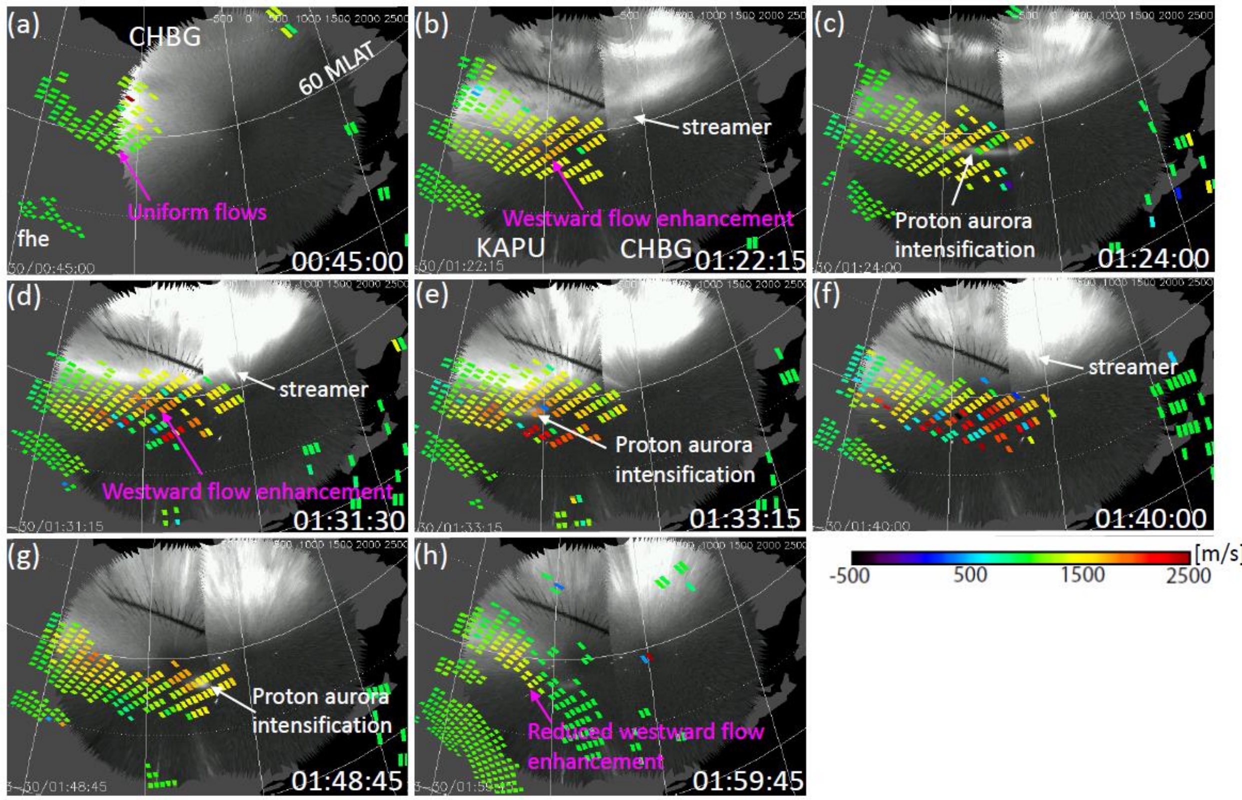

Figure 4.5. Temporal evolution of SAPS flow enhancements associated with auroral streamers and proton aurora intensifications on March 30, 2013. The format is the same as in figure 3.

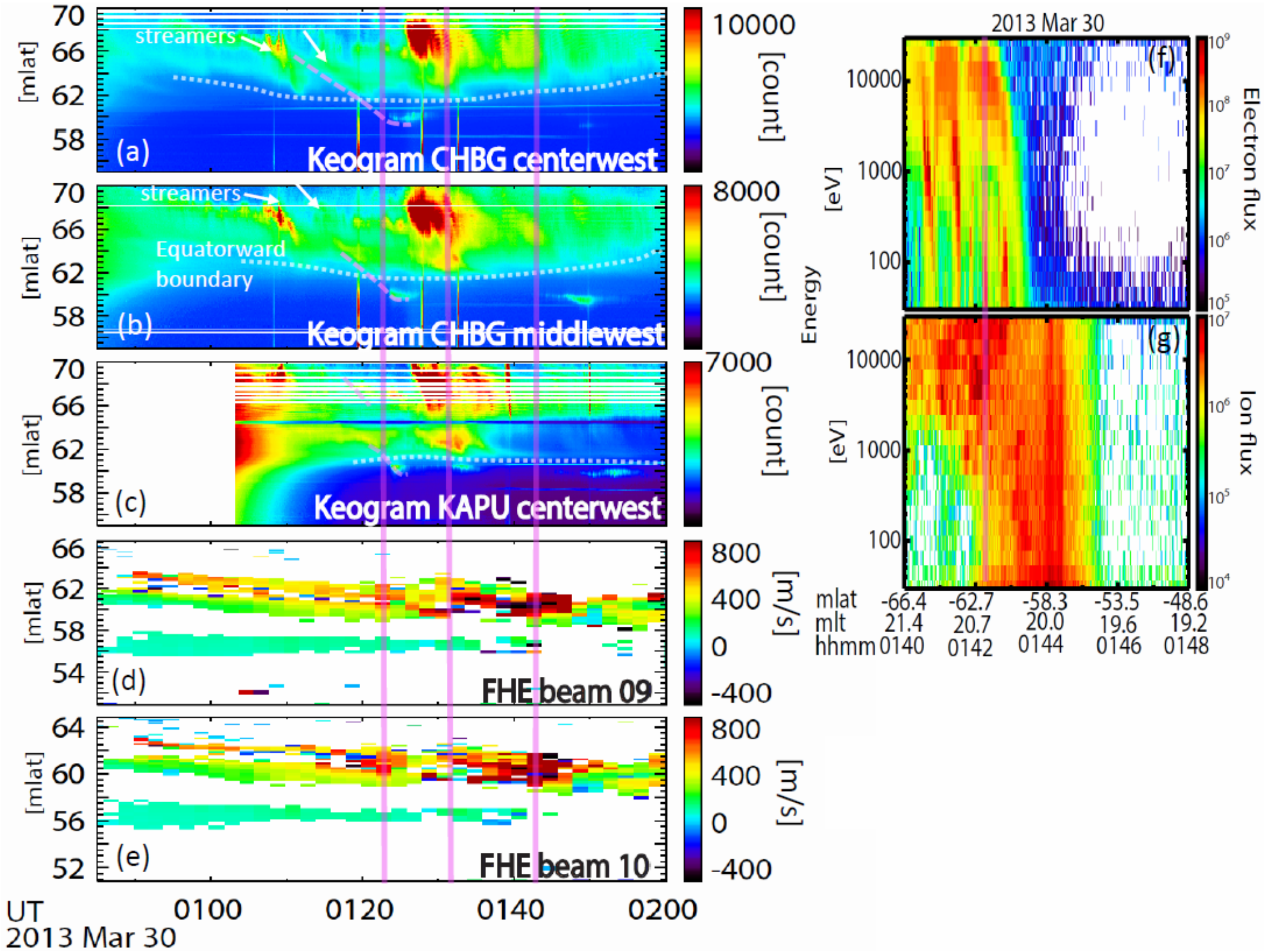

Figure 4.6. (a-e) Time series of the of SAPS flow enhancements associated with auroral streamers and proton aurora intensifications on March 30, 2013. From top to bottom the panels represent two keograms from CHBG ASI station centerwest and middlewest. Third panel shows a keogram from KAPU ASI. Fouth and fifth panel respresent the *fhe* radar l-o-s flow velocity for beams beams 09 and 10. (f-g) From top to bottom the panels represents the energy flux for electrons and ions measured by DMSP 16. Pink vertical line indicates the location of the electron equatorward boundary at 62.5° mlat in the southern hemisphere (~62° mlat when mapped to the northern hemisphere).

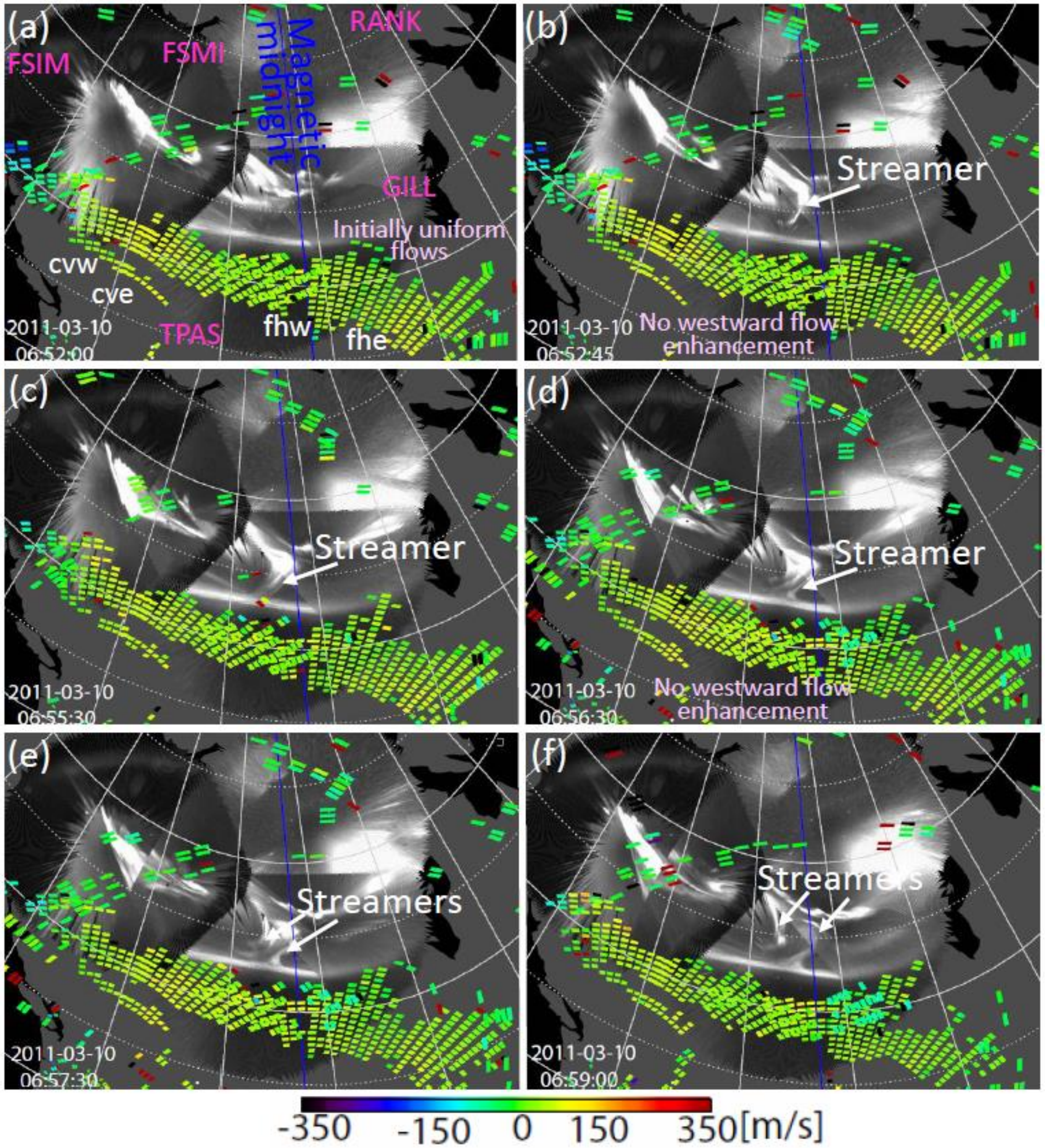

Figure 4.7. Temporal evolution of an uncorrelated event. In the sequence we observed an auroral streamer in absence of SAPS flow enhancement on March 10, 2011.Blue line correspond to magnetic midnight. The format is the same as in figure 3.

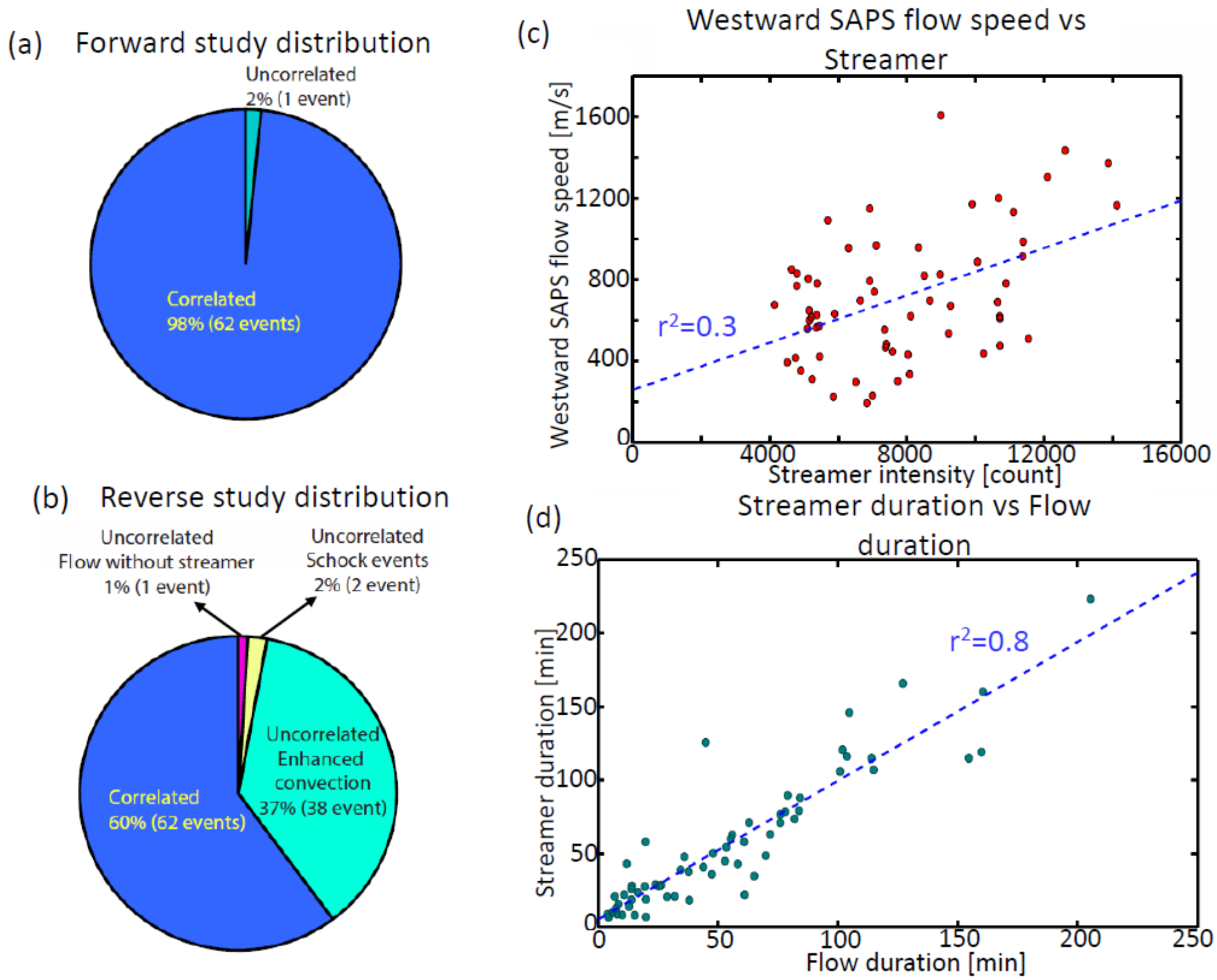

Figure 4.8. (a-b) Pie charts indicating the distribution of events for forward and reverse study respectively. (c) Westward SAPS flow enhancements as a function of streamer intensity. (d) Streamer duration as a function of flow duration.

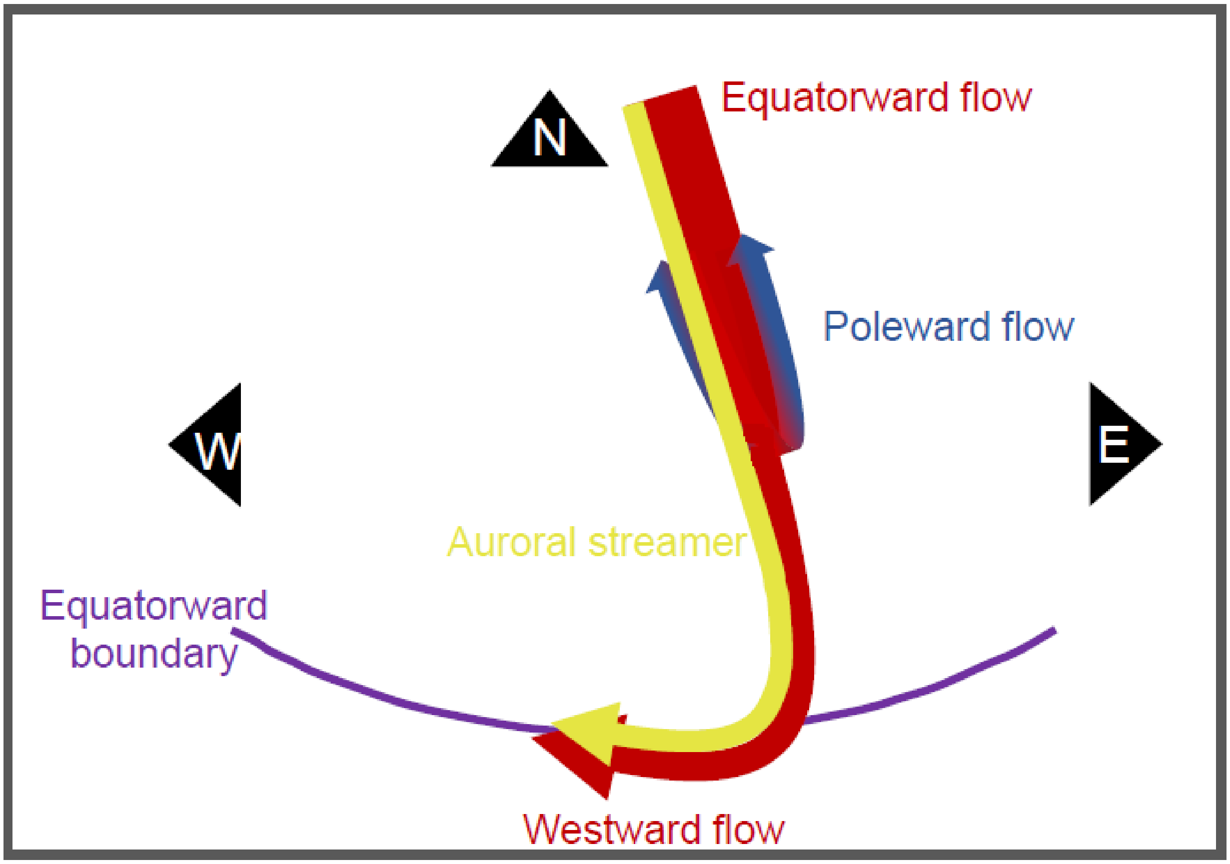

Figure 4.9. Schematic illustration of the association between auroral streamers and flow enhancements in the auroral and subauroral ionosphere.

CHAPTER 5

Summary and Concluding Remarks

The ultimate goal of this Ph.D. research is to analyze the contribution of mesoscale ionospheric flows at auroral and subauroral latitudes. In order to achieve this, during the first part of this Ph.D. thesis we have: (1) Analyzed and characterized ionospheric flows associated with auroral streamers, by using THEMIS ASIs and SuperDARN radars between 2007 and 2010; (2) Examined high resolution data to established the ionospheric flow pattern associated with substorm auroral onset beads. We have used THEMIS ASIs and SuperDARN THEMIS mode (6s resolution) data; (3) analyzed the influence of auroral streamers on rapid evolution of auroral streamers by using THEMIS ASIs, SuperDARN radars, MSP and DMSP satellite data.

.

5.1 Coordinated SuperDARN-THEMIS ASI observations of mesoscale flow bursts associated with auroral streamers

We investigated statistically the properties of ionospheric flows related to auroral streamers, by selecting 135 isolated streamers roughly aligned with the radar l-o-s directions,

1. We found that all streamers are correlated with fast flows around the streamers, and most of them were directed equatorward.
2. The equatorward flows invariably lie just to the east of their respective streamer. While observed less frequently, we found evidence for two poleward flows to the east and west of the equatorward flow, giving a three-flow structure as illustrated in Figure 2.8.
3. The western edge of the equatorward flow is collocated with the streamer, which highlights an upward FAC sheet. While the eastern edge of the equatorward flow does not have any auroral emission, it is likely the location of a downward FAC sheet that is a counterpart of the upward FAC.
4. We calculated the azimuthal width of the equatorward and poleward flow enhancements obtaining an average of about 74km for both cases.
5. We also calculated the azimuthal shift of the maximum flow speed relative to the maximum intensity of the streamer obtaining an average of 58km for both equatorward and poleward flow enhancements.
6. The flow structure we found is consistent with MHD simulations [Birn et al., 2004] and multi-satellite observations [Keiling et al., 2009] during BBFs in the plasma sheet. Our results suggest that ground-based observations are quite useful for identifying the 2-D structure of localized flows and FACs that cannot be easily obtained by in situ observations in the plasma sheet.
7. We have mapped the flow channel widths for the case studies from the ionosphere to the magnetosphere using Tsyganenko 2001 as an external model and the

International Geomagnetic Reference Field (IGRF) model for the Earth's magnetic field, and we obtained an average flow channel width of 1.5RE.

5.2 Ionospheric flow structures associated with auroral beading at substorm auroral onset

We identified the flow structure associated with the auroral beading observed at substorm onset.

1. In all three of our events over North America, we found extremely fast (~1000 m/s), longitudinally narrow, flows with a strong flow shear simultaneously with the initiation of the auroral beading.
2. We have found excellent temporal and spatial correlations between the beading and the alternation of fast equatorward and poleward flows.
3. For the event in Iceland (eastward-looking radar beams), westward flow perturbations were associated with eastward propagating beads, although the flow magnitude (~100 m/s) was much smaller than the north-south flows found in the north-south looking beam events.
4. The measured flow oscillations observed in all the events can be interpreted as a spatial structure passing across the radar beam that maintain its wavy pattern as it grows in time for several wave periods.

5. Clockwise flow shears are associated with upward FACs in the center of the flow shear and can be seen as the auroral beads, and counter-clockwise flow shears between the beads are associated with downward FAC.
6. An important feature is the clear difference between the flow magnitudes measured in the north-south (N-S, events 1-3) direction compared with the east-west (E-W, event 4) direction, with the azimuthal component of the flows being significantly slower than that in the north-south orientation. A possible explanation for the difference observed in the N-S and E-W flows is that the N-S flows are confined to a longitudinal width that is much shorter than the latitudinal extend of the flows. The broad latitudinal extent of the N-S flows is an indication that the E-W flows connecting to these N-S flows extend substantially poleward and equatorward of the onset arc.
7. We roughly estimated the magnetotail size of the observed structure by mapping the beads observed by the all-sky cameras to the equatorial plane using the Tsyganenko 2001 magnetic field model. We obtained an azimuthal wavelength of ~1800 km (0.28 Re), similar to what was obtained by Motoba et al. [2012].
8. The latitudinal extent of the flow oscillation in the ionosphere is ~3.5° or larger (limited by the echo coverage), corresponds to >~4R_E extension in the x-direction in the magnetotail, although this number likely has a large uncertainty that depends on the magnetic field configuration.
9. The present study suggests that the substorm onset process involves formation of fast earthward/tailward flow structures

10. Our result indicates that ballooning interchange instability (BICI) modes may be a viable candidate for the instability that is responsible for the auroral beading and initiates the auroral onset. We, however, do not rule out other potential mechanisms for substorm onset, and more quantitative comparisons are needed for determining the onset mechanism.

5.3 Influence of auroral streamers on rapid evolution of SAPS flows

We evaluated the connection of these characteristic phenomena in the auroral and subauroral regions by taking advantage of the high-resolution simultaneous observations from the THEMIS ASIs and SuperDARN radars. Additionally, we determined the influence of plasma sheet flow bursts, as seen via auroral streamers, on SAPS flow evolution to understand the role of transient flows in the plasma sheet in driving the subauroral ionosphere and its conjugate region within the magnetosphere. Our study therefore shows the importance of plasma sheet-inner magnetosphere-subauroral ionosphere coupling by fast flows.

1. We found that 60% for our events SAPS flow are associated with auroral streamers.
2. Our analysis revealed that typically before the streamers are present within the ASI, the radars measure a uniform flow of ~0-100 m/s. Once the streamers are observed closer to the radars FOV, the flow increases to ~700 m/s on average. Streamers then propagate equatorward and drift westward in the pre-midnight region following the large-scale convection pattern. When the streamers no

longer appear closer to the radars FOV we observed a decrease in westward flow velocity.

3. The remaining 40% of the events corresponds to uncorrelated cases in which westward flow enhancements are not associated with streamers; most of these events (90%) are composed of enhanced convection events. These events typically present changes in the IMF conditions (southward turnings) and a southward propagation of the auroral oval equatorward.
4. We have also characterized typical parameters of auroral streamer and SAPS flow enhancements for the aforementioned correlated events. In doing so, we determined that a good correlation exists between streamer duration and flow duration for isolated and non-isolated events (r^2=0.8). In addition, we established a rough correlation (r^2=0.3) between westward flow enhancement and streamer intensity.
5. We have proposed a flow system in which at higher latitudes, the flows within the auroral oval are consistent with the description above (i.e. an equatorward flow enhancement surrounded by two poleward flow enhancements). The auroral streamer then propagates to lower latitudes with part of the equatorward flow enhancement located to the east. Once the streamer reaches the equatorward boundary and turns westward following the large-scale convection pattern in the pre-mid-night sector, the corresponding equatorward flow enhancement also turns westward to follow the streamer and consequently produces a transient increase in the SAPS region flows.

6. Our analysis is supported by MSP and DMSP satellite data to clearly identify the equatorward boundary. The observed flow enhancements are located equatorward of the auroral emissions and measured electron precipitation; therefore, these flows are detected in the suburoral ionosphere.
7. These results suggest that ring current modulations are due to particle injections into the inner magnetosphere, and that the ring current is highly variable. This variability is associated with auroral streamers and westward SAPS flow enhancements.

APPENDIX A

Additionally, during the course of this Ph.G. research, a study on external triggering of substorms was conducted; although the results of this study are not included in the main section of this thesis, they can be found in this appendix.

External triggering of substorms identified using modern optical versus geosynchronous particle data

An important question for understanding substorms is whether substorm onset is the result of a change in the external conditions or is the result of an instability that is purely internal to the magnetosphere. The primary external factor that has been considered as a cause of onset is a turning towards the north in the direction of the IMF, since the IMF direction is the dominant modulator of the strength of solar wind coupling to the magnetosphere. However, there has been a long debate as to the extent to which substorms are externally triggered by IMF changes. Even after many reports of an association between northward turning of the IMF and substorm onset [Foster et al., 1971; Can et al., 1975, 1997; Rostoker et al. 1983; McPherron et al., 1986], cases without northward turning have also been presented [e.g., Henderson et al., 1996] and thus the external triggering of substorms is still a very controversial issue. Lyons et al. [1997] proposed quantitative criteria of the IMF B_z changes that are effective for substorm triggering (see section 2 for criteria details). Using the criteria, they found a high occurrence probability of triggering for a limited number of events (14 of 20 events, 70%).

Hsu et al. [2003] examined the triggering hypothesis using an onset list based on the *AL* index and Pi 2 pulsations. They used two different approaches, the Lyons et al. criteria and a visual inspection, which is essentially a relaxed version of the Lyons et al. criteria (see section 2 for details), and determined the occurrence of external substorm triggering. They obtained a remarkably high (60%) triggering percentage using the visual inspection, while it was much lower (33%) for the Lyons et al. criteria. This result suggests that the Lyons et al. criteria may be too strict for identifying triggering, or that triggering occurs less frequently than obtained by Hsu et al.

Statistical analysis related to events occurring randomly in space and time [e.g., Cox, 1955; Hsu et al., 2002] were used by Morley et al. [2007] to analyze the association between IMF triggering and substorm onsets, and they did not find significant evidence for triggering, in contrast to the finding by Lyons et al. A recent study by Newell et al. [2011] also showed a low occurrence probability (24%) of triggering using the same triggering criteria as used by Lyons et al. In their study, the triggering percentage for the onset list created by Frey et al. [2004] was compared to triggering percentages for completely random epochs, and quasi-random epochs. Similar triggering percentages were obtained for all three types, suggesting that northward turnings may not be a significant trigger for the substorm onset.

As can be seen in the studies mentioned above, the issue of substorm external triggering still remains controversial. Although the Lyons et al. criteria have been shown to give low triggering occurrences [Hsu et al., 2003; Morley et al., 2007; Newell et al., 2011] the attempt of the visual inspection by Hsu et al. suggests that more triggered events could be found by adjusting the triggering criteria. This would be plausible because the Lyons et al. criteria are based on a limited number of events and could indicate that triggering by northward turnings might indeed be important. In chapter 3 we examine the triggering hypothesis by applying three different triggering criteria to three different lists of substorms. We choose three different criteria because different criteria have been used in the above earlier studies, and it is not known which is the most realistic. Thus a result that holds for all of these criteria would indicate that the result is not dependent on the specifics of the criteria and is therefore more likely to be correct than a result that is found for only one set of criteria. The different onset lists identify substorms with different minimum strengths, smallest being by high-resolution ground-based imaging and largest being the traditional identification by large dispersionless geosynchronous particle injection events. We show that the triggering percentage is significantly higher when applying relaxed criteria and including IMF B_y triggering, suggesting that the external triggering could be common even while the Lyons et al. criteria give a low percentage. Furthermore, the large injection events are found to give higher triggering occurrence than the lists in which weaker substorm are included, indicating that triggering may be more likely for larger events and that the corresponding IMF orientation changes may be larger and thus more easily identified.

A.1 Data set and methodology

This study uses three different lists of substorm onsets. The THEMIS All Sky Image (ASI) list [Nishimura et al., 2010] includes 190 isolated auroral onset events obtained from November 2007 to April 2008. The THEMIS ASIs have the capability to detect substorm auroral onsets in high spatial and temporal resolution as well as high sensitivity. This advantage allows obtaining onset timing unambiguously and identifying weak substorms that maybe missed in the *AL* index and space-based auroral imaging. The ASIs can also distinguish other types of auroral disturbances (e.g. poleward boundary intensifications and auroral streamers) that lead to similar ground magnetic field perturbations as substorms. The present analysis focuses on isolated onsets, which occur more than 30 minutes after preceding onsets.

The second list of onsets used in this analysis is composed of substorm onsets observed by the IMAGE-FUV from May 2000 to December 2002 [Frey et al., 2004]. The FUV imager on board the IMAGE spacecraft provides global auroral imaging in the far ultraviolet. This list has a large number (2437) of events, which help to increase the statistical significance. This list was also used for the IMF triggering study by Newell et al. [2011].

The third list of onsets corresponds to 64 events of large electron injection from Los Alamos National Laboratory (LANL) geosynchronous energetic particle data obtained from January 2000 to April 2001. Here electron injections were analyzed using the Synchronous Orbit Particle Analyzer (SOPA) instrument which measures electrons from 50 keV to 26 MeV in 16 energy channels. Although the injection events do not have supportive auroral observations, rapid increases in energetic particle fluxes without energy dispersion are known as a substorm-related phenomenon [Reeves et al., 1996]. As a list of large substorm we selected large dispersionless injection events, where electron fluxes at one of the spacecraft for any two energy channels were enhanced by more than one order of magnitude. Dispersionless injections seen at more than one spacecraft where not included because they can result from the magnetospheric compressions from solar wind dynamic pressure enhancements. Solar wind parameters were obtained from the OMNI database with 1 min resolution.

We use three different set of criteria for external triggering of substorms. The first is based on the Lyons et al. [1997] criteria, and three major categories are established: B_z-triggered, B_y-triggered and non-triggered. B_z-triggered events represent clear northward turning of the IMF B_z by more than 2 nT with respect to the average value for the 20 min preceding the northward turning, and this point should be located within ±15 minutes of the onset time. B_z should be negative with a standard deviation less than 2 nT during the 20 minutes preceding the northward turning, and B_z should remain more than 2 nT above its average over the preceding 20 min for the 10 minutes following the northward turning. Figure A.1 shows an example satisfying these criteria. The panels show (a) the IMF B_y; (b) IMF B_z; (c) dynamic pressure and (d) *AL* index. This event shows a significantly large northward turning starting at 0522 UT and remaining elevated for more than 10 minutes. If an event does not satisfy the B_z criteria, it is considered if the magnitude of the IMF B_y decreases by at least 2 nT from its average over the preceding 20 min and remain decreased by at least 2 nT for 5 min. Also, the standard deviation of B_y must be less than 2 nT during the preceding 20 minutes. Events with a sign change in B_y are also counted if B_y changes by more than 4 nT. Figure A.2 provides an example of a B_y triggered event, the IMF B_z showing a ~2nT reduction starting at 0605 UT while the IMF B_z stayed essentially constant.

The rest of the events, which are classified as non-triggered, are divided into three subcategories: mostly south, mostly north and fluctuating. The mostly south subdivision corresponds to events where the IMF B_z remains negative for at least 75% of the 1-hour time period (±30 min) around the substorm onset time. The events are called mostly north if the IMF B_z is positive at least 75% of the 1-hour time period. Events that do not satisfy either of the above two criteria are called fluctuating. Figure A.3 presents examples of non-triggered events: (A) mostly south, (B) mostly north and (C) fluctuating.

We relax the Lyons et al. criteria for defining external triggering substorms in two ways. The first is based on the visual criteria proposed by Hsu et al. [2003]. Their criteria follow the Lyons et al. criteria except that a northward turning by 2 nT at one point is required to be detected within ±15 minutes of the substorm onset time and the IMF B_z should remain elevated by any magnitude for 5 minutes after the northward turning. Figure A.4 shows an example of a B_z-triggered event applying the criteria based on the visual criteria established by Hsu et al. [2003]. The northward turning occurring at 0520 UT has a change of ~3.5 nT and remains elevated for 6 minutes. This event is not counted in the Lyons et al. criteria because of the short duration of the elevated IMF but is included in the Hsu et al. definition.

As a further relaxation of the Lyons et al. criteria, we use the same requirements as for the Hsu et al. criteria above, but we do not require a steady southward IMF prior to the northward turning. However, a northward turning of the IMF B_z by more than 2 nT with respect to the average value for the 20 min preceding the northward turning is required. With this relaxation, a northward turning is counted as a trigger even if the preceding IMF is northward IMF. This allows for the possibility of a growth phase to develop under northward IMF, as can occur when there are large fluctuations in the IMF [Kim et al., 2009; Lyons et al., 2009], or when the IMF B_y is large. Figure A.5 illustrates an example showing a northward turning starting at 0221 UT with brief northward excursions prior to the northward turning.

A.2 Results

Tables A.1-A.3 show the results for the statistical study for the onset lists applying the three different triggering criteria. The rows represent the triggering percentage applying the criteria of Lyons et al. [1997]; Hsu et al. [2003] and Hsu et al. without requirement for the preceding southward IMF. The tables are divided into B_z-triggered, B_z or B_y-triggered and Non-triggered events. "B_z or B_y-triggered" includes the B_z-triggered events and By-triggered events defined in the previous section, and thus indicates the total IMF triggered events. The non-triggered category is divided into three subcategories mostly south, mostly north and fluctuating according to the definitions established above. The values in the tables represent percentages.

Table A.1 provides the results for the THEMIS ASI event list. The percentage of the B_z-triggered events is low (17%) for the Lyons et al. criteria, while it is significantly higher (27%) for Hsu et al. and (36%) for Hsu et al. without the requirement of the preceding IMF B_z. Similarly, the percentage of the B_z or B_y-triggered events increases from 22 to 41% with relaxing the criteria. The total percentage of non-triggered events conversely decreases from 78% for Lyons et al. to 59% for Hsu et al. without requirement for preceding IMF B_z.

Table A.2 provides the results for the list of onset from IMAGE-FUV. Consistently with the results in Table A.1, the percentage of the triggered events significantly increases with relaxing the triggering criteria. The percentage of the B_z-triggered events is limited to 22% for Lyons et al. This is a similar percentage as and thus consistent with the finding by Newell et al. [2011]. In contrast, the percentage is significantly higher for the Hsu et al. (32%) and relaxed Hsu et al. criteria (43%). The triggering percentage increases more when including the B_y-triggered events and reaches close to 50%.

The results above indicate that almost half of the substorm may be triggered by IMF orientation changes by considering the relaxed criteria. While we can not ascertain whether or not the Lyons et al. criteria are too strict to identify many IMF triggering, this is a possibility to explain the changes in the triggering percentage. However, the other half of the events cannot be explained by the triggering hypothesis unless triggering occurs under conditions not envisioned in previous studies.

It is interesting the triggering percentage is larger for all criteria for the IMAGE-FUV events than for the THEMIS ASI events, despite the effect that substorms are more accurately distinguishable from other auroral activation by the THEMIS ASI. However, the ground-based ASIs are far more sensitive to small substorm auroral activations than in the spacecraft IMAGE-FUV camera, suggesting that it may be easier to identify IMF triggers for larger events or that larger events are more likely to be triggered than are smaller events. To examine this possibility, we first considered the magnitude of the *AL* index drop associated with the onset However, perhaps due to the sparsity of *AL* stations, an *AL* dependence was not observed, and in fact little or no *AL* response was observed for many onsets. We thus examined the list of large geosynchronous dispersionless injections.

Table A.3 clearly shows that the percentage of the IMF triggering increases substantially as compared to Tables A.1 and A.2, the highest percentage reaching up to 63%. This result leads us to suggest that it may indeed be possible that IMF triggering may be easier to identify for larger events or that larger events are triggered than are smaller events. It also interesting that the percentage of non-triggering substorms that occur under mostly southward IMF conditions increases with substorm size, which is consistent with the idea that larger substorms are more likely to be non-triggered under southward IMF conditions than for the other IMF conditions.

A.3 Discussion and conclusions

We have evaluated the external substorm triggering by IMF orientation changes, using three different criteria and three substorm onset lists. We have found that the triggering percentage is limited to 17% and 22% when applying the Lyons et al. criteria for the THEMIS ASI and IMAGE-FUV event lists, respectively. The percentage increases slightly by including IMF B_y triggering. More interestingly, the relaxed triggering criteria, which follow the Hsu et al. method but without requirements for southward IMF prior onset, give significantly higher percentages, reaching close to 50% (41 and 48% for the THEMIS and IMAGE lists including the By triggering). Our analysis does not allow us to ascertain whether or not the relaxation of the criteria indicates that the real triggering percentage is larger than given by the Lyons et al. criteria. However, our results suggest that this is a possibility that this should be considered, particularly because the Lyons et al. criteria were based on very few events.

We have also investigated the substorm external triggering for large, dispersionless injections at the geosynchronous orbit, in order to examine if it is possible that the IMF variation leading to substorm can be more pronounced for large substorms. The triggering percentage is found to reach up to 63% for the relaxed criteria, and 34% even using the Lyons et al. criteria. This remarkable increase suggests that the external triggering can be more easily found for larger substorms than for smaller substorms, and possibility that warrants further considerations. This tendency leads us to suggest that it is possible that the triggering condition for some events in the THEMIS and IMAGE lists may be missed due to short duration changes and the artificial triggering conditions we have used. Our results suggest that more work is warranted on both determination of realistic triggering criteria and on the possibility that triggers are more easily identified, or triggering is more common, for larger than for smaller substorm events. We have also found evidence that larger substorms may be more likely to be non-triggered under mostly southward IMF conditions than for other IMF conditions.

	B_z	$B_z + B_y$	Non triggered: Mostly South	Mostly North	Fluctuating
(A) Lyons et al.	17	22	32	21	25
(B) Hsu et al.	27	33	31	17	19
(C) relaxed Hsu et al.	36	41	29	16	14

Table A.1. Percentages of IMF triggering for the THEMIS events. The first row (A) represents the results applying the Lyons et al. criteria. The second row (B) provides the triggering percentage applying the Hsu et al. visual criteria. The third row (C) shows the results applying the same criteria used in row (B) but without requirements for the preceding IMF B_z. The values in the tables represent percentages.

	B_z	$B_z + B_y$	Non triggered		
			Mostly South	Mostly North	Fluctuating
(A) Lyons et al.	22	30	38	18	14
(B) Hsu et al.	32	40	33	17	13
(C) relaxed Hsu et al.	43	48	33	6	13

Table A.2. Same as Table A.1 but for the event list from IMAGE-FUV.

	B_z	$B_z + B_y$	Non triggered		
			Mostly South	Mostly North	Fluctuating
(A) Lyons et al.	34	42	44	6	8
(B) Hsu et al.	40	54	33	6	7
(C) relaxed Hsu et al.	41	63	27	5	5

Table A.3. Same as table A.1 but for the large dispersionless injections.

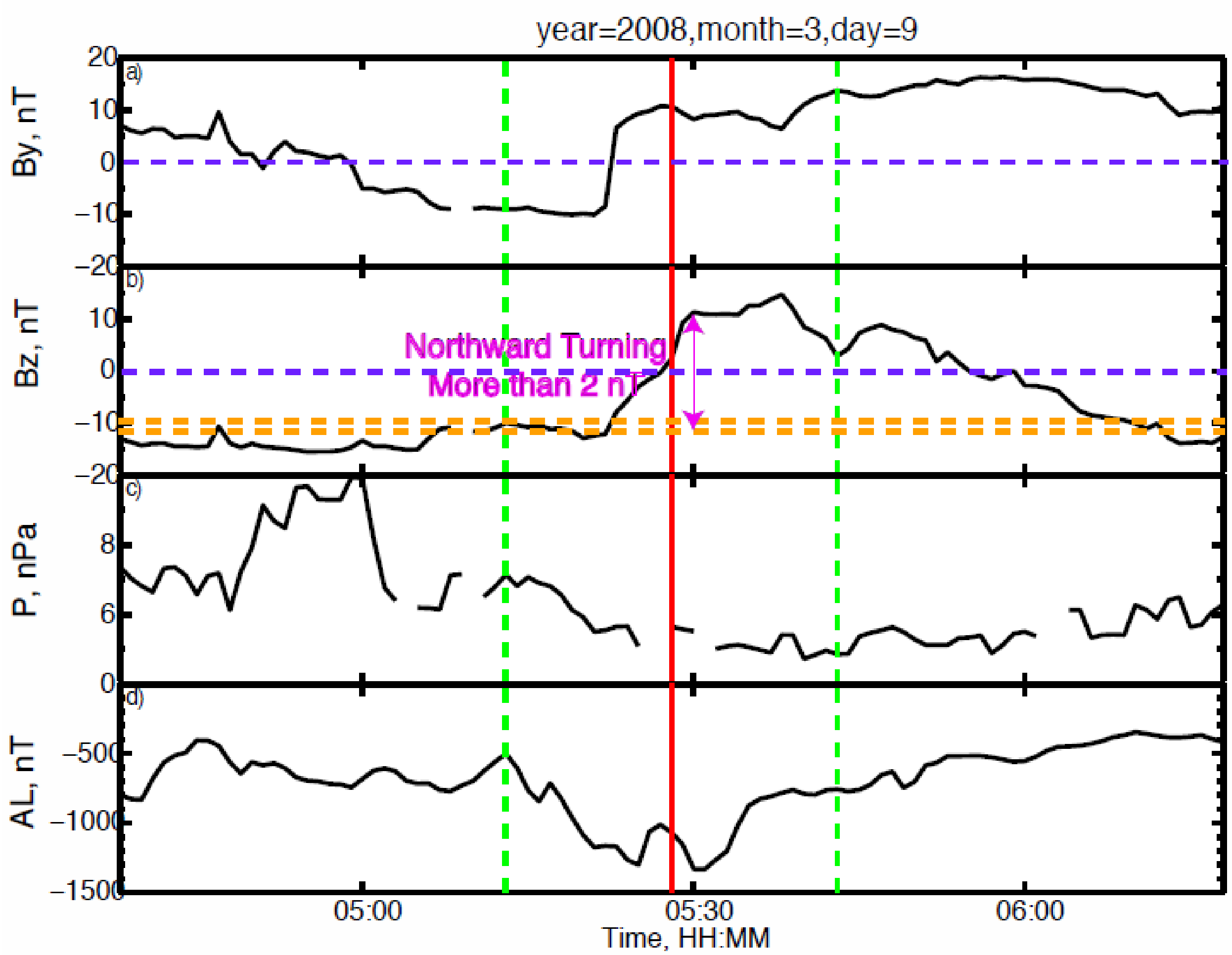

Figure A.1. Example of a Bz-triggered event applying the criteria based on Lyons et al. The first panel (a) represents By, (b) shows Bz, (c) indicates dynamic pressure and (d) AL index. The red line indicates the onset time. The two vertical green lines indicate ±15 min around the onset time. The horizontal orange lines indicate a 2 nT change of the IMF Bz starting at the initial point of the northward turning. The horizontal blue line indicates the location of zero for reference.

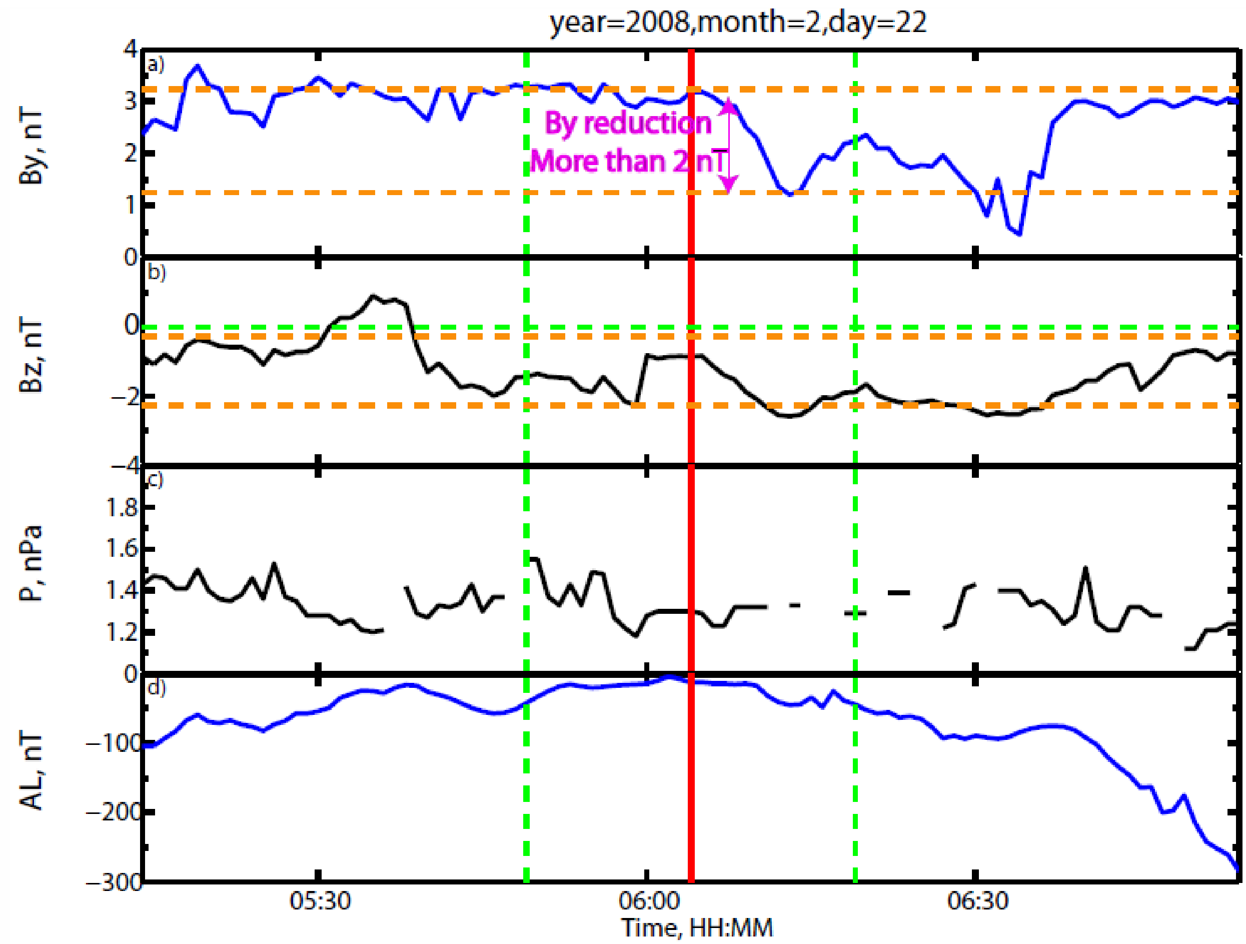

Figure A.2. Example of a By-triggered event in the same format as Fig. A.1.

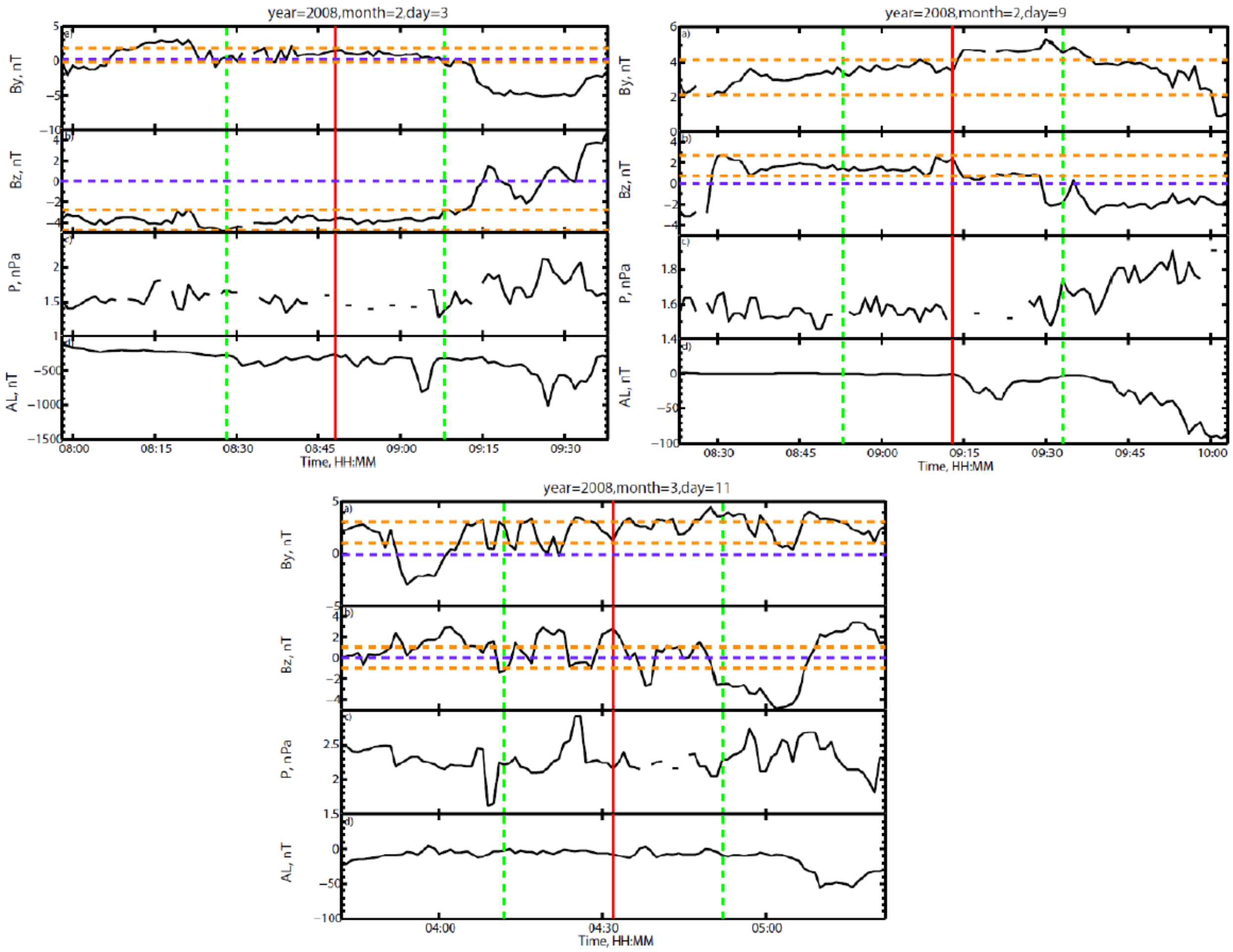

Figure A.3. Examples of Non-triggered events in the same format as Fig. A.1.

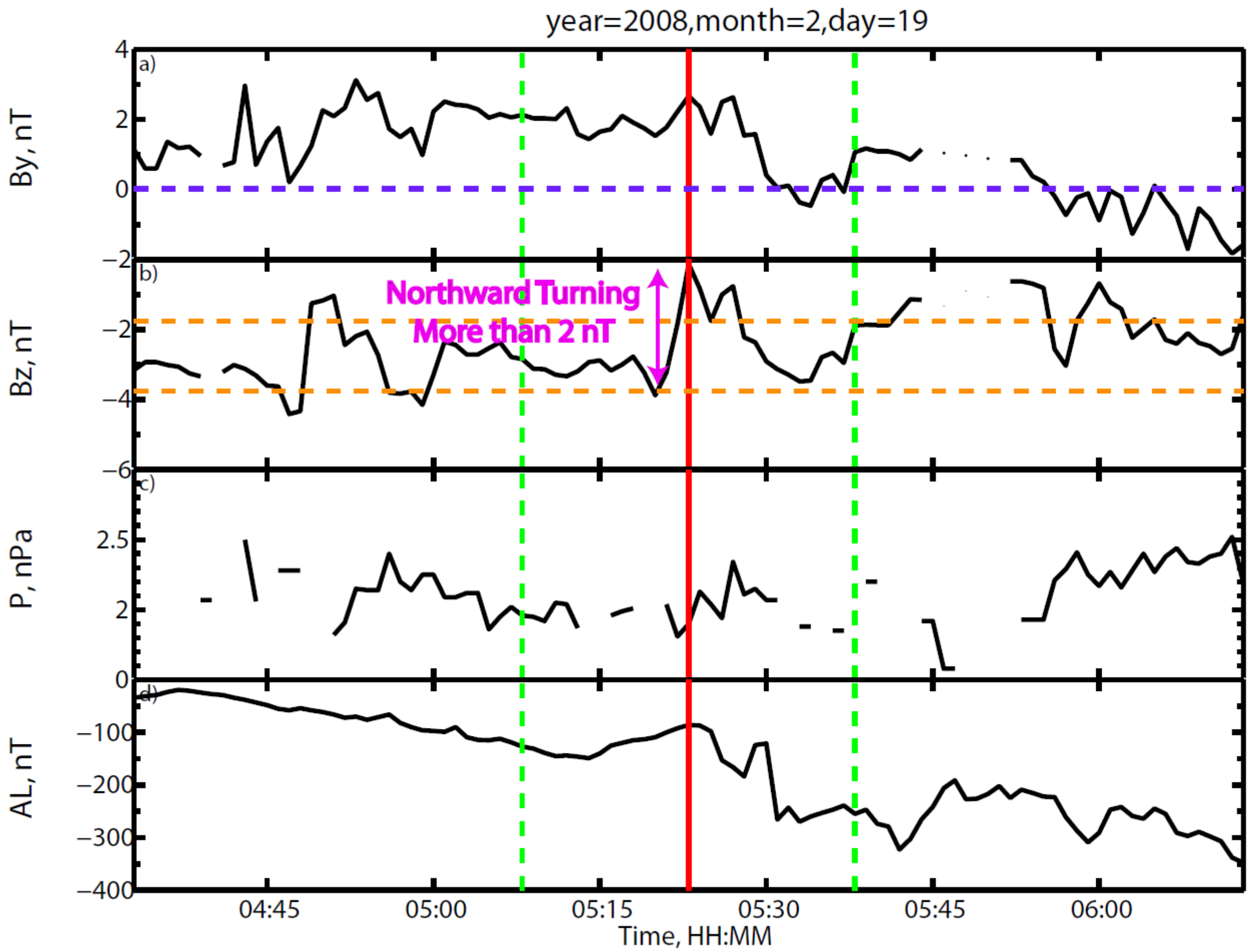

Figure A.4. Example of a B_z-triggered event applying the criteria based on Lyons et al. and the visual criteria in Hsu et al. in the same format as Fig. A.1.

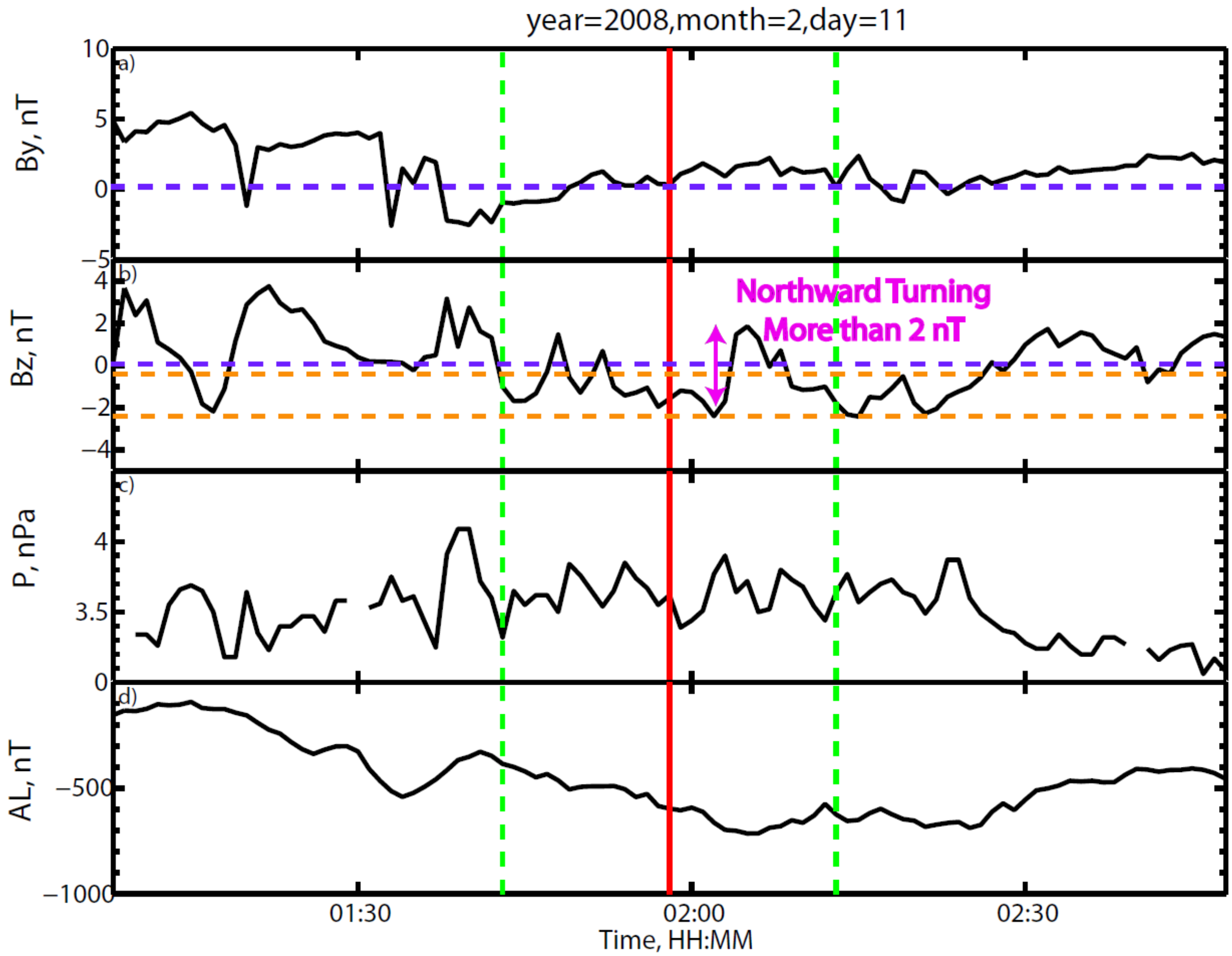

Figure A.5. Example of a B_z-triggered event applying the criteria based on Lyons et al. and the visual criteria in Hsu et al. without requirements for the southward IMF growth phase in the same format as Fig. A.1.

Bibliography

Akasofu, S.-I. (1964), The development of the auroral substorm, Planet. Space Sci., 12, 273-282.

Angelopoulos, V., et al. (2008), Tail reconnection triggering substorm onset, Science, 321, 931, doi:10.1126/science.1160495.

Amm, O., A. Pajunpaa, and U. Brandstrom (1999), Spatial distribution of conductances and currents associated with a north-south auroral form during a multiple-substorm period, Ann. Geophysicae 17, 1385.

Anderson, P. C., R. A. Heelis, and W. B. Hanson (1991), The ionospheric signatures of rapid subauroral ion drifts, J. Geophys. Res., 96, 5785–5792.

Anderson, P. C., W. B. Hanson, R. A. Heelis, J. D. Craven, D. N. Baker, and L. A. Frank (1993), A proposed production model of rapid subauroral ion drifts and their relationship to substorm evolution, J. Geophys. Res., 98, 6069–6078.

Anderson, P. C., D. L. Carpenter, K. Tsuruda, T. Mukai, and F. J. Rich (2001), Multisatellite observations of rapid subauroral ion drifts (SAID), J. Geophys. Res., 106, 29,585–29,599.

Angelopoulos, V., W. Baumjohann, C. F. Kennel, F. V. Coroniti, M. G. Kivelson, R. Pellat, R. J. Walker, H. Lühr, and G. Paschmann (1992), Bursty bulk flows in the inner central plasma sheet, J. Geophys. Res., 97, 4027–4039, doi:10.1029/91JA02701.

Angelopoulos, V., C.F. Kennel, F.V. Coroniti, R. Pellat, M.G. Kivelson, R.J. Walker, C.T. Russell, W. Baumjohann, W.C. Feldman, and J.T. Gosling, Statistical characteristics of bursty bulk flow events, J. Geophys. Res. 99, 21257, 1994.

Angelopoulos, V., F. V. Coroniti, C. F. Kennel, M. G. Kivelson, R. J. Walker, C. T. Rusell, R. L. McPherron, E. Sanchez, C.-I. Meng, W. Baoumjohann, G. D. Reeves, R. D. Belian, N. Sato, E. Friis-Christensen, P. R. Sutcliffe, K. Yumoto, and T. Harris (1996), Multipoint analysis of a bursty bulk flow event on April 11, 1985 , J. Geophys. Res., 101, 4967.

Angelopoulos, V., T. D. Phan, D. E. Larson, F. S. Mozer, R. P. Lin, K. Tsuruda, H. Hayakawa, T. Mukai, S. Kokobun, T. Tamamoto, D. J. Williams, R. W. McEntire, R. P. Lepping, G. K. Parks, M. Brittnacher, G. Germany, J. Spann, H. J. Singer, K. Yumoto (1997), Magnetotail flow bursts: Association to global magnetospheric circulation, relationship to ionospheric activity and direct evidence for localization, Geophys. Res. Lett., 24, 2271.

Baumjohann, W. (1993), The near-Earth plasma sheet: An AMPTE/IRM perspective, Space Sci. Rev., 64, 141-191.

Birn, J., J. Reader, Y. L. Wang, R. A. Wolf, and M. Hesse (2004), On the propagation of bubbles in the geomagnetic tail, Ann. Geophys., 22, 1773-1786.

Caan, M., R. McPherron, and C. T. Russell (1975), Substorm and Interplanetary Magnetic Field Effects on the Geomagnetic Tail Lobes, J. Geophys. Res., 80(1), 191-194.

Caan M. N., R. L. McPherron, C.T. Russell (1977), Characteristics of the association between interplanetary magnetic field and substorms, J. Geophys. Res., 82, 4837 - 4842.

Cheng, C. Z. (2004), Physics of substorm growth phase, oset, and dipolarization, Space Sci. Rev., 113, 207 – 270.

Clausen, L. B. N., et al. (2012), Large-scale observations of a subauroral polarization stream by midlatitude SuperDARN radars: Instantaneous longitudinal velocity variations, J. Geophys. Res., 117, A05306, doi:10.1029/2011JA017232.

Cox D. R. (1955), Some statistical methods connected with series of events, J. R. Stat. Soc., Ser. B, 17(2), 129 – 164.

Donovan, E., et al. (2006), The azimuthal evolution of the substorm expansive phase onset aurora, in Proceedings of ICS-8, edited by M. Syrjäsuo, and E. Donovan, pp. 55–60, Univ. of Calgary, Calgary, Alberta, Canada.

Dungey, J. W. (1961), Interplanetary magnetic fields and the auroral zones, Phys. Rev.

Let., 6, 47-48.

Elphinstone, R. D., et al. (1995), Observations in the vicinity of substorm onset: Implications for the substorm process, J. Geophys. Res., 100(A5), 7937–7969, doi:10.1029/94JA02938.

Erickson, P. J., J. C. Foster, and J. M. Holt (2002), Inferred electric field variability in the polarization jet from Millstone Hill E region coherent scatter observations, Radio Sci., 37(2), 1027, doi:10.1029/2000RS002531.

Foster, J., D. Fairfield, K. Ogilvie, and T. Rosenberg (1971), Relationship of Interplanetary Parameters and Occurrence of Magnetospheric Substorms, J. Geophys. Res., 76(28), 6971-6975.

Foster, J., and W. Burke (2002), A new categorization for sub-auroral electric fields, Eos Trans. AGU, 83(36), 393–394, doi:10.1029/2002EO000289.

Foster, J., P. Erickson, F. Lind, and W. Rideout (2004), Millstone Hill coherent-scatter radar observations of electric field variability in the sub-auroral polarization stream, Geophys. Res. Lett., 31, L21803, doi:10.1029/2004GL021271.

Frey, H. U., S. B. Mende, V. Angelopoulos, and E. F. Donovan (2004), Substorm onset observations by IMAGE-FUV, J. Geophys. Res, 109, A10304, doi:10.1029/2004JA010607.

Gallardo-Lacourt, B., Y. Nishimura, L. R. Lyons, S. Zou, V. Angelopoulos, E. Donovan, K. A. McWilliams, J. M. Ruohoniemi, and N. Nishitani (2014), Coordinated SuperDARN THEMIS ASI observations of mesoscale flow bursts associated with auroral streamers, J. Geophys. Res. Space Physics, 119, 142–150, doi:10.1002/2013JA019245.

Galperin, Y. (2002), Polarization jet: Characteristics and a model, Ann. Geophys., 20, 391–404

Galperin, Y., Y. Ponomarev, and A. Zosinova (1974), Plasma convection in the polar ionosphere, Ann. Geophys., 30, 1–7.

Greenwald, R. A., et al. (1995), DARN/SuperDARN: A global view of high-latitude convection, Space Sci. Rev.,71, 763-796.

Heppner, J. P. (1972), Polar-cap electric field distributions related to the interplanetary magnetic field direction, J. Geophys. Res., 77(25), 4877–4887.

Haldoupis, C. (1989), A review on radio studies of auroral E region ionospheric irregularities, Ann. Geophys., 7, 239.

Henderson, M., G. Reeves, R. Belian, and J. Murphree (1996), Observations of magnetospheric substorms occurring with no apparent solar wind/IMF trigger, J. Geophys. Res., 101(A5), 10773-10791.

Henderson, M. G., G. D. Reeves, J. S. Murphree (1998), Are north-south structures an ionospheric manifestation of bursty bulk flows?, Geophys. Res. Lett., 25, 3732, 1998.

Henderson, M. G., L. Kepko, H. E. Spence, M. Connors, J. B. Sigwarth, L. A. Frank, H. J. Singer, and K. Yumoto (2002), The evolution of north-south aligned auroral forms into auroral torch structures: The generation of omega bands and Ps6 pulsations via flow bursts, Proc. ICS-6, Ed. R. M. Winglee.

Henderson, M. G. (2009), Observational evidence for an inside-out substorm onset scenario, Ann. Geophys., 27, 2129-2140, doi:10.5194/angeo-27-2129-2009.

Hori, T., K. Maezawa, Y. Saito, and T. Mukai (2000), Average profile of ion flow and convection electric field in the near- Earth plasma sheet, Geophys. Res. Lett., 27(11), 1623–1626.

Hosokawa, K., S. E. Milan,M. Lester, A. Kadokura, N. Sato, and G. Bjornsson (2013), Large flow shears around auroral beads at substorm onset, Geophys. Res. Lett., 40, doi:10.1002/grl.50958.

Hsu, T.-S., and R. L. McPherron (2002), An Evaluation of the Statistical Significance of the Association between Northward Turnings of the IMF and Substorm Expansion Onsets, Journal of Geophysical Research, 107(A11), 1398, doi:1310.1029/2000JA000125.

Hsu T.-S., and R.L McPherron (2003), Occurrence frequencies of IMF triggered and nontriggered substorms, J. Geophys. Res, 108(A7), 1307, doi:10.1029/2002JA009442.

Kauristie, K., V. A. Sergeev, M. Kubyshkina, T. I. Pulkkinen, V. Angelopoulos, T. Phan, R. P. Lin, J. A. Slavin (2000), Ionospheric current signatures of transient plasma sheet flows, J. Geophys. Res., 105, 10 677- 10 688.

Keiling, A., V. Angelopoulos,J. M. Weygand, O. Amm, E. Spanswick, E. Donovan, S. Mende, J. McFadden, D. Larson, K.-H. Glassmeier, and H. U. Auster (2009), THEMIS ground-space observations during the development of auroral spirals, Ann. Geophys., 27, 4317-4332, doi:10.5194/angeo-27-4317-2009

Kim H.-J., L. R. Lyons, S. Zou, A. Boudouridis, D.-Y. Lee, C. Heinselman, and M. McCready (2009), Evidence that solar wind fluctuations substantially affect the strength of dayside ionospheric convection, J. Geophys. Res., 114, A11305, doi:10.1029/2009JA014280.

Koustov, A. V., D. W. Danskin, R. A. Makarevitch, and J. D. Gorin (2005), On the relationship between the velocity of E region HF echoes and E x B plasma drift, Ann. Geophys.,23, 371, doi: 10.5194/angeo-23-371-2005.

Liang, J., E. F. Donovan, W. W. Liu, B. Jackel, M. Syrjäsuo, S. B. Mende, H. U. Frey, V. Angelopoulos, and M. Connors (2008), Intensification of preexisting auroral arc at Substorm expansion phase onset: Wave-like disruption during the first tens of seconds, Geophys. Res. Lett., 35, L17S19, doi:10.1029/2008GL033666.

Lin, N.,H. Frey, S. Mende, F. Mozer, R. Lysak, Y. Song, andV.Angelopoulos (2009), Statistical study of substorm timing sequence, J. Geophys. Res., 114, A12204, doi:10.1029/2009JA014381.

Lui, A. T. Y. (2004), Potential plasma instabilities for substorm expansion onsets, Space Sci. Rev., 113, 127 – 206.

Lui, A. T. Y., (2009), Comment on Tail reconnection triggering substorm onset, Science, 324, 1391, doi:10.1126/science.1167726.

Lyons R.L., G.T. Blanchard, J.C. Samson, R.P. Lepping, T. Yamamoto, T. Moretto (1997), Coordinated observations demonstrating external substorm triggering, J. Geophys. Res., 102(A12), 27, 039-27, 051

Lyons, L. R., T. Nagai, G. T. Blanchard, J. C. Samson, T. Yamamoto, T. Mukai, A. Nishida, S. Kokobun (1999), Association between Geotail plasma flows and auroral poleward boundary intensifications observed by CANOPUS photometers, J. Geophys. Res., 104, 4485- 4497.

Lyons, L. R., E. Zesta, Y. Xu, E. R. Sanchez, J. C. Samson, G. D. Reeves, J. M. Ruohomiemi, J. B. Sigwarth (2002), Auroral poleward boundary intensifications and tail bursty flows: A manifestation of a large-scale ULF oscilation?, J. Geophys. Res., 107(A11), 1352, doi: 10.1029/2001JA000242.

Lyons L. R., H.-J. Kim, X. Xing, S. Zou, D.-Y. Lee, C. Heinselman, M. J. Nicolls, V. Angelopoulos, D. Larson, J. McFadden, A. Runov, K.-H. Fornacon (2009), Evidence that solar wind fluctuations substantially affect global convection and substorm occurrence, J. Geophys. Res., 114, A11306, doi:10.1029/2009JA014281.

Lyons, L. R., Y. Nishimura, H.-J. Kim, E. Donovan, V. Angelopoulos, G. Sofko, M. Nicolls, C. Heinselman, J. M. Ruohoniemi, and N. Nishitani (2011), Possible connection of polar cap flows to pre- and post-substorm onset PBIs and streamers, J. Geophys. Res., 116, A12225, doi:10.1029/2011JA016850.

Lyons, L. R., et al. (2015), Azimuthal flow bursts in the inner plasma sheet and possible connection with SAPS and plasma sheet earthward flow bursts, J. Geophys. Res. Space Physics, 120,5009–5021, doi:10.1002/2015JA021023.

Makarevich, R. A., and P. L. Dyson (2007), Dual HF radar study of the subauroral polarization stream, Ann. Geophys., 25, 2579–2591.

Makarevich, R. A., A. C. Kellerman, J. C. Devlin, H. Ye, L. R. Lyons, and Y. Nishimura (2011), SAPS intensification during substorm recovery: A multi-instrument case study, J. Geophys. Res., 116, A11311, doi:10.1029/2011JA016916.

McPherron, R. L., T. Terasawa, and A. Nishida (1986), Solar wind triggering of substorm expansion onset, J. Geomagn. Geoelectr., 38(11), 1089– 1108.

Mende, S. B., S. E. Harris, H. U. Frey, V. Angelopoulos, C. T. Russell, E. Donovan, B. Jackel, M. Greffen, M. Peticolas (2008), The THEMIS array of ground-based observatories for the study of auroral substorms, Space Sci. Rev., 141, 357, doi:10.1007/s11212-008-9380-x.

Mishin, E., J. Foster, A. Potekhin, F. Rich, K. Schlegel, K. Yumoto, V. Taran, J. Ruohoniemi, and R. Friedel (2002), Global ULF disturbances during a stormtime substorm on 25 September 1998, J. Geophys. Res., 107(A12), 1486, doi:10.1029/2002JA009302.

Mishin, E.,W. Burke, C. Huang, and F. Rich (2003), Electromagnetic wave structures within subauroral polariza- tion streams, J. Geophys. Res., 108, 1309, doi:10.1029/2002JA009793.

Mishin, E., W. Burke, and A. Viggiano (2004), Stormtime subauroral density troughs: Ion-molecule kinetics effects, J. Geophys. Res., 109, A10301, doi:10.1029/2004JA010438.

Mishin, E.V., and W.J. Burke (2005), Stormtime coupling of the ring current, plasmasphere, and topside ionosphere: Electromagnetic and plasma disturbances, J. Geophys. Res., 110, A07209, doi:10.1029/ 2005JA011021.

Morley, S. K., and M. P. Freeman (2007), On the association between northward turnings of the interplanetary magnetic field and substorm onsets, Geophysical Research Letters, 34, 08104, doi:08110.01029/02006GL028891.

Motoba, T., K. Hosokawa, A.Kadokura, and N. Sato (2012), Magnetic conjugacy of northern and southern auroral beads, Geophys. Res. Lett., 39, L08108, doi:10.1029/2012GL051599.

Nakamura, R., W. Baumjohann, R. Schödel, M. Brittnacher, V. A. Sergeev, M. Kubyshkina, T. Mukai, K. Liou (2001), Earthward flow bursts, auroral streamers, and small expansions, J. Geophys. Res., 106, 10 791-10 804.

Nakamura, R., W. Baumjohann, C. Mouikis, L. M. KIstler, A. Runov, M. Volwerk, Y. Asano, Z. Vörös, T. L. Zhang, B. Klecker, H. Rème, and A. Balogh (2004), Spatial scale of high-speed flows in the plasma sheet observed by Cluster, Geophys. Res. Lett., 31, L09804, doi:10.1029/2004GL019558.

Newell P. T., and K. Liou (2011), Solar Wind Driving and Substorm Triggering, J. Geophys. Res., 116, A03229, doi:10.1029/2010JA016139.

Nishida, A. (1968a), Coherence of geomagnetic DP 2 fluctuations with interplanetary magnetic variations, J. Geophys. Res., 73(17), 5549–5559.

Nishida, A. (1968b), Geomagnetic Dp 2 fluctuations and associated magnetospheric phenomena, J. Geophys. Res., 73(5), 1795–1803.

Nishimura, Y., J. Wygant, T. Ono, M. Iizima, A. Kumamoto, D. Brautigam, and R. Friedel (2008), SAPS measurements around the magnetic equator by CRRES, Geophys. Res. Lett., 35, L10104, doi:10.1029/ 2008GL033970.

Nishimura, Y., L. Lyons, S. Zou, V. Angelopoulos, and S. Mende (2010), Substorm triggering by new plasma intrusion: THEMIS all-sky imager observations, J. Geophys. Res., 115, A07222, doi:10.1029/2009JA015166.

Nishimura, Y., J. Bortnik, W. Li, L. R. Lyons, E. F. Donovan, V. Angelopoulos, and S. B. Mende (2014), Evolution of nightside subauroral proton aurora caused by transient plasma sheet flows, J. Geophys. Res. Space Physics, 119, 5295–5304, doi:10.1002/2014JA020029.

Oguti, T. (1973), Hydrogen emission and electron aurora at the onset of the auroral breakup, J. Geophys. Res., 78(31), 7543–7547, doi:10.1029/JA078i031p07543.

Pritchett, P. L., and F. V. Coroniti (2010), A kinetic ballooning/interchange instability in the magnetotail, J. Geophys. Res., 115, A06301, doi:10.1029/2009JA014752.

Pritchett, P. L., and F. V. Coroniti (2011), Plasma sheet disruption by interchange- generated flow intrusions, Geophys. Res. Lett., 38, L10102, doi:10.1029/2011GL047527.

Pritchett, P. L., and F. V. Coroniti (2013), Structure and consequences of the kinetic ballooning/interchange instability in the magnetotail, J. Geophys. Res. Space Physics, 118, 146–159, doi:10.1029/2012JA018143.

Pitkänen, T., A. T. Aikio, O. Amm, K. Kauristie, H. Nilsson, K. U. Kaila (2011), EISCAT-Cluster observations of quiet-time near-Earth magnetotail fast flows and their signatures in the ionosphere, Ann. Geophys., 29, 299-319, doi: 10.5194/angeo-29-299-2011.

Pu, Z., et al. (1999), Ballooning instability in the presence of a plasma flow: A syntheses of tail reconnection and current disruption models for the initiation of substorms, J. Geophys. Res., 104, 10,235 – 10,248.

Reeves G. D. (1996), Radial propagation of substorm injections, International Conference on Substorms-3, Eur. Space Agency Spec. Publ., ESA SP-339, 579-584.

Rostoker, G., S.-I. Akasofu, J. Foster, R. A. Greenwald, A. T. Y. Lui, Y. Kamide, K. Kawasaki, R. L. McPherron, and C. T. Russell (1980), Magnetospheric substorms—Definition and signatures, J. Geophys. Res., 85, 1663–1668, doi:10.1029/JA085iA04p01663.

Rostoker, G. (1983), Triggering of Expansive Phase Intensifications of Magnetospheric Substorms by Northward Turnings of the Interplanetary Magnetic Field, J. Geophys. Res., 88(A9), 6981-6993.

Roux, A., S. Perraut, P. Robert, A. Morane, A. Pedersen, A. Korth, G. Kremser, B. Aparicio, D. Rodgers, and R. Pellinen (1991), Plasma sheet instability related to the westward traveling surge, J. Geophys. Res., 96(A10), 17697–17714, doi:10.1029/91JA01106.

Sakaguchi, K., K. Shiokawa, A. Ieda, Y. Miyoshi, Y. Otsuka, T. Ogawa, M. Connors, E. F. Donovan, and F. J. Rich (2007), Simultaneous ground and satellite observations of an isolated proton arc at subauroral latitudes, J. Geophys. Res., 112, A04202, doi:10.1029/2006JA012135.

Sakaguchi, K., K. Shiokawa, A. Ieda, R. Nomura, A.Nakajima, M. Greffen, E. Donovan, I. R. Mann, H. Kim, and M. Lessard (2009), Fine structures and dynamics in auroral initial brightening at substorm onsets, Ann. Geophys., 27, 623–630.

Samson, J. C., L. R. Lyons, P. T. Newell, F. Creutzberg, and B. Xu (1992), Proton aurora and substorm intensifications, Geophys. Res. Lett., 19, 2167–2170, doi:10.1029/92GL02184.

Sergeev, V. A., O. A. Aulamo, R. L. Pillinen, M. K. Vallinkoski, T. Bosinger, C. A. Cattell, R. C. Elphic, D. J. Williams (1990), Non-substorm short-lived injection events in the ionosphere and magnetosphere, Planet. Space Sci., 38,231.

Sergeev, V. A., V. Angelopoulos V., C. A. Cattell, C. T. Russell (1996), Detection of localized, plasma-depleted flux tubes or bubbles in the midtail plasma sheet, J. Geophys. Res., 101(A5), 10817-10826

Sergeev, V. A., K. Liou, C.-I. Meng, P. T. Newell, M. Brittnacher, G. Parks, G. D. Reeves (1999), Development of auroral streamers in association with localized impulsive injections to the inner magnetotail, Geophys. Res. Lett., 26(3), 417-420.

Sergeev, V. A., J.-A. Sauvaud, D. Popescu, R. A. Kovrazhkin, K. Liou, P. T. Newell, M. Brittnacher, G. Parks, R. Nakamura, T. Mukai, G. D. Reeves (2000), Multiple spacecraft observation of a narrow transient plasma jet in the Earth's plasma sheet, Geophys. Res. Lett., 27(6),851-854.

Sergeev, V. A., K. Liou, P. T. Newell, S.-I Ohtani, M. R. Hairston, F. Rich (2004), Auroral streamers: Characteristics of associated precipitation, convection and field-aligned currents, Ann. Geophys., 22,537-548, doi: 10.5194/angeo-22-537-2004.

Shi, Y., E. Zesta, L. R. Lyons, J. Yang, A. Boudouridis, Y. S. Ge, J. M. Ruohoniemi, and S. Mende (2012), Two-dimensional ionospheric flow pattern associated with auroral streamers, J. Geophys. Res., 117, A02208, doi:10.1029/2011JA017110.

Spiro, R. W., R. A. Heelis, and W. B. Hanson (1979), Rapid subauroral ion drifts observed by Atmospheric Explorer C, Geophys. Res. Lett., 6, 657–660.Yeh et al., 1991

Voronkov, I., E. Friedrich, and J. C. Samson (1999), Dynamics of the substorm growth phase as observed using CANOPUS and SuperDARN instruments, J. Geophys. Res., 104, 28491–28505, doi:10.1029/1999JA900362.

Voronkov, I., E. F. Donovan, B. J. Jackel, and J. C. Samson (2000), Large-scale vortex dynamics in the evening and midnight auroral zone: Observations and simulations, J. Geophys. Res., 105(A8),18505–18518, doi:10.1029/1999JA000442.

Wang, C., L. Lyons, J. Weygand, T. Nagai, and R. McEntire (2006), Equatorial distributions of the plasma sheet ions, their electric and magnetic drifts, and magnetic fields under different interplanetary magnetic field B-z conditions, J. Geophys. Res.- SPACE Phys., 111(A4), doi:10.1029/2005JA011545.

Weimer, D. R. (1995), Models of high-latitude electric potentials derived with a least error fit of spherical harmonic coefficients, J. Geophys. Res., 100(A10), 19595.

Yang, J., F. R. Toffoletto, R. A. Wolf, and S. Sazykin (2011), RCM-E simulation of ion acceleration during an idealized plasma sheet bubble injection, J. Geophys. Res., 116, A05207, doi: 10.1029/2010JA016346.

Yang, J., F. R. Toffoletto, R. A. Wolf, S. Sazykin, P. A. Ontiveros, and J. M. Weygand (2012), Large-scale current systems and ground magnetic disturbance during deep substorm injections, J. Geophys. Res., 117, A04223, doi: 10.1029/2011JA017415.

Zesta, E., L. R. Lyons, E. Donovan (2000), The auroral signature of Earthward flow burst observed in the magnetotail, Geophys. Res. Lett., 27, 3241-3244, doi:10.1029/2000GL000027.

Zesta, E., E. Donovan, L. Lyons, G. Enno, J. S. Murphree, and L. Cogger (2002), The two-dimensional structure of auroral poleward boundary intensification (PBIs), J. Geophys. Res., 107(A11), 1350, doi:10.1029/ 2001JA000260.

Zesta, E., L. Lyons, C.-P. Wang, E. Donovan, H. Frey, and T. Nagai (2006), Auroral poleward boundary intensification (PBIs): Their two-dimensional structure and associated dynamics in the plasma sheet, J. Geophys. Res., 111, 111, A05201, doi:10.1029/2004JA010640.

Zou, S., L. R. Lyons, M. J. Nicolls and C. J. Heinselman (2009), PFISR observations of strong azimuthal flow bursts in the ionosphere and their relation to nightside aurora, J. Atmos. and Solar-Terr. Phys., doi:10.1016/j.jastp.2008.06.015.

Zou, S., L.R. Lyons, M. J. Nicolls, and C. J. Heinselman (2009), PFISR observations of strong azimuthal flow bursts in the ionosphere and their relation to nightside aurora, J. Atmos. Sol. Terr. Phys., doi:10.1016/j.jastp.2008.06.015.

Zou, S., M. B. Moldwin, L. R. Lyons, Y. Nishimura, M. Hirahara, T. Sakanoi, K. Asamura, M. J. Nicolls, Y. Miyashita, S. B. Mende, and C. J. Heinselman (2010), Identification of substorm onset location and pre-onset sequence using Reimei, THEMIS GBO, PFISR and Geotail, J. Geophys. Res., 115, A12309, doi:10.1029/2010JA015520.

Zou, Y., Y. Nishimura, L. R. Lyons, E. F. Donovan, J. M. Ruohoniemi, N. Nishitani, *and* K. A. McWilliams *(*2014*),* Statistical relationships between enhanced polar cap flows and PBIs, J. Geophys. Res. Space Physics, 119, *doi:*10.1002/2013JA019269.